

An Investigation into the Fabrication of Nanomechanical Switches

by

Carlo Schenke

*Thesis presented in partial fulfilment of the requirements for
the degree of Master of Science in Engineering at
Stellenbosch University*



Supervisor: Prof. W.J. Perold
Department of Electrical and Electronic Engineering

March 2010

Declaration

By submitting this thesis electronically, I declare that the entirety of the work contained therein is my own, original work, that I am the owner of the copyright thereof (unless to the extent explicitly otherwise stated) and that I have not previously in its entirety or in part submitted it for obtaining any qualification.

March 2010

Abstract

This report intends to show how able the Stellenbosch Electrical and Electronic Engineering Department's micro fabrication laboratory is to manufacture nanomechanical switches and similar structures. Following the investigation, an attempt will be made to produce these devices.

In attaining this goal, a literature study was performed focusing on mechanical switching and nanotechnology. Their origins, development and current application are investigated, as well as the requirements for developing these devices.

Having completed the literature study, a series of current nanomechanical switches were investigated, selecting those most likely to be manufactured at the available facilities and having the required attributes for taking the place of silicon transistors in low speed, hostile environments.

The most common method of manufacturing nanoswitches is simulated using several methods of predicting device failure. This will aid in the selection of manufacturing process guidelines, such as dimensions in the photoresist templates and layer thickness before etching, allowing for the repeated production of functional switches.

The two manufacturable nanomechanical switches are investigated, using techniques and materials available at the micro fabrication laboratory to manufacture them. Subsequently, their electrical properties will be determined and used in simulating their failure characteristics.

In conclusion, the results are discussed along with advice and improvements for the continued investigation and production of nanodevices at Stellenbosch University.

Opsomming

Die doel met hierdie tesis is om die vermoë van die Departement Elektriese en Elektroniese Ingenieurswese se mikro-elektronika laboratorium te ondersoek ten opsigte van die vervaardiging van nanomeganiese skakelaars en aanverwante komponente. Na afloop van die ondersoek sal 'n poging aangewend word om hierdie toestelle te vervaardig.

In nastrewing van hierdie doel is 'n literatuurstudie uitgevoer wat fokus op meganiese skakeling en nanotegnologie. Die oorsprong, ontwikkeling en huidige aanwending van hierdie skakelaars word ondersoek, sowel as die vereistes vir die ontwikkeling daarvan.

Na voltooiing van die literatuurstudie word 'n reeks van bestaande nanomeganiese skakelaars ondersoek. Skakelaars word dan geïdentifiseer op grond van hul waarskynlike vervaardigbaarheid met die beskikbare fasiliteite. Die vereiste eienskappe vir lae spoed toepassings in omgewings waar silikon-skakelaars nie kan werk nie, word ook in ag geneem.

Die mees algemene metode vir die vervaardiging van nanoskakelaars word gesimuleer met behulp van verskeie tegnieke wat toestelfaling voorspel. Die simulاسies sal help in die keuse van vervaardigingsriglyne van die proses, soos die dimensies van die fotolak template en die laagdiktes voor etsing, sodat goeie resultate verkry kan word wanneer die skakelaars vervaardig word, met goeie herhaalbaarheid.

Die twee gekose vervaardigbare nanomeganiese skakelaars word dan ondersoek ten opsigte van die tegnieke en materiale wat in die mikro-elektronika laboratorium beskikbaar is. Daarna sal die elektriese eienskappe van die skakelaars bepaal word.

Ter afsluiting word die resultate bespreek, saam met aanbevelings vir die voortsetting van die navorsing om nanomeganiese skakelaars by die Universiteit van Stellenbosch te vervaardig.

Acknowledgements

I would like to thank my parents, Richard and Tertia Sandra Schenke, for their love and unwavering support.

A word of thanks to my supervisor, Prof W.J. Perold, for all the aid and guidance.

My appreciation to Gareth van der Westhuizen for all the evenings stuck in the laboratory.

Much of what was done in this report would not have been viable without the help of Ulrich Büttner and the people at SED. Thanks to Ulrich Büttner, Wessel Croukamp, Lincon Saunders en Nicklaas van Graan.

Also to iThemba Labs I would like to express my appreciation for providing materials for the construction process.

Lastly a thank you to all the family and friends that kept me going in the hard times.

Contents

Declaration	i
Abstract	ii
Opsomming	iii
Acknowledgements	iv
Contents	v
List of Figures	viii
List of Tables	xi
Nomenclature	xii
1 Introduction	1
1.1 Research Objectives and Motivation	2
1.2 Report Overview	2
2 Literature Study	3
2.1 Steam powered thinking	3
2.2 Nanotechnology and NEMS	14
2.3 To summarise	35
3 Mechanical Nanoswitches	36
3.1 Device overview	36
3.2 Silver Sulfide Switches	37
3.3 Photoswitches	40
3.4 Carbon Nanotube Switches	43

3.5	Organically Actuated Switches	46
3.6	To Summarise	48
4	Procedure and Methodology	49
4.1	Procedure	49
4.2	Methodology	51
4.3	To Summarise	51
5	Design and Manufacture	52
5.1	About the Microelectronics Laboratory	52
5.2	Basic Procedures in the Microelectronics Laboratory	56
5.3	Choosing a Device	66
5.4	Manufacture	68
5.5	Results	86
5.6	To Summarise	91
6	Simulation	92
6.1	CNT Simulation Theory	93
6.2	Implementation of Simulation Theory	96
6.3	To Summarise	103
7	Conclusion	104
	Appendices	107
A	Clean Room	108
A.1	Servicing Procedure	108
A.2	Clean room Rules and Regulations	110
A.3	Personnel Entrance Procedure	112
A.4	Emergencies	113
B	Deposition Materials	114
C	XRD Results	118
C.1	Calibration Sample	118
C.2	Silver	120
C.3	Silver Sulfide	121
C.4	Palladium	122

C.5 Aluminium	123
List of References	124

List of Figures

2.1	A box of Napier's bones	3
2.2	Schickardt's mechanical calculator	4
2.3	Pascal's computer	5
2.4	Leibnitz's geared calculating machine	5
2.5	Charles Babbage	6
2.6	Difference Engine Nr 2 replica	11
2.7	Lego Difference Engine	12
2.8	A visual relation of scales	15
2.9	AFM theory	18
2.10	STM theory	18
2.11	Representation of TEM and SEM microscopy	20
2.12	The photolithography process	25
2.13	The effects of positive and negative photoresist	26
2.14	Dip pen nanolithography setup	27
2.15	Self assembled polymer sheet	29
2.16	Magnetically folded blank	30
2.17	Drug capsule after completion	30
2.18	Nano-origami procedure	30
3.1	Silver sulfide as an ionic conductor	37
3.2	Silver sulfide switch model	38
3.3	Silver sulfide reversible particle model	39
3.4	Schematic and topographic views of a phototransistor	40
3.5	Model of a F ₁₆ CuPc photoswitch	41
3.6	Functional model of the organic insulator photoswitch	41
3.7	Representation and SEM image of a basic CNT switch	43
3.8	Model of the CNT trench switch	44

3.9	Model of the telescoping nanoswitch	45
3.10	C ₇₀ Switch model	45
3.11	Nanomotor from liquid spheres	46
3.12	Organically actuated contact switch	47
5.1	Nick van Graan working in the cleanroom (1986)	52
5.2	Transistor manufactured in microelectronics laboratory	53
5.3	Photoresist spinner and associated chemicals	56
5.4	UV exposer	57
5.5	Chrome Mask	58
5.6	PCB mask	58
5.7	Printed mask	58
5.8	Rubber mask	58
5.9	Photoresist profile of a chrome mask	59
5.10	Photoresist profile of a PCB mask	59
5.11	Photoresist profile of a printed mask	59
5.12	Photoresist profile of a rubber mask	59
5.13	Thermal evaporation unit	61
5.14	Thermal evaporation unit crucible	62
5.15	Thermal evaporation unit during annealing process	62
5.16	QCM sensor and housing	63
5.17	AFM station	64
5.18	The AFM and motorised sample base	64
5.19	Test run photoswitches	68
5.20	Diagram for thin film theory	70
5.21	Organic layer components and equipment	72
5.22	Polystyrene spun on at 3000rpm	73
5.23	Polystyrene spun on at 4000rpm	73
5.24	Polystyrene spun on at 5000rpm	73
5.25	Graph for layer thicknesses	74
5.26	Colour map AFM scan an organic layer	75
5.27	3D graph AFM scan of an organic layer	75
5.28	3D graph AFM scan of a scratched organic layer	75
5.29	Cross section of the AFM scratch	76
5.30	Cross section along the AFM scratch	77
5.31	First complete photoswitch	78

5.32	3D graph AFM scan of the ITO glass	78
5.33	Cross section of the ITO glass surface	78
5.34	SEM image of an actual Ag ₂ S switch	79
5.35	Niello Silverware	80
5.36	Liver of sulphur	81
5.37	The impregnated silver tested in nitric acid	81
5.38	The impregnation solution and heating base	82
5.39	Impregnated silver samples	82
5.40	XRD sample holder	83
5.41	XRD results for silver sulfide development	83
5.42	Test run device for the silver sulfide switch	84
5.43	Photoswitch testing area	86
5.44	UV exposure zone	86
5.45	Photoswitch with water cavitation	87
5.46	Layer damage from water drops	87
5.47	Aluminium distortion transition	88
5.48	Magnified view of aluminium deformation	88
5.49	Arc damaged samples	88
5.50	Magnified ITO fractures	88
6.1	Schematic of a cantilever switch	92
6.2	Graph of the pull-in voltages	97
6.3	Graph of the nanotube lengths	98
6.4	Graph of the gap heights	99
6.5	Raw data simulation models	100
6.6	Surf plot of the error percentage of the two simulation models . . .	101
6.7	Contour plot of the two simulation's error function	102
C.1	XRD results for ITO substrate	118
C.2	XRD results for silver deposition	120
C.3	XRD results for silver sulfide development	121
C.4	XRD results for palladium deposition	122
C.5	XRD results for aluminium deposition	123

List of Tables

2.1	Differnce Engine Principle	9
2.2	Differnce Engine Principle	9
5.1	Photoresist equipment	57
5.2	Pugh's matrix for nanoswitches	67
5.3	Photoswitch device configurations for manufacture	68
5.4	Material Properties for the Organic Layer	72
5.5	Organic layer thickness readings	76
5.6	Material Data for Thermal Deposition (in Celsius)	84

Nomenclature

MEMS	-	Microelectromechanical System
CMOS	-	Complementary Metal Oxide Semiconductor
NEMS	-	Nanoelectromechanical System
ASCC	-	Automatic Sequence Controlled Calculator
DARPA	-	Defense Advanced Research Projects Agency
AFM	-	Atomic Force Microscope
STM	-	Scanning Tunneling Microscope
MFM	-	Magnetic Force Microscope
MRI	-	Magnetic Resonance Imaging
SEM	-	Scanning Electron Microscope
TEM	-	Tunnelling Electron Microscope
UV	-	Ultra Violet
PLD	-	Pulse Laser Deposition
PLE	-	Pulse Laser Etching
PMMA	-	Polymethylmethacrylate
ITO	-	Indium Tin Oxide
PS	-	Polystyrene
CNT	-	Carbon Nanotube
SWNT	-	Single Wall Nanotube
PECVD	-	Plasma Enhanced Chemical Vapour Deposition
MWNT	-	Multi Wall Nanotube
DWNT	-	Double Wall Nanotube
DNA	-	Deoxyribonucleic Acid
RF	-	Radio Frequency
ESR	-	Electron Spin Resonance
XRD	-	X-Ray Diffraction
ESD	-	Electrostatic Discharge

UWC	-	University of the Western Cape
UCT	-	University of Cape Town
PCB	-	Printed Circuit Board
QCM	-	Quartz Crystal Microbalance
MD	-	Molecular Dynamics
Ag ₂ S	-	Silver Sulfide
Ag	-	Silver
<i>F</i> ₁₆ <i>CuPc</i>	-	Hexadecafluorophthalocyanine
C ₇₀	-	Ellipsoidal Molecule of 70 Carbon atoms
Au	-	Gold
Al	-	Aluminium
CuPc	-	Copper Phthalocyanine
Pt	-	Platinum
Pd	-	Palladium
HNO ₃	-	Nitric Acid
\hat{H}	-	Hamiltonian
\hbar	-	Plancks constant divided by 2π
m	-	Mass
V(r)	-	External Potential of a particle
r	-	Distance between Nuclear Particles
Z	-	Electron Charge Number
e	-	Electron Charge
h	-	Height
K	-	Overall Calibration constant
C	-	Polymer Concentration
μ	-	Intrinsic Viscosity
ω	-	Rotational Speed
ρ	-	Density
t	-	Time
N	-	Number of parts in a system
\bar{x}	-	Mean value
x_i	-	i-th term if N
S	-	Standard deviation
σ	-	Stress
ϵ	-	Strain
E	-	Young's modulus
e_0a	-	Small scale effect parameter

q	-	Force working in on a system
Q	-	Shear force in a structure
M	-	Bending moment
y	-	Displacement
I	-	Second moment of area
F_e	-	Force due to electrostatic effects
F_n	-	Force due to intermolecular effects
ϵ_0	-	Permittivity of a vacuum
A	-	Hamaker's constant
γ	-	Poisson's ratio
g	-	Gap distance from Cantilever to base
c	-	Constant speed of light
Tera	-	10^{12}
Giga	-	10^9
Mega	-	10^6
Kilo	-	10^3
Milli	-	10^{-3}
Micro	-	10^{-6}
Nano	-	10^{-9}
Angstrom	-	10^{-10}
Pico	-	10^{-12}

Chapter 1

Introduction

Currently only basic nanodevices can be produced with some degree of control [1]. Microelectromechanical Systems (MEMS) and microsystems made the breakthrough to commercial products in the 1990's, adding a well developed understanding of Complementary Metal Oxide Semiconductor (CMOS) manufacturing technology and the experience already garnered from extensive work in the field [2]. At the same time the discovery of the nanotube added to the interest of the then emerging nanotechnology, and in the dawning of the 21st century, commercial sub-micron manufacturing technologies are being developed, allowing for the steady breakthrough of Nanoelectromechanical Systems (NEMS)

So from the concept of current silicon technology switches and their shortcomings, we look at something different, also contrasted with Babbage and his difference engine, on top of the growing field of nanotechnology brought to us in practice at the dawn of the 21st century by Richard Feynman in spirit and Maxwell in theory.

Currently technology is falling behind Moore's law due to size restrictions and increasing material tolerances. Ten-atom devices are greatly affected by a deviation in doping concentration and interlinks have become bottle necking structures. Computing speed thus no longer doubles, with an accompanying halving in price, every 1.5 years, as Moore predicted in his later life.

The requirement for faster switching speeds thus necessitates a look at the available technologies world wide, for switch production and the methods and techniques available at Stellenbosch University for the fabrication of these types of nanodevices.

1.1 Research Objectives and Motivation

The objective of this thesis is the of nanomechanical switches and then their application as logic gates. These devices will be designed, simulated and then manufactured.

1.2 Report Overview

This report can be broken down into three main parts, namely investigation, manufacture and simulation. In Chapter 2, the broader aspects of the investigation are addressed. It starts with the origins of mechanical calculation and its founder, followed by a discussion of nanotechnology and its subsidiary considerations.

In Chapter 3 nanomechanical switching and current nanomechanical switches are investigated and discussed. Particular attention is given to the driving principal of the devices, as well as the different applications thereof.

This is followed by a discussion of the procedure and methodology that was followed during the course of the project and in writing the report. This is done ahead of the manufacturing section in order to ease qualms as to the approach used in following through with the research.

Chapter 5 discloses the selection process for the manufactured switches as well as the formulation of the manufacturing methods. Each nanoswitch was analysed for possible obstacles to their construction, which were then addressed in full before the attempted production of functional switches.

An attempt was made, in Chapter 6 to simulate the function and failure mechanisms of cantilever style nanodevices, in particular those using carbon nanotubes. This was done because of the extensive use of this type of device in current micro- and nanoscale devices.

Finally, the results of the report are discussed in the conclusion. Possible additions for the laboratory are suggested and improvements to the developed devices are suggested.

Chapter 2

Literature Study

2.1 Steam powered thinking

In the advances leading to the modern day personal computer, the transistor is heralded as the most fundamental piece, the original building block making the subsequent evolution of the technology possible. However, before the advent of the solid-state switch, the idea for computing difficult functions with the aid of machines already existed.

If we go to the very beginning of computing there was the abacus from 3000 B.C. This was followed by the Scottish mathematician, John Napier's logarithm sticks from 1594. The logarithm sticks led to the development of logarithm tables and Napier's bones. This cylinder spool method of realigning logarithm tables can be seen in Figure 2.1.



Figure 2.1: A box of Napier's bones [3]

This inspired the Englishman William Oughttred to invent the slide rule. Although these were the forerunners to the saga of computing, they were still far from automated.

Next came the mechanical calculator. While the first of this new breed is impossible to pinpoint, the earliest that has been catalogued is that of the German Professor Wilhelm Schickardt in 1623.



Figure 2.2: Schickardt's mechanical calculator [4]

While this machine, seen in Figure 2.2, was of simple construction, it could already add, subtract, multiply and divide, while keeping track of carry over values for tens and hundreds. This device was soon to be followed by Pascal's addition to the field with Pascal's computer, a representation of which can be seen in Figure 2.3. The Philosopher Thomas Hobbes said of this device:

"Brass and iron have been invested with the function of brain, and instructed to perform some of the most difficult operations of mind."



Figure 2.3: Pascal's computer [5]

Up to this point the mechanical calculators were no more than a child's toy. Gottfried Wilhelm Von Leibnitz however was to construct a geared calculating machine in 1671, like the one in Figure 2.4. At the same time he also envisaged the binary system and its 2 value logic.

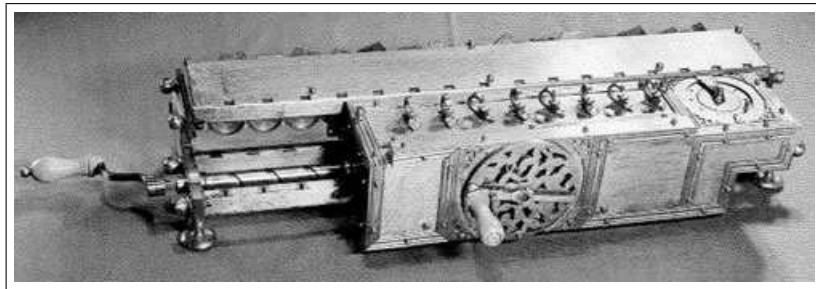


Figure 2.4: Leibnitz's geared calculating machine [6]

All these attempts at mechanical calculation were still, however, highly expensive and laborious with little increase in the speed of calculation. Only seen as curiosities, they were never taken much further than a few models for the rich.

It was on 3 July 1822 that a man named Charles Babbage wrote a letter to the president of the Royal Society. The letter proposing the construction of a machine to do arithmetical calculations, to free man from this the lowest occupation of man's faculties. He called this device the Difference Engine.

Charles Babbage



Figure 2.5: Charles Babbage (1791-1871) [7]

When the English government withdrew from the endeavour of the difference engine, Babbage was distraught. This also came at the point where Babbage believed that he had completed all the necessary refinement and development to be able to finish the machine. Babbage said that when someone else finally constructs his dream, only then, and that person alone, would be able to appreciate his labour and vision. He believed that it would occur within 50 years of his death. It would however be more than 80 years before Professor Aiken eventually realised the computer.

Even as a child, Charles Babbage was mechanically minded. Having been a sick child and therefore being stuck indoors often, he would disassemble his toys in order to find out how they worked. As he grew up he continued with his inquisitive pursuits, trying to improve the world around him. One such event is rather well documented by others and himself, where he tried to make shoes that could walk on water. They worked well at first but when the current

changed deeper into the river he was testing it on, the right shoe gave in. It took some time for him to free himself from the grip of his invention and the river.

The seeds of the difference engine were sown while Babbage was at college. Some sources say that it occurred while he was working with a colleague on star charts, others say it was during a mathematics lesson. But agree, however, that it was in connection with logarithm tables, which at the time were prone to faults. Having come across another fault in the table he was working with exclaimed:

"...wish to God these calculations had been executed with steam!"

He wanted to produce the tables mechanically, hence excluding the possibility of calculation and copy errors due to human involvement.

Since the French government had produced such tables by breaking the calculations down into a series of additive and subtractive operations, Babbage thought that a repetitive operating machine would be able to do the same. Why, he asked himself, would a machine of gears and levers not be able to replace humans in these tedious low level operations? So he went about designing a device that would be able to produce accurate tables of squares, roots, cubes, logarithms and the like.

Babbage was undoubtedly far ahead of his time. He proposed a telegraph system six years before Morse was to patent the electric telegraph. Flat rate postage, earthquake detectors and an impromptu submarine, were some of the other things he came up with during the course of his life. But alas, as with most others who were ahead of their time, he would not be appreciated. One of his school time friends said of him, "*. . . not only bad, but who would never get on in the world*".

The Difference and Analytic Engines

By 1822 Babbage had developed a pilot model of his difference engine. The device performed so well that the government provided funding for a larger, more expensive, version to be constructed.

While the Difference Engine may have become a success, it was in its own right already an ambitious undertaking. Babbage, however, had an even grander vision. He wanted to build a calculating machine that could take its own calculations and feed them back to itself, and calculate further. He referred to it as “. . . *moving forward by biting its own tail*”.

From those ambitions the Analytic Engine was conceived. It was an automated device that could be programmed in advance, having a large number memory and was able to print its own tables. The printing was another of Babbage’s additions in order to eliminate human error from the process of calculation and tabulation.

Babbage produced over 200 drawings detailing the approximately 50,000 parts that would be needed to make the Analytic Engine. These drawings were the finest of his time, but all the parts were non-standard sizes and shapes. In addition, they also had tolerances that the technology of his time would be hard pressed to achieve.

Even though the Analytic Engine was never finished, the funds provided by the government were more than compensated for by Babbage’s endeavours. The advances in manufacturing processes, machines and production methods that came about as a peripheral, bolstered efficiency and productivity. The first steps toward industrial engineering.

Beyond even the economic yield of their investment, the analytic engine was to assure England’s freedom. The Automatic Sequence Controlled Calculator (ASCC), developed by Professor Aiken, would run around the clock during World War 2. It solved complex problems for the American military, enabling them to aid England against the Nazi’s.

The Difference Engine worked on the theory that a mathematical equation could be represented by a table of differences. Take a linear equation such as

$$y = 3 \times x$$

as an example. Every integer of the series will, as shown in Table 2.1, differ

from the previous by a constant value of 3.

Table 2.1: Differnce Engine Principle

x	y	Difference
1	3	
2	6	3
3	9	3
4	12	3
5	15	3

For a 2nd degree equation this no longer holds true, but the difference of the differences is still a constant value. This yields the result of Table 2.2, for the equation

$$y = x^2.$$

Table 2.2: Differnce Engine Principle

x	y	Diff1	Diff2
1	1		
2	4	3	
3	9	5	2
4	16	7	2
5	25	9	2

In this way numerous different mathematical systems may be constructed by using the sequence of cumulative differences through this progression. Since it is such a simple principle, Babbage wished to incorporate it in a machine, the construction of which was started in 1821.

The Difference Engine was to perform these operations and tabulate polynomial functions. Being revised often, it consisted of 28,000 parts by 1830, and was to be able to calculate with 16 digits and 6 orders. In 1833, however, construction halted after Babbage had a falling out with his head engineer. The machine was never built and the existing 12,000 pieces where smelted

down. At this point the English government had already spent £17,500 on the endeavour, roughly the cost of 20 new steam engines or 2 war ships [8].

The Analytic Engine was conceived in 1834 and bears the closest resemblance to what we today recognise as a computer. It was programmed using punch cards, with separate areas for number storage, iterative results and processing. It was also capable of several low level programming functions, such as looping, latching and iteration.

Finally came the Difference Engine Nr 2. Its design was completed in 1849, having started in 1847. This was to be the big one, being more efficient than the first Difference Engine and requiring only a third of the parts. It utilised the same printing device as the Analytic Engine, which allowed page printing or the printing of a template.

Babbage today

The first time that the Difference Engine Nr 2 that Babbage envisioned was built in totality was in 2002, 153 years after its inception. It consisted of 8000 parts and weighted in at 5 tons. An identical engine, shown in Figure 2.6, is on display at the computer history museum in California since March 2008 [8].

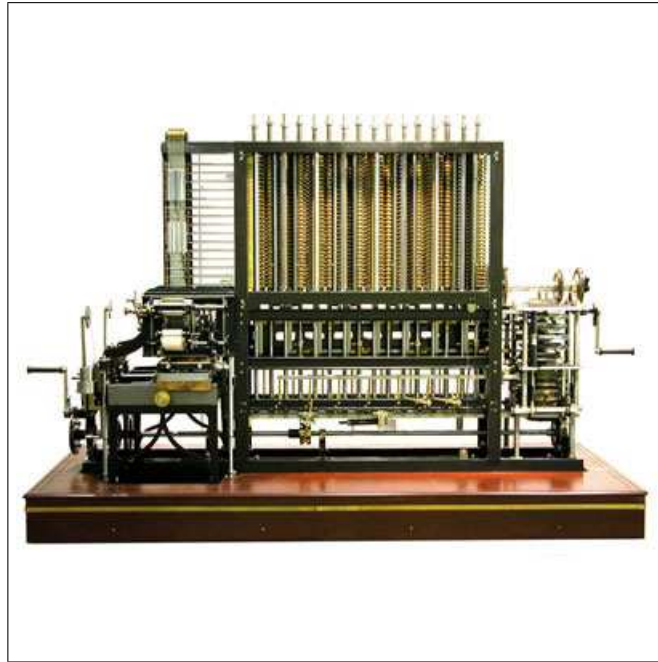


Figure 2.6: Difference Engine Nr 2 replica at the computer history museum [8]

Since its replication, hobbyists have also had a go at Babbage's work. Some have built his machines out of washing pegs, Mechano or even Lego. Every styling has its individual challenges, but most of these can be solved by looking at Babbage's own earlier work and designs. In Figure 2.7 we can see one such rendition.

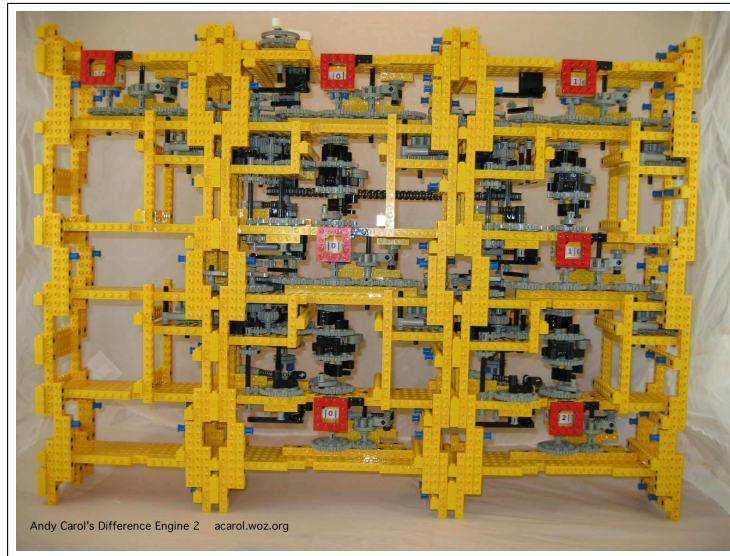


Figure 2.7: Lego recreation of the Difference engine Nr 2 [9]

But aside from replicas and toys, mechanical computing has resurfaced in the branch of nanotechnology. This time, instead of weighing several tons the components are at a scale of millionths of a millimeter. This new wave of interest was sparked by the United States Defense Advanced Research Projects Agency (DARPA) who are in search of computers that are durable enough to survive harsh environments that would destroy conventional semiconductors [10].

From initial research done to achieve this aim, it has been shown that mechanical computers will be more energy efficient, produce less heat, have greater resistance to energy spikes and last longer in harsh environments. Several applications in the industrial and medical sectors are also evident.

While mechanical switches offer such benefits, research is still ongoing due to the slow progress in the field. It has only recently been shown that mechanical parts can be manufactured, is able to move and be actuated, and at a scale of current nanoscale silicon transistors. Another problem is the diverse solutions offered by nanotechnology, each being a unique case with its own governing principals. This makes simulation and production a costly and time consuming endeavour.

A type of mechanical switch that has received most of the attention is the nanotube cantilever switch. Since it has been shown that a suspended nan-

otube can be deflected using electrostatic forces, several institutions have been researching this particular device. Predominantly, they have been attempting to develop it into a 3 terminal relay.

Although mechanical switches may never reach the speeds of solid state silicon based technologies, being restricted to 2GHz, research is already going into hybrid circuits. If the mechanical switches are used for latching and memory, the calculations can still be done with CMOS circuits, having a layer of mechanical switches on top of the silicon transistors.

2.2 Nanotechnology and NEMS

In 1871, a Scottish Physicist named James Clerk Maxwell proposed a thought experiment. In an attempt to disprove the second law of thermodynamics, picture a infinitesimal room with a miniscule entity inside this room. The experiment stated that this entity would sort molecules coming through the room into high energy and low energy groups. The experiment failed to disprove the law, but the thought was born.

Nearly a century later the renowned physicist, Richard Feynman, while at a social dinner, broached the topic. He said that no physical law prevented the building of machinery on the atomic scale. To put it eloquently, there is plenty of room at the bottom. Fifteen years following his statement, the first nanoscale components were produced.

Nanotechnology is a buzz word that has been tossed around for the last decade following the discovery, by scientists, statesmen and Hollywood producers. The definition thrown around by most people amounts to nanotechnology being the field of applied science and technology which entails the control of matter on the molecular scale and the fabrication of devices in that size range. While true, it says just enough to propagate uncertainty as to what nanotechnology really is.

Nanoscience is the study of fundamental principals of molecules and structures in the size range, or having a critical dimension, between 1 and 100 nanometres, where unique phenomena allow for novel applications [11]. Nanotechnology is the application of these nanostructures into useful nanoscale devices.

To understand and apply nanotechnology, researchers need to have an understanding of biology, chemistry, physics, engineering and computer science. Depending on the specific application, many other fields may also be necessary, such as protein engineering, surface physics and material science [1].

This being said, it doesn't seem to explain the large amount of attention and publicity that nanotechnology has received. To appreciate this, one needs to understand where nanotechnology stands. It has been said that the scale is in the nanometre scale, which while being small, is a unique kind of small.

A nanometre is one millionth of a millimeter, or one billionth of a metre. A human hair is 50,000nm across, a bacterial cell measures a few hundred

nm across and the latest microchips produced by Intel uses transistors at 35nm size. The smallest things visible to the human eye is 10,000nm across [12]. 1nm can accommodate 10 hydrogen atoms or 3 uranium atoms. An approximation of the differences in scale can be seen in Figure 2.8, where the basic nanostructures are shown in comparison to conventional small things and then to every day items.

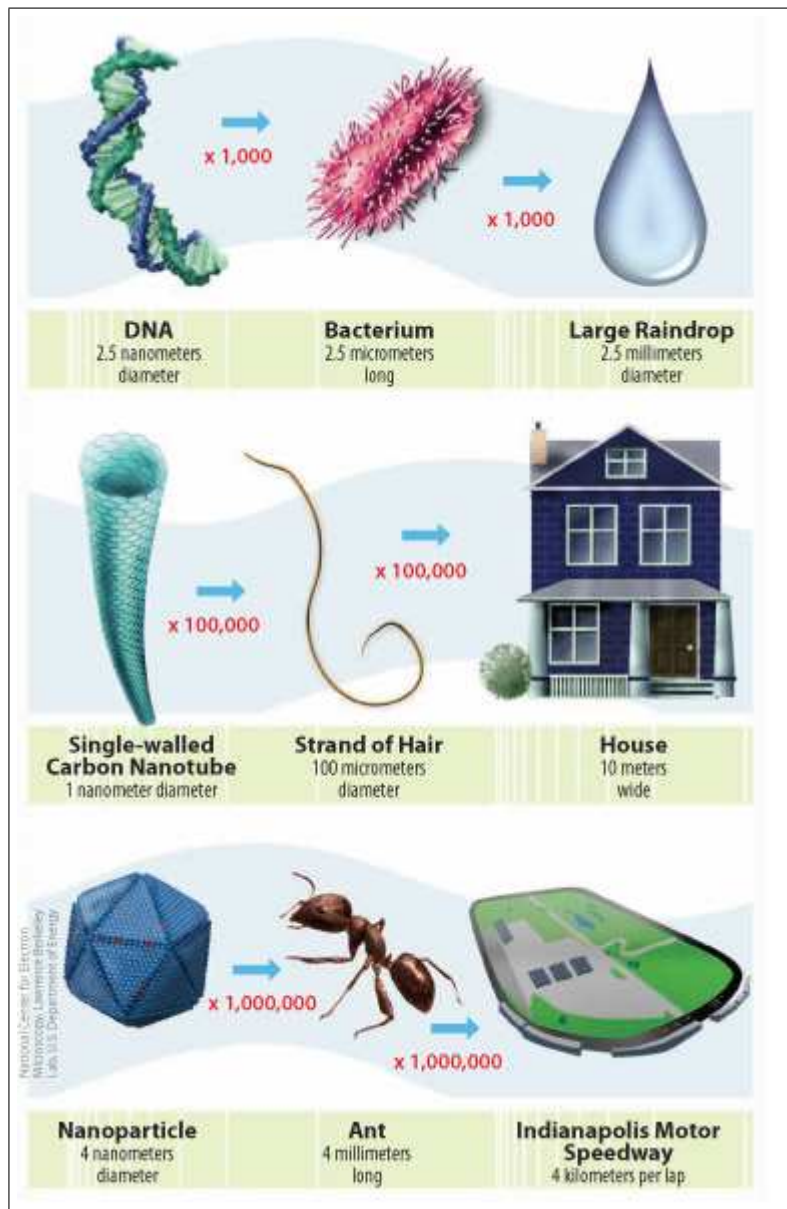


Figure 2.8: A visual relation of scales [11]

Still this does not explain the unique properties of this size range. Let us equate it with the forging of a Japanese katana. The starting material is iron and carbon, forming steel that is folded repeatedly, until it consists of near on a million layers. Now instead of plain hard and light steel, the blade is flexible, even stronger, and sharpens itself with each cut, a change in properties and behaviour by subdivision.

This is where the crux of the matter is exposed, the nanoscale is where the conventional everyday properties of materials like conductivity, hardness or melting point meet the more exotic properties of the atomic and molecular world such as wave-particle duality and quantum effects [12]. At nanoscale a wire will not obey Ohm's Law, due to the small scale. The transmission line is only a few atoms wide, so the electrons are not able to flow as easily, or in some extreme cases need to travel single file.

To emphasise this point let us take a bar of gold with which everyone is familiar as an example. The yellow metallic lustre, electric and thermal properties are well documented and used in several capacities. Now, if one were to cut the bar along each axis, there will be eight golden rhomboids with the same properties as the original. Cut it the same way again and again, eventually the dimensions sink into the micrometre range and still the properties are the same. Continue cutting again, using specialised equipment, we reach the nanometre dimensions and suddenly, the properties change. Colour alone may change to orange, purple, red or greenish, depending on the actual size of the gold nanoparticles. This was known by alchemists during the middle ages, and was used to colour the stained glass windows in churches [13].

Seeing the Infinitesimal

In order to investigate, manufacture and then test nanostructures one must first be able to see and examine structures of that size. Barely being able to see things of 10,000nm size with the naked eye, a strong microscope will allow the spotting of things at 5nm. But seeing nanostructures as specks is not conducive to scientific experimentation, so ways needed to be developed to improve imaging techniques.

Some of the methods developed in this capacity are scanning microscopy, spectroscopy, electrochemistry and electron microscopy.

Scanning Probe Instruments

One of the first methods to be developed, was the scanning probe devices. Intuitive to us as tactile creatures, this method uses a probe or tip that is slid along a surface. Imagine it as your finger dragged across a surface, the feel of the material already provides information, such as whether it is steel, wood, velvet or tar. Furthermore, the process of moving your finger along the surface also gives an impression of the features and topography of the surface.

Fundamental to this method is that the tip be on the same scale as the surface that is to be scanned, since any profile details smaller than the tip will not be registered by the probe. Therefore it is common for a scanning probe instrument's tip to be honed down to the size of a single atom where it is to scan the target.

In this family the main devices for microscopy are the Atomic Force Microscope (AFM), the Scanning Tunnelling Microscope (STM) and the Magnetic Force Microscope (MFM) [12].

The AFM uses electronics to measure the force exerted on the probe tip as it moves over the surface. There are two methods or modes that can be used for this measurement, contact or non-contact mode. The contact mode procedure uses the same method as your finger, by pulling along the surface with physical contact. The non-contact mode uses the attractive force between the tip and the surface at close proximity. In Figure 2.9 the measurement and interpretation cycle of the AFM can be seen.

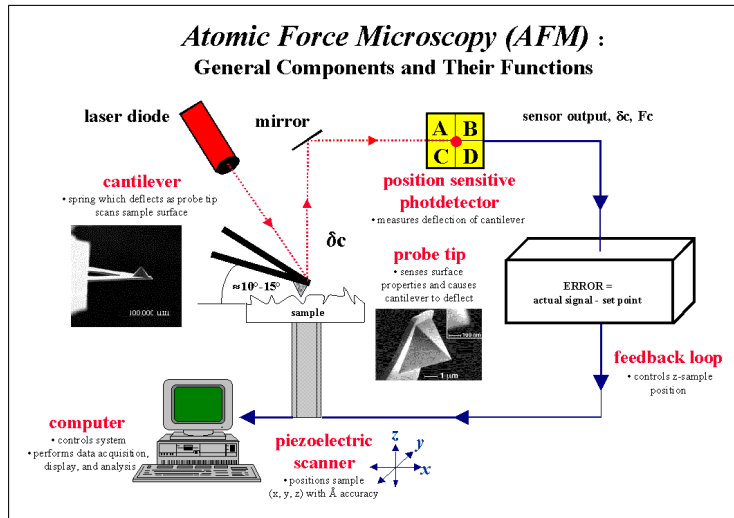


Figure 2.9: A visual representation of AFM theory [14]

The STM, as depicted in Figure 2.10, uses a conductive base and platinum tip to pass an electrical current through the sample surface and measure it. Depending on the setup of the system, the STM can either measure the sample geometry, or measure the local electrical conductive properties. The STM was the first of the scanning probe techniques to be developed, earning Gerd Binnig and Heinrich Rohrer the 1986 Nobel Prize.

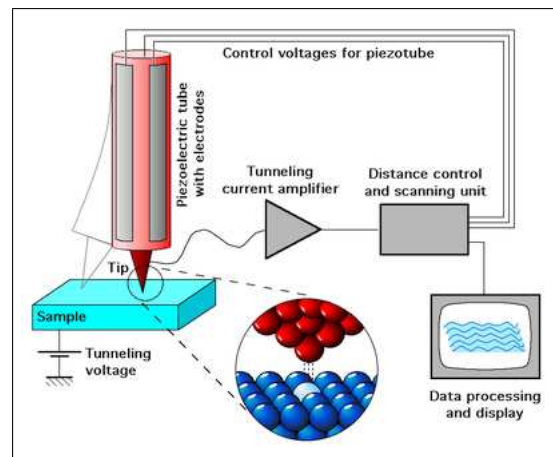


Figure 2.10: A visual representation of STM theory [15]

In the MFM the scanning tip is magnetic. As it traverses the surface it senses the local magnetic structure. It works in a similar way to the reading head on a hard disk drive or audio cassette player.

With most scanning probe instruments computer enhancement is used to produce usable images, compiling the linear sets of height, force, current or field strength measurements into a total picture. Software enhancement is occasionally used to reduce noise and distortion on the image.

Spectroscopy

Spectroscopy refers to shining a light of a specific wavelength on a sample and observing the absorption, scattering or other properties of the material under those conditions.

Spectroscopy is the oldest technique, having many applications and forms, offering a variety of insights. Some of these are familiar, like X-rays, where high energy radiation is passed through an object to see how the radiation is scattered by the heavy nuclei of substances like steel or bone. Magnetic Resonance Imaging (MRI) is another form of spectroscopy.

The difficulty with spectroscopy is that it can only be used to study structures with sizes larger than the wavelength of light being used. Since the wavelengths of visible light ranges between 400 and 900 nanometres, this doesn't help for looking at single nanostructures, but is handy for studying them in groups [12].

Electrochemistry

Electrochemistry entails the changes in chemical processes by the application of an electric current and the generation of electrical currents by chemical reactions. A common example is voltaic cells, where energy is produced by a chemical reaction. The inverse process can be used in electroplating, whereby a metal is made to deposit on an electrically charged surface.

While the method of electrochemistry is widely used to manufacture nano-devices, it can also be used to analyse them. Using electrochemistry, the nature of surface atoms can be measured from the emitted current. More advanced techniques can be used in conjunction with other microscopy methods to glean further details about a nanostructure [12].

Electron Microscopy

The first technique that was used to observe nanostructures was electron microscopy, even before scanning probe microscopy. Instead of using light, like spectroscopy, electron microscopy uses electrons to examine the structure and behaviour of the devices.

While there are several forms of electron microscopy, they all function on the principal of accelerating electrons and passing them through the sample. As the electrons encounter nuclei and other electrons, they scatter and by collecting these scattered electrons, an image can be constructed. This is done by predicting where the particles were that scattered the collected electrons.

Two examples of these techniques, seen in Figure 2.11, are Scanning Electron Microscopy (SEM) and Transmission Electron Microscopy (TEM). A TEM image can have resolutions sufficient to see individual atoms, but unfortunately samples must be stained before they can be scanned. Another drawback is that it cannot measure forces or electric fields, but still, it is the best method for acquiring physical images of nanostructures for analysis and interpretation [12].

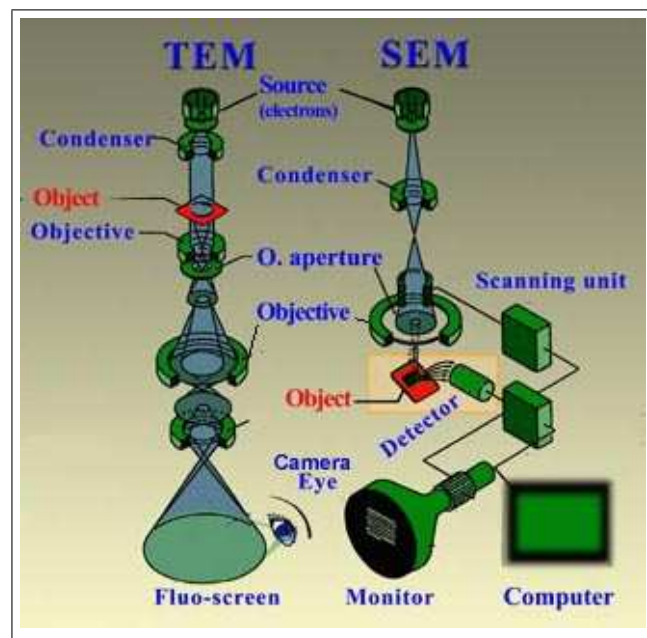


Figure 2.11: Representation of TEM and SEM microscopy [16]

Simulating Nanodevices

Product and device development used to be exceedingly time and cost intensive, due to the necessity of prototypes and physical testing. Thanks to breakthroughs in computational power and the sciences, most systems can be mathematically modelled and run to obtain results in a faster, cheaper manner. While simulation does not eradicate the necessity of physical testing, it does speed up the production time, provide comparable results and lessen the number of prototypes needed considerably.

One of the first implementations of computational simulation was during the Second World War, involving the behaviour of neutrons. To set up and run the experiment over and over again with the possibility of collisions was arduous, time consuming and very expensive. Since the basic principals of the reactions were known, mathematicians where consulted and a model drawn up. The system that was set up was able to predict the outcome of the neutron reactions with remarkable accuracy. After the war many new technologies were being developed or adapted, providing ample opportunity for the expansion of simulation.

However in order to simulate the system the basic principles behind the processes incumbent on that system need to be understood. For something like a bending beam, classical mechanical theory has an empirical solution. So, given the material, physical dimensions and applied load, the curve of the beam, deflection along its length and even failure can be predicted.

With nanotechnology, however, the interaction between atoms in smaller devices moves the ball from the mechanical theory court into the domain of quantum theory, the science of all things infinitesimal. Having large, by comparison, devices with atomic scale components mean that the governing equations need to contain elements of both mechanical and quantum theory. Since the two theories tend to be contradictory [17], compromises are inevitable.

Nanotechnology makes design a crucial part of the development process, since, with the right knowledge, the same goal can be achieved in any number of ways, limited only by the imagination. In this world where the question has changed from "*What can we do?*" to "*What do we want to do?*", simulation has become important for the evaluation of these products.

The many particle system problems of nanotechnology have found four types of numerical solutions, namely quantum theoretical calculation (or *ab*

initio), molecular mechanics, Monte Carlo and molecular dynamics.

The *ab initio* techniques commonly use self-consistent field methods, linear combinations of atomic orbitals or the density functional method [1]. These techniques all have to do with molecule to molecule gravity and potentials in respect to all other particles in the system. If one takes a look at the Hamiltonian, an operator pertaining to the total energy of a system (2.1), of a system containing N particles of masses m_i we see the possible problems.

$$\hat{H} = \sum \left[-\frac{\hbar^2}{2m_i} \nabla_i^2 + V_i(r_i) \right] + \sum V_{ik}(r_i, r_k) \quad (2.1)$$

$$V_{ik}(r_i, r_k) = \frac{Z_i Z_k e^2}{(r_k - r_i)} \quad (2.2)$$

A system's complexity will determine the length of the simulation, because an increase in particles results in a exponential increase in calculations. In a simple 100 argon atom system, a summation of 10^{11400} volume elements would be required to reach a solution [1].

Due to this exponential increase in calculations, *ab initio* techniques revolve around simplifications and assumptions made for individual cases, in order to minimise the computational intensity of its equations.

Molecular mechanics uses the approximation of chemistry models where a molecule is simulated using balls and sticks. The balls are atoms and the bonds between them is represented by the sticks connecting them. The aim of this method is to find stable configurations for the system out of its potential energy, in other words finding the minimum energy considering the bond tension, bending, torsion, Van der Waal's and Coulomb interactions [18].

For this method to work effectively the initial conditions need to be fairly close to equilibrium for a convergent answer. An improvement on this system is the molecular dynamics method that uses similar approximations, but solves for the system using Newton's equations of motion. This allows the change in the system to be modelled over discrete time steps where the total information is available [1].

The molecular mechanics and mechanics methods are both mechanical models however, and as such cannot include the effects of quantum interactions in the system. Systems modelled using these methods must be approached with an understanding of the quantum effects on the system, keeping in mind

how they may cause differences in the result.

Finally, there is the Monte Carlo method that uses sampled data from the system and time steps statistically determined by a Boltzmann distribution. The Monte Carlo method evaluates the system with various random values and is particularly useful for systems that are nonlinear, complex or have coupled variable parameters.

Each of these methods have their own strengths and limitations, depending on the assumptions made and computational methods used. Here the best technique becomes the one whose assumptions are nearest to the implemented system. The mechanical models do not account for quantum effects, causing limited precision and validity. However, they are able to handle large systems better. The quantum theoretical method is highly accurate, but becomes laborious for larger systems. The Monte Carlo method needs to be tailored for each configuration with respect to the time steps used, and the data required can be hard to obtain for the simulation [1].

Manufacturing of NEMS

Many breakthroughs have been made at a rapid rate over the last few years, but they have yet to make the transition into technology. This can be attributed to hindrances in the manufacturing of nanodevices. For example, while shrinking dimensions may hold the answer to memory requirements, this cannot, however, be implemented without a way to connect the individual bits, a process that would require the connection of wire billions of nanodevices.

Most research is focused on manufacturing and manipulating a few, to several hundred particles or molecules into the required setup. In order to commercialise the technology, the aim changes to being able to replicate the configurations and devices into large production volume synthesis techniques, while having a robust and reliable process. After producing the devices, ways must be found to incorporate them in microstructures, larger systems and then a finished product [13].

There are two main approaches to the fabrication of nanostructures and devices. The first is the Top-Down approach, which uses larger machines to form smaller devices similar to cutting a structure from a larger chunk of material. The second is the Bottom-Up approach, where the device is put together from smaller parts, like a house is built of bricks.

The solution for commercial fabrication is believed to be a combination of these two approaches, cutting out of the main structure, adding in the more complicated devices, and then grow them together.

Nanoscale Lithography

Lithography comes from the Greek word *lithos*, meaning stone and *graphein* meaning to write, referring to the process of inking a stone and transferring the image to paper.

This later evolved into photolithography, a process by which a mask on glass is transferred to thin photosensitive films by means of a Ultraviolet (UV) light. This process has little tolerance for non-planar topography, hence being an exclusively two-dimensional process [19].

The photolithographic process will be explained using an oxidised silicon wafer and negative photoresist as an example. See Figure 2.12 for the step by step guide. After cleansing the silicon wafer with acetone, it is coated with negative photoresist and baked (B). The sample is placed below a piece

of glass with the structure to be transferred, blanked out. UV light is then shone through this mask onto the photoresist to harden the exposed sections (C). The sample is then immersed in a developing chemical to remove the soft photoresist (D). The sample is then immersed in a chemical capable of etching the silicon dioxide (E), followed by an immersion in a chemical that will remove the remaining photoresist (F) [19].

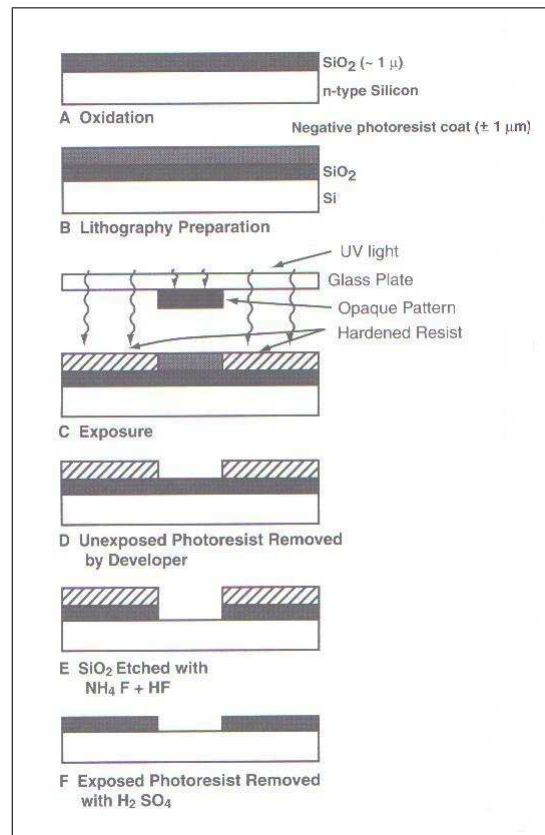


Figure 2.12: The photolithography process [19]

Some variations should be mentioned at this point. In the case of positive photoresist, the exposed area is softened and removed from the sample by development. A comparison of the effects of positive and negative photoresist can be seen in Figure 2.13. Instead of etching away at the substrate, material can be added onto the developed photoresist. When the photoresist is then removed, it takes the material above it away, leaving additional material in the patterned form behind.

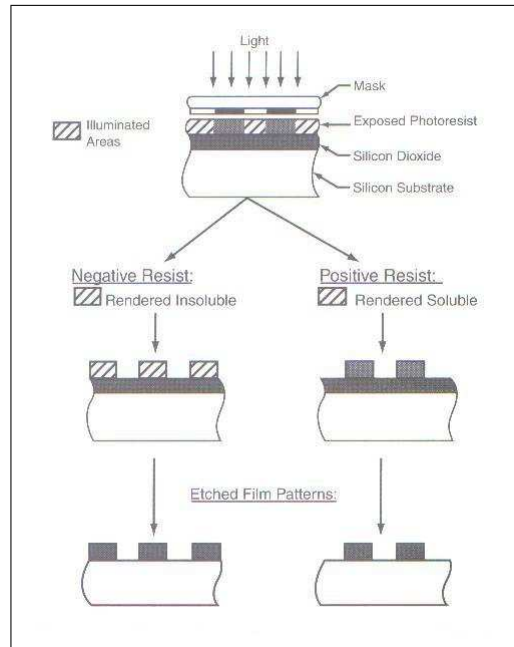


Figure 2.13: The effects of positive and negative photoresist [19]

As the dimensions of a structure shrink, however, the chemicals needed to make the film and the method of developing the resist has to adapt. The resist, exposure and etching techniques change, but the principle remains the same. A few of the techniques developed to overcome the scale barrier are now discuss.

Dip Pen Nanolithography

This is a rather direct way to put structures onto a substrate by writing on it, as one would write with ink or in wax. In both cases a pen is needed, fine enough to make nanoscale markings, which an AFM tip is ideal for.

In the first instance, a reservoir of atoms or molecules is kept on the probe, and as the tip moves, these particles are manipulated down the tip and onto the surface, as in Figure 2.14. Where the tip thus moves, the lines and patterns are left behind, like an old fashioned dip pen, hence the name.

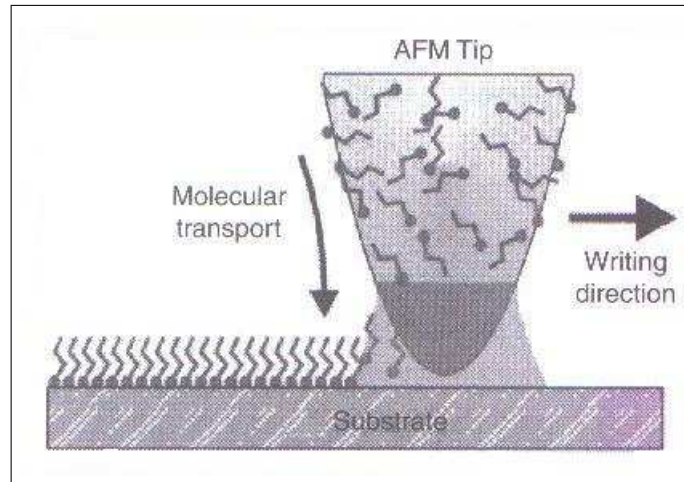


Figure 2.14: Dip pen nanolithography setup [13]

In the second instance, the sample is coated with photoresist beforehand and the AFM tip is used to remove the pattern. Alternatively, the sample may be coated with the desired material and the excess scratched away to reveal the pattern.

Of this method's many advantages, two should be highlighted. Most importantly, nearly anything can be used as nano-ink and almost any surface can be written on. The other great advantage is that detailed and complex patterns can be created since an AFM tip is easy to control and manipulate. The drawback of this method, however, is that it is slow and not conducive to mass production [12].

E-Beam Lithography

As was mentioned before, the large wavelengths of visible light are not able to produce the small features required for nanodevices. A solution might be to use smaller wavelengths of light, but this has the side-effect of introducing large quantities of energy, that may harm the surface and structure that is being worked on.

So instead, like with spectroscopy and electron microscopy, light is replaced with electrons. This electron beam may be employed to etch away material at high power levels, or to cut away photoresist. It is also possible to push loose nanostructures around on the surface with the E-beam method.

Nanosphere Liftoff Lithography

In the early days of printing, the dot matrix method was used, where letters were made up of a series of ink dots. Similarly, working at nanoscale, material dots or spheres can be put down and used as a mask. At its most extreme, individual molecules can be used as the mask. In an array of spheres, where each sphere is surrounded by 6 others, the deposition of material will put triangular structures with concave sides onto the surface.

The benefits of this technique is that multiple layers can be put down sequentially. There are a variety of materials that can be used as the mask and deposition material alike. This method is also an exclusively linear method, building upwards without the need for etching, and for commercial or high definition application, millions of the triangular dots can be made simultaneously [12].

Self-Assembly

Self-assembly deals with the way things in nature come about under their own initiative. In nature nothing needs to be built, they form and grow on their own. Most other fabrication techniques require a lot of time, effort and energy to produce a result, and researchers began to wonder if they might not be able to tap into nature's secret for having things build themselves.

Many disciplines have used this concept, and each has its own description of what self-assembly means. Taking a general view of this field, one can say that self-assembly pertains to the spontaneous formation of organised structures through a stochastic process that involves pre-existing components, is reversible and can be controlled by proper design of the components, the environment and the driving force [20].

To help picture this concept, think of a memory alloy like nitinol wire. If the wire is shaped into a structure, for simplicity say a square, and heated, it sets into this form for high energy states. Once cooled the wire can be straightened to its original shape, however, now when it is heated it will return to the square shape that it was formed to during the heating phase.

A common method of employing self-assembly would be to introduce a unique atom or molecule to an existing nanostructure. What makes this particle unique is that, in combination with the nanostructure, they attempt to move to a lower state of energy, changing position and forming bonds [12].

Large structures can be formed in this way, without the attention and consistent input required by some other methods.

The advent of nanotechnology has given self-assembly a big push to the forefront, since nanodevices of only several thousand atoms are highly reliant on the position of some of these particles. Now the addition of another atom or molecule can have a large effect on the overall structure, or functionality of such a device.

In Figure 2.15 an example of current self-assembly can be seen. This is an endeavour by Massachusetts Institute of Technology (MIT) to make easily assembled nano-motors, capacitors and memory elements. This technique is referred to as nano-origami, moving planes relative to one another by enabling the folds [21].

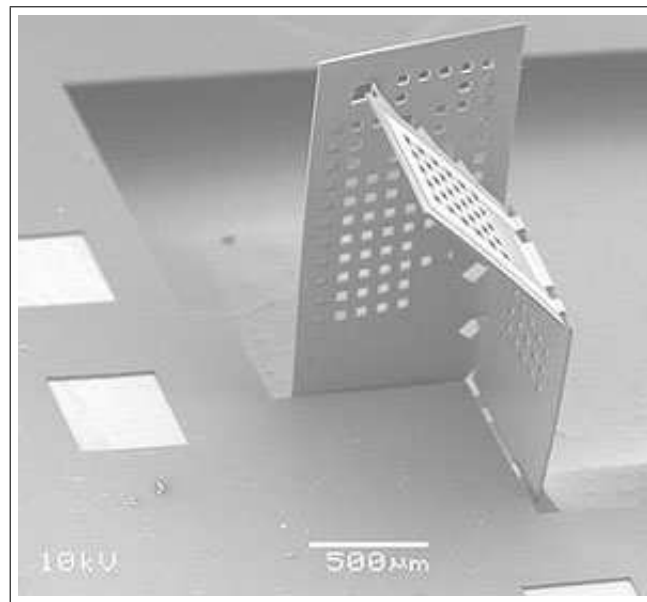


Figure 2.15: Self assembled polymer sheet [21]

At the Information Sciences Institute a similar project has been undertaken to improve drug delivery systems. A package is self assembled from polysilicon to carry the drug into the body and transport it to the relevant areas. Figure 2.16 shows the capsule before being closed and Figure 2.17 shows the complete product.

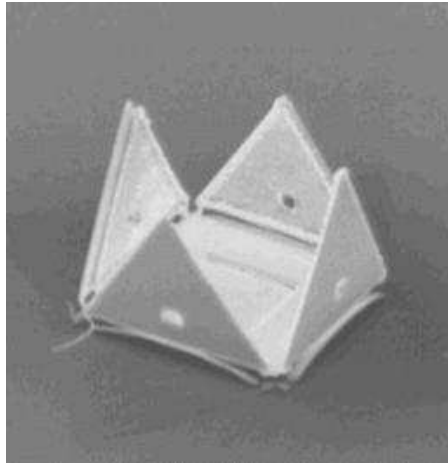


Figure 2.16: Magnetically folded blank

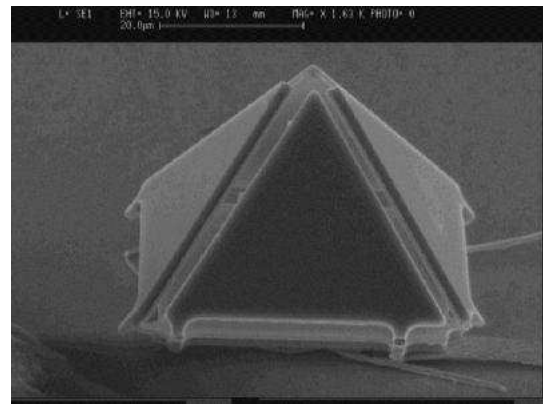


Figure 2.17: Drug capsule after completion

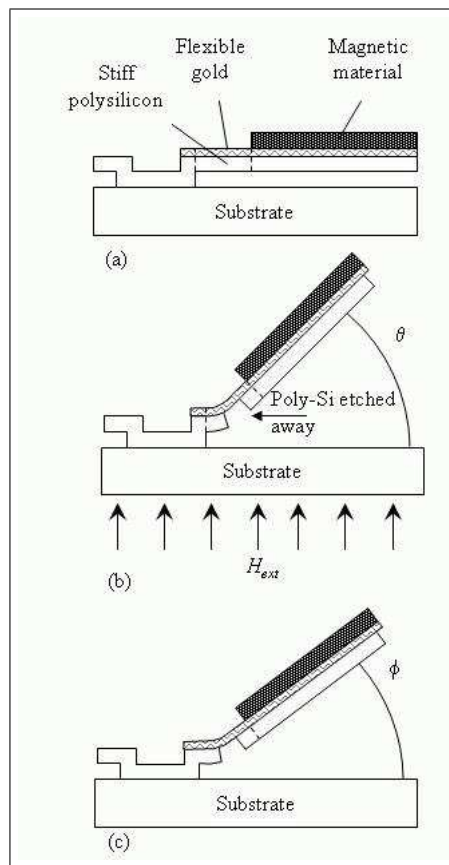


Figure 2.18: Nano-origami procedure [22]

One way of manufacturing nano-origami structures can be seen in Figure 2.18. First a silicon structure is prepared and a layer of gold deposited on it. A magnetic component is then deposited on the area that is to be lifted, followed by the etching away of the silicon at the fold lines. Once a magnetic field is applied across the structure, the magnetic section moves away, bending at the sections where only the flexible gold is now present for reinforcement.

Aqueous Solution Growth

Many children at some point will have grown sugar or copper sulfate crystals in their mother's kitchen, with saturated solutions. It is a fun and harmless entertainment that introduces us to the beginnings of chemistry. In recent years this aqueous solution growth has cropped up in nanotechnology, since it allows for the controlled growth of materials from a seed molecule.

As research into this branch expanded, it was found that more complex features could be attained by this method, like nanotubes, nanowires, nanoribbons and structured crystal configurations. Processes have even been developed to produce thin films [23] with specified particle orientation.

Laser Techniques

Lasers can either be used to deposit material by means of Pulse Laser Deposition (PLD), or to remove material using Pulse Laser Etching (PLE).

PLE is usually limited to removing material at the edges of a structure, since the beam width usually is in the micron range. With the inclusion of glass micro-beads to focus the beam further, narrower beams can be achieved and profile work may be attempted. It should be noted that with longer pulse lengths, more heat is dissipated in the substrate, which may be undesirable.

PLD uses the laser to blast a material target in a vacuum in order to liberate atoms from its solid state. These atoms that have been rendered to a vapour by the plasma plume created by the laser, fall onto the waiting sample, either patterned or for total surface coverage. This method has the benefit of being fast, robust and cost effective.

Thermal Deposition

Thermal deposition is accomplished in a vacuum using a heating element for the material to be deposited and a support for the substrate. The heating

element can be a wire or crucible made from tungsten, stainless steel, molybdenum or inconel, depending on the material that is to be deposited.

The system is placed under vacuum and the deposition material is heated to its sublimation temperature, while being shielded from the sample by a screen. When the sublimation temperature is reached, the screen is removed and the sublimated material steadily deposits on the substrate.

While this process takes a long time, it yields high quality films, and the system can be modified in a variety of ways to make for a versatile and robust deposition method.

Sputter Deposition

Similar to the PLD technique, material is liberated from a target to be deposited on the substrate. The difference is that the plasma is not produced by a laser, but rather by high current application in a gas environment (usually argon) and the vapour isn't allowed to float down on its own, instead being propelled towards the substrate due to an applied electric field.

Like PLD this method is part of the physical vapour deposition family, hence the similarity. Also the film is of similar quality, but the deposition takes considerably longer, especially if the substrate needs to be heated.

Testing Nanodevices

When testing nanodevices, instead just using standard practice and equipment for the experimental test plan, the additional factor of the size range must also be considered. Actually, the size factor needs to be considered first. In order to take the required measurements, and follow test plan procedures, the test equipment has to be chosen to accommodate the small outputs that might be expected.

First, in order to take measurements, the weight, lengths, voltages, currents and orientations need to be accessible. With nanodevices this is impossible via normal means. Depending on the lengths and angles that are to be measured, an AFM, STM or SEM can be used if the structure has been manufactured in such a way as to make these dimensions accessible for these microscopy techniques. In order to access the voltage or current information, contacts need to be provided, since direct contact to the device can easily be damaging, if not all out destructive. To measure mass, the device must be manufactured in such a manner that it can be transferred to a scale where it can be isolated from material that isn't part of the device.

Here it can be seen that, instead of the experiments starting after production, the methodology and approach must already be considered during the design phase. This will allow the device to accommodate the test procedures, making it easier, faster and not an arduous task.

Now the test plan can be started. Having chosen the variables to be measured, the variables that influence them need to be determined and classified as independent or dependent variables. An independent variable can be changed independently of other variables, a dependent variable cannot be changed independently of the other variables [24]. Independent variables will have no effect on the overall experiment. The dependant variables, however, need to be measured and controlled if possible. Variables that influence the measured variable, but cannot be controlled, are called extraneous variables.

The experiment should follow a series of repetitions to even out the values in the individual device, and a series of replications to eliminate the effect of the test equipment on the results. Using some probability theory, data from the replications and the repetitions in each of the said replications can be condensed into a set of values that are fairly independent of the test equipment and individual devices.

Now we consider the effect of a nanoscale device on the test equipment. The values to be measured may be very small. Currents in the pico-amperes and masses in the micro-grams are not unusual. Equipment suited for these kinds of measurements must thus be used. The range, resolution and accuracy of the equipment must also be taken into account [24]. Manufacturers usually include a section in the manual where they state the possible linearity, hysteresis, sensitivity and zero shift errors that may be encountered while using their equipment.

2.3 To summarise

The pioneers of each of the mentioned fields were legends of their time and the fields that they opened for us have revolutionised the way things were done during their age. We must now try to combine these contributions in order to move even further along the path.

The discoveries of nanotechnology bring the scientific disciplines ever closer together, into a collusive whole. 2400 years after Aristotle formed the disciplines of science [25], we can reform them, with the same logic he taught us.

Using nanotechnology to miniaturise Babbage's engines would open up a new field of possibilities in what used to be impossible areas, producing tiny systems of near infinite complexity.

Yet in order to do so, the starting point is the small of the small. Manufacturing the components and producing mechanical switches in the nanoscale that will rival their solid state counterparts.

At a surprising rate, however, researchers have stepped up and are producing ever more ingenious and varied solutions to these first stumblings into nanomechanical switching. Much promise is being show in this field and followed up with a remarkable vigour.

Chapter 3

Mechanical Nanoswitches

A lot of effort has gone into researching alternatives to modern day silicon technology for switching purposes. The trouble is being able to go ever smaller, while remaining reliable and maintaining high levels of power.

3.1 Device overview

MEMS switches were lucrative as a replacement for conventional relays and solid state switches due to their size and speed advantages. Also, they do not suffer as much from on-resistance and parasitic capacitance [13].

NEMS promise to offer an increase in these benefits. Apart from the operational benefits, they increase the available avenues of implementation and application.

Switch activation is largely achieved using electrostatic and magnetic means. In this chapter several types of switches will be investigated, some using electrostatic switching, but predominantly alternative switching techniques will be sought, as led by current research or particularly promising avenues of research.

Since it is mechanical switches which are going to be researched, it should be remembered that part of the power going into the switch is being used to maintain contact in either the on- or off-state. This force is the remainder and differs from what is needed to close the switch. This small force is a major factor influencing the area and quality of the contact. Another issue is that this force cannot be made too large, because it may result in negative consequences, lastly and in the worst case, device failure.

3.2 Silver Sulfide Switches

A recent eureka moment led to the exploitation of the unique conductive properties of silver sulfide. While scanning a silver sulfide surface with a STM, the researchers discovered that little mounds of silver were forming on the surface of the sample [26]. Further study showed that the silver mounds were formed due to the proximity of the electrified platinum tip and grounded sample.

Silver sulfide (Ag_2S) is an ionic conductor, meaning that in its crystal lattice ions may assume many possible positions, allowing them to move around freely. More so, it exhibits these properties at room temperature. Another material that shares these properties is copper sulfide.

When one layer of silver sulfide is between two silver layers, as in Figure 3.1, and the silver electrodes are connected to a battery, the effect of this ionic conduction can be observed. At the positive electrode, Ag^+ ions are formed at the $\text{Ag}-\text{Ag}_2\text{S}$ interface, while at the negative electrode interface Ag^+ ions are reduced [26].

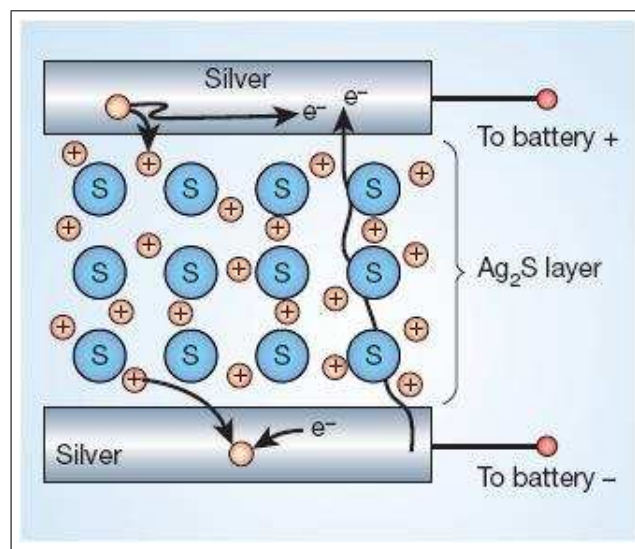


Figure 3.1: Silver sulfide as an ionic conductor [26]

This provided a material that could, at room temperature, conduct ions (allowing material transfer), conduct electrons (allowing current transfer) and actuated by a low voltage. A device was then developed that would use these properties to make a switch that grows its contact in a reversible manner.

While many switching mechanisms have been reported between STM tips and substrates in recent years, these required an STM to function, whereas the silver sulfide only needs a reversible power source and small contact area. With this in mind, Terabe *et al.* [27] were able to come up with a cunning solution. A layer of Ag_2S on top of a silver wire is in contact with a thick platinum wire through a 1nm thick silver layer.

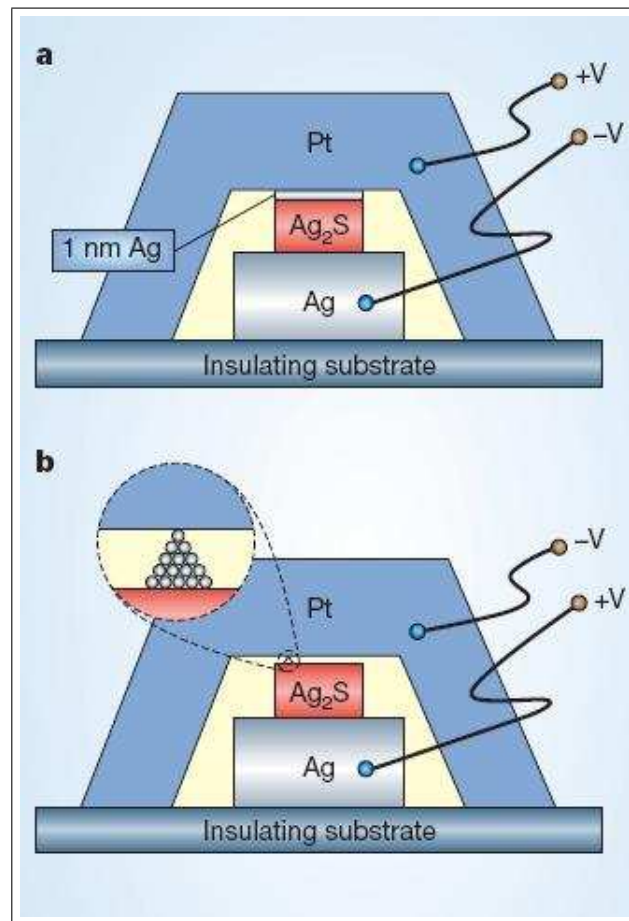


Figure 3.2: Silver sulfide switch model [26]

A voltage is then applied over the platinum and silver terminals. When current flows from the platinum to the silver, as in Figure 3.2a, Ag^+ ions are transported into the Ag_2S causing the silver layer to vanish, breaking contact and putting the device in the "off" state. When the current flows from the silver to the platinum contact, as in Figure 3.2b, localized connections form from the silver sulfide to platinum, as Ag^+ ions grow back out putting the

device into the "on" state. This process is reversible and very rapid, since only a few atoms are involved [26]. In Figure 3.3, the full switching process is depicted in a particle model.

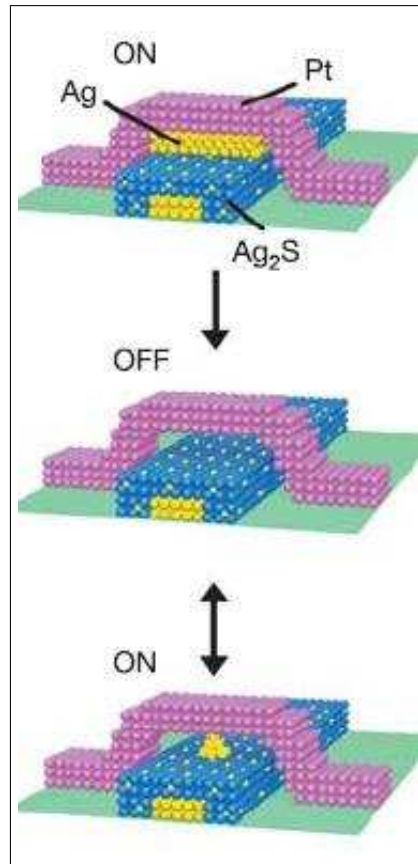


Figure 3.3: Silver sulfide reversible particle model [27]

Since a voltage higher than 100mV is required to change states, the state of a device can be read non-destructively at voltages below this. This makes memory, as well as switching applications, ideal for this type of device.

3.3 Photoswitches

Photons seem poised to take over from electrons as demand for high storage density and fast data-processing rates increase. As such, many approaches have been used to develop binary switches, memory and logic devices. Some of the promising materials in the field are zinc oxide nanotubes, polymer-coated carbon nanotubes, spiropyrans and doped polymethylmethacrylate (PMMA), although most of them exhibit low on/off ratios and high light intensity requirements. A high on/off ratio and low light intensity requirements will be critical for future optoelectronic devices [28].

Photonic devices using organic semiconductors and insulators are becoming increasingly popular, due to their advantages over their inorganic counterparts. Some of these are lower cost, flexibility and large area application [29].

Phototransistors have been developed to improve the sensitivity and noise values of simple photodiodes. Following their development, attempts have been made to incorporate organic semiconductors to improve the device functionality. One case study, using hexadecafluorophthalocyanine ($F_{16}CuPc$), showed particular promise in its stability and self organising properties.

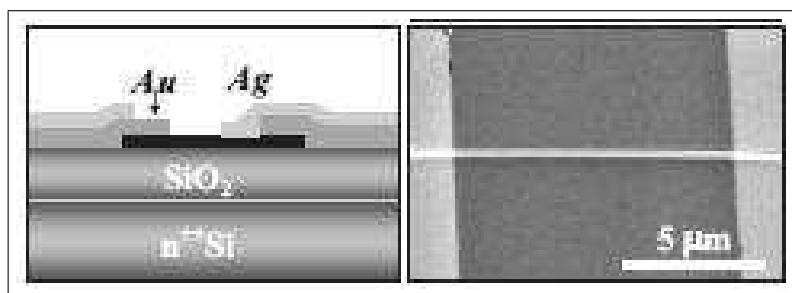


Figure 3.4: Schematic and topographic views of a phototransistor [29]

A single-crystalline ribbon of $F_{16}CuPc$ is used as the functional component, as shown in Figure 3.4. Under bombardment with light of a photonic energy equal or higher than the materials bandgap energy, charge carriers are liberated [29], which is depicted in Figure 3.5. In the absence of a gate electrode the device operates directly as a photoswitch. While the on/off ratio of the photoswitch, roughly 100Hz, is two to three orders of magnitude lower

than that of the phototransistor, it removes the addition of the gate electrode, which is a difficult task due to the nanoscale alignments required.

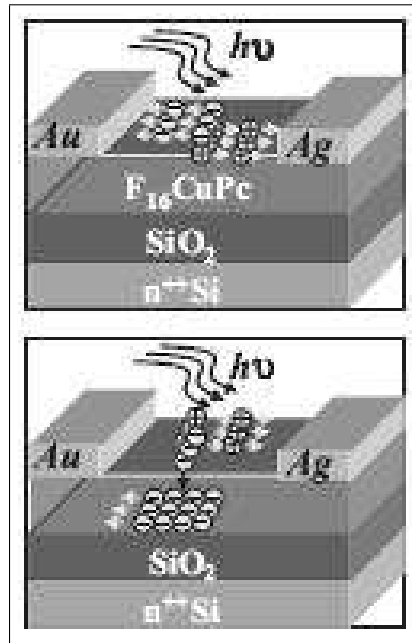


Figure 3.5: Model of a $F_{16}CuPc$ photoswitch [29]

In electrically bistable devices of the form metal/organic insulator/metal, as in Figure 3.6, the switching phenomenon is due to metal filament penetration through the organic insulator. Xinjun Xu *et al.* investigated the possibility of a photo response in these devices [28].

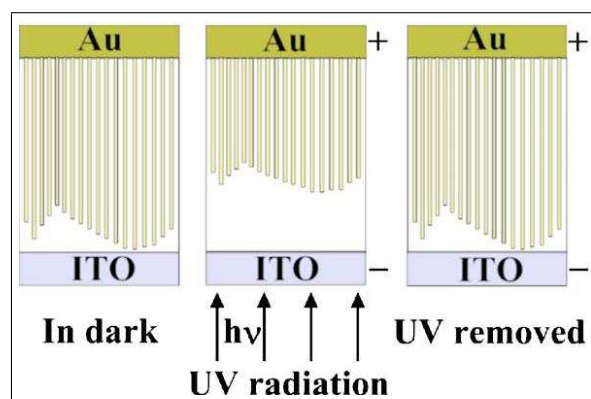


Figure 3.6: Functional model of the organic insulator photoswitch [28]

The initial device specifications were Indium Tin Oxide (ITO) coated glass used as the substrate and bottom contact, polystyrene (PS) as organic insulator and gold as the top metal contact. Three different material thicknesses were tested, as well as other organic insulators, most prominently PMMA. The top metal contact was also exchanged for aluminium during some tests.

The devices worked admirably. Below a threshold voltage determined by device geometry, the device switches reliably between the on and off states, once a calibration run is made. The calibration run consists of a prolonged UV exposure to push the metal filaments through the organic insulator.

The role of the radiation pressure, provided by the photons can be explained as follows. After activation, the metal filaments are formed in the organic insulator, some of which are then very close to the ITO. Due to the organic insulator being very thin, large currents caused by tunnelling occur when voltage is applied. This is then referred to as the on state. When the device is then exposed to UV radiation, the metal filaments are pushed back from the ITO causing greater distance to lessen the current flow. The device is now in the off state. When the UV radiation is then removed, filament stretching due to the electric field force brings the filaments closer to the ITO again, causing current recovery [28]. On/off ratios in the order of 10^6 were achieved.

Nanofibers have been undergoing a lot of research in the area of light generation and further applications, specifically on device light sources. This research has shown a myriad of applications for organic nanofibers, such as the already named light sources, detectors, sensors and also switches.

Once the fibers have been deposited on the substrate, the state of the host polymer can be altered from the transparent state (off) to a coloured/opaque state (on) using UV light. The reverse can be achieved using green light. Like the nano-ribbon photoswitches these polymer fiber switches also present a switching ratio of around 100Hz [30].

3.4 Carbon Nanotube Switches

The Carbon nanotube (CNTs) was the second fundamental nano building block to be discovered. The first was the buckminsterfullerene, or buckyball, which was discovered in 1985, six years before the carbon nanotube.

Since being able to look at, grow and manipulate them reliably, carbon nanotubes have formed the basis of many nanodevices. This is due to its well characterized chemical and physical structures, low mass and dimensions, exceptional directional stiffness and range of electrical properties [31]. Single Wall Nanotubes (SWNT's) have even shown changes in their electronic properties depending on its interaction with the environment [2].

Traditional methods of manufacturing carbon nanotubes are arc discharge, laser ablation, thermal synthesis and Plasma Enhanced Chemical Vapour Deposition (PECVD) [32], followed by a gleaning procedure to attain the nanotubes of appropriate chirality, size and length.

Due to the human tendencies towards following what they know, the first set of CNT nanoswitches resemble press switches, much like a telegraph tap switch. Figure 3.7 shows such a device. A nanotube is made to hang over the silicon dioxide substrate from a substrate silicon pillar, much like a single side supported cantilever. Two metal contacts are present under the nanotube and a layer of metal is deposited onto the pillar, to serve as a contact to the nanotube.

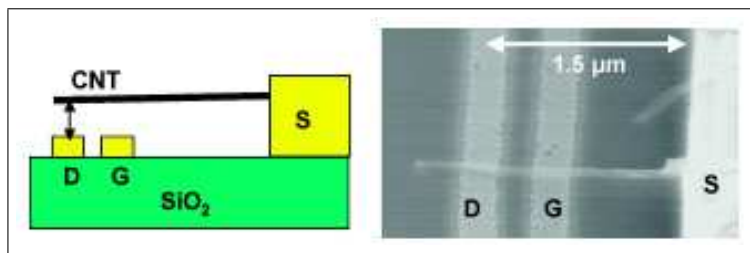


Figure 3.7: Representation and SEM image of a basic CNT switch [31]

The inner of the two substrate terminals is defined as the gate and the outer terminal is the drain, while the conducting tip of the pillar is the source. When charge is induced in the nanotube by applying a voltage to the gate electrode, the resulting capacitive force between them causes the nanotube to

bend. Once the nanotube has bent far enough, it contacts the drain, completing the electrical contact [31].

Another nanotube switch, using the same principle with a bit of a twist is the double supported cantilever design, as in Figure 3.8. The nanotube is placed over a trench like a bridge over a trench, at the bottom of which is a conductive material. This bottom region serves as a puller when a voltage is applied, since the induced charge in the nanotube and the resulting capacitive force forces the nanotube to deflect, to form a bend in the structure.

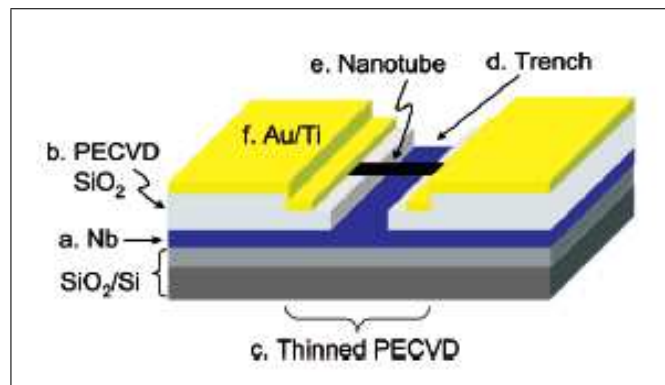


Figure 3.8: Model of the CNT trench switch [33]

This bending restricts electron tunnelling between the two sides of the trench through the nanotube. When the applied voltage is removed, the nanotube corrects itself and standard electron flow resumes. There are labs that have reported switching speeds of up to 1MHz using this technique.

The novel linear bearing nanoswitches also uses a CNT suspended over a trench, only this time the nanotube is severed by ramping the current till the nanotube breaks down, forming a gap in the bridge. Now in the case of Multi-walled nanotubes (MWNT) and Double-walled Nanotubes (DWNT) this leaves two sides, each with concentric nanotubes. Taking advantage of the low intershell friction the inner nanotubes can be actuated to telescope out of the outer shell using electrostatic forces [34]. When the two sides meet, electrical contact is restored. By introducing a gate in the DWNT device, the process can be reversed repeatably.

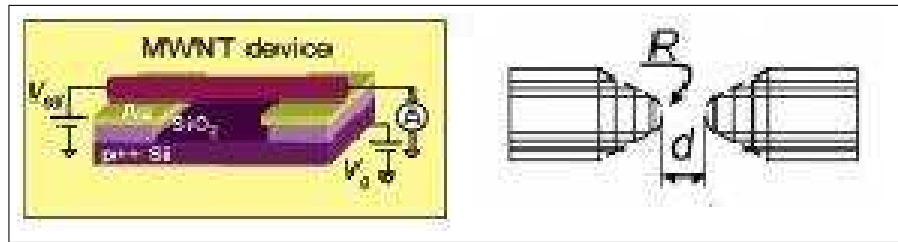


Figure 3.9: Model of the telescoping nanoswitch and representation of the breakdown gaps [34]

One of the major advantages of this switch is that the contacts are self-aligning. After the nanotube is placed, or grown in place, all the ensuing steps require no additional mechanical work.

One of the more unique switching solutions is the placing of a C_{70} molecule between two CNTs with open ends. The configuration is depicted in Figure 3.10.

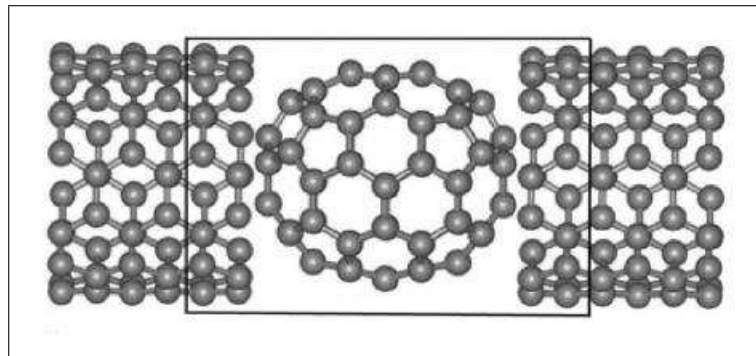


Figure 3.10: C_{70} Switch model [35]

The C_{70} is an interesting molecule due to its particular electrical and thermal properties, as well as its large energy bandgap, however, much is left to investigate of its properties. Here however, the highly directional nature of its molecular structure is used. At 60° intervals the molecule has distinct repeating features that are conducive to electron flow, and alternative between these points the flow decreases. A change of current in the region of 3 orders of magnitude is experienced between the on/off states.

3.5 Organically Actuated Switches

One of the main impedances to the evolution of NEMS beyond static and dynamic nanostructures to fully fledged molecular machinery, is the lack of nanoscale actuators, such as linear and cyclic motors, pumps and turbines. There have been many discoveries pertaining to actuators, some very promising, but they tend to be difficult to position.

An example of this is the droplet nanomotor developed by scientists at Berkeley. It consists of 2 spheres of liquid metal, one large and one small, as can be seen in Figure 3.11. They are placed on a carbon nanotube through which an electric current is allowed to flow. This forces atoms to migrate from the larger sphere to the smaller one. Once the smaller sphere is large enough to touch the other one, difference in surface tension causes atom migration to the larger sphere, restoring the earlier state. On its scale it gives about 100 million times the power output of a V6 225 horsepower engine [36].

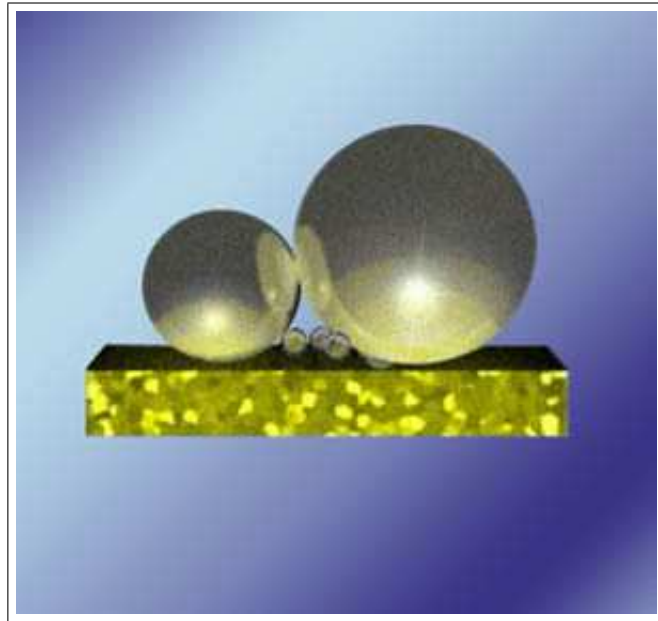


Figure 3.11: Nanomotor from liquid spheres [36]

Once again, for a simple efficient solution we turn to nature. Evolution has long since created means of actuation at a small scale. In this particular case, Deoxyribonucleic Acid (DNA) strands and muscle tissue.

Organic bistable compounds hold particular promise in regards to artificial molecular actuation. Two specific examples are DNA molecules that walk and rotaxanes that contract, both when exposed to ionised fluid.

The DNA motion can be used to move loose connection blocks to form a closed circuit. An organic walking path is deposited and the connector is placed on this track with DNA legs deposited on its underside. A SEM image of such a configuration can be seen in Figure 3.12. The rotaxane can be placed onto cantilevers and bend them when contacted.

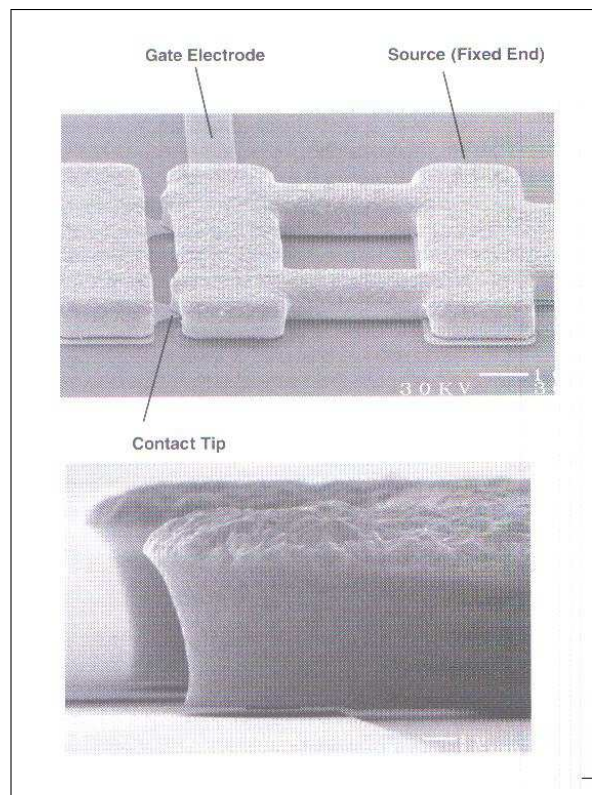


Figure 3.12: Organically actuated contact switch [13]

The force generated in the rotaxane molecule is approximately 40pN. Along a bar of 1 μm , this equates to a total deflection of 45nm.

3.6 To Summarise

In this chapter, a brief overview of current mechanical nanoswitches was given. First, it was explained why NEMS are being considered as an alternative solid state switches in some applications and what some of the drawbacks might be.

Following this explanation, a series of nanoswitch types and some of their variations, were given. Each switch was discussed in terms of the driving principle and the ways in which it has been implemented to date.

Chapter 4

Procedure and Methodology

The aim of this report is to investigate mechanical switches in the current field of nanotechnology. Following this, it will be attempted to reproduce such switches with the in house facilities of the microelectronics laboratory of the Electrical and Electronic Engineering Department of Stellenbosch University.

4.1 Procedure

To effectively follow through on these goals, a road map needs to be set for the course of the activities to accomplish them. This requires the implementation of base-lining, milestones and deliverables.

To start incorporating these ideas into the project, it must first be subdivided into its objectives and the elements contributing to each objective. The objectives of the project are two-fold:

1. The investigation of nanomechanical switches
2. Attempt the manufacture of nanomechanical switches

The sub-objectives contributing to each of these main objectives have been identified as follows:

The investigation of nanomechanical switches

- Mechanical switching as logic and calculating aid
- Nanotechnology

Attempt the manufacture of nanomechanical switches

- Identify and verify the manufacturing capabilities of the microelectronics laboratory
- Identify the switch/switches that are to be reproduced
- Manufacture of the nanoswitches, with attention to the manufacturing methods
- Testing of the nanomechanical switches produced

Each of the objectives produce a deliverable, whether tangible or intangible. Objective one yields the background and understanding of the relevant technologies to manufacture the devices. Each of its sub-objectives brings a different facet of these technologies as its deliverable.

Milestones are important achievements within an objective. The completion of each sub-objective would be a major milestone. After a milestone has been reached, that part of the project should not be revisited unless it is of large importance to the success of the project. This is called base-lining.

Base-lining sections of the project is important to prevent rehashing of old sections without sufficient cause, whether to implement the latest research, adding in novelties, or expand further on a topic. This sort of behaviour can cost valuable time and reek havoc on a design process.

4.2 Methodology

As important as reaching the aim of the project, is the quality of the research. Without reliable research, the result cannot be repeated or improved upon, hence useless. So in order to ensure the validity of the project results, proper scientific method needs to be adhered to and a stringent methodology followed.

To this end objectivity should be maintained at all times so that pre-held assumptions do not contaminate the choices made or results obtained. The rules of the used facilities will need to be adhered to and all procedures used in the manufacture and testing will be recorded. The specific equipment used will be listed and used as indicated by the manufacturer.

At best the results obtained during this project are an approach to the truth, but by keeping track of equipment, techniques and extraneous variables, this estimation will be as close to the truth as the available resources allow [37].

This report is meant to be original work, unifying previous research into this area and to expand the processes and achievable devices in this context at the microelectronics laboratory of the Electrical and Electronic Engineering Department of Stellenbosch University, to Show insight into the work done and bring a critical approach to bear on the choices and results obtained with impartiality.

4.3 To Summarise

Here the approach for the manufacturing in this investigation has been laid out. This has been done to ensure repeatable results of a calibre acceptable in scientific research.

Chapter 5

Design and Manufacture

5.1 About the Microelectronics Laboratory

Construction of the microelectronics laboratory began in 1980 and by 1984 it was able to begin full operation. The original staffing included Adrian Vader, Willie van Niekerk and Nicklaas van Graan, later to be joined by Martie Kruger from Pretoria University.

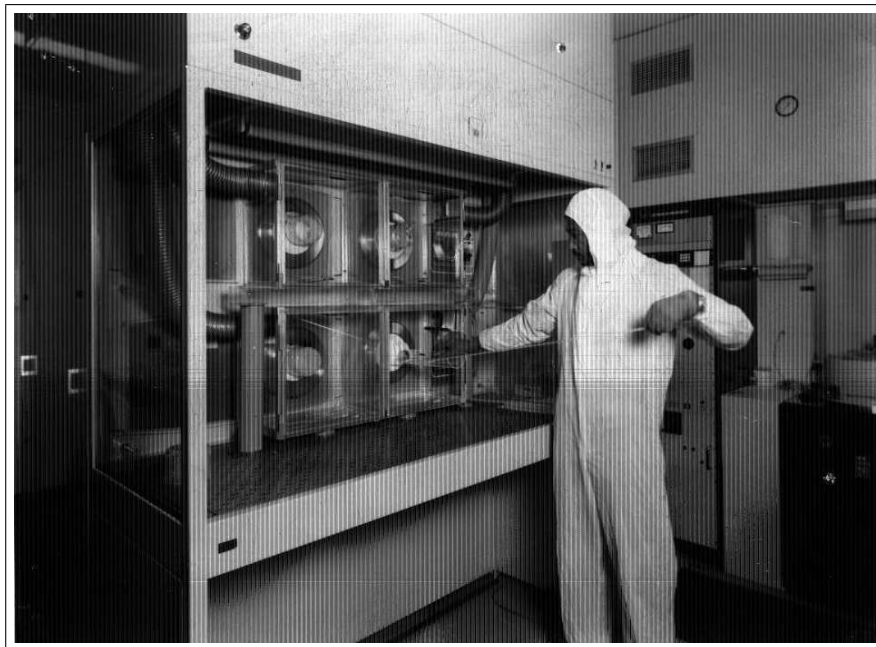


Figure 5.1: Nick van Graan working in the cleanroom (1986)

They had facilities to make their own lithography masks, quartz ovens to bake the samples, hydrofluoric sample cleansing, pre-treatment and impregnation of samples with boron and phosphorous, metal plating and multi-layered structure development on both sides of a sample.

When the Class 1000 cleanroom was finally sealed, it was found, by a verification process done by Natal University, that the cleanroom was beyond expectation. The class of a cleanroom is an indication of how many particles are present in the air within the room, as well as the average size of these particles. A Class 1000 cleanroom is limited to 1000 particles per cubic foot of air, with a particle size of no larger than 0.5 microns [38]. The cleaning and conduct protocols for the cleanroom are given in Addendum A.

Due to the volatility and poisonous nature of some of the chemicals that are required for processes used, a chemical detection and warning system was built into the laboratory. An example of such a process is the etching of nickel. One of the techniques involve using a solution that consists of 2 parts HNO_3 , 1 part Acetic acid and 1 part acetone. This solution explodes after a time period of about 10 minutes.

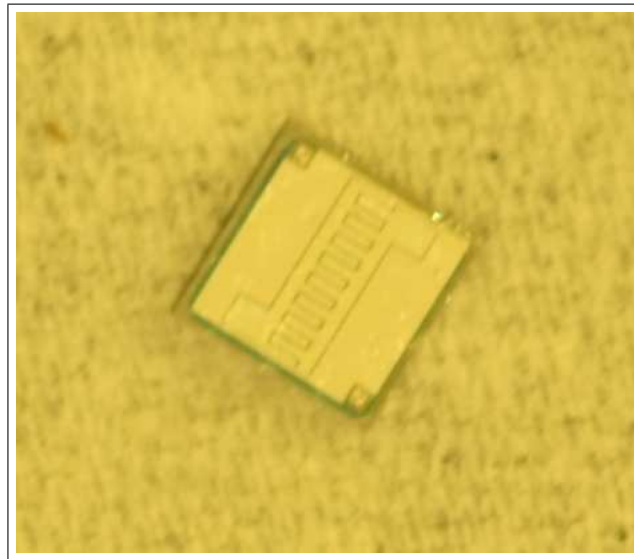


Figure 5.2: Transistor manufactured in microelectronics laboratory

Projects in the laboratory ranged from making solar cells and solar cell packs, to transistors, diodes and cutting their own resistors. An example

of this work is provided in Figure 5.2. Aside from making transistors, the laboratory also made thyristors, inorganic solar cells, inverters, Schotky diodes and INPATT diodes.

Eventually, with declining interest and funding, work on microelectronics ceased. Eventually the laboratory was adapted to aid in the research and manufacture of superconductors and nanodevices.

While funding is still required to restore the cleanroom to its Class 1000 status, operation can continue due to superconductors being largely single layer structures, simple 3 layer structures or manufactured in a sealed environment. Nanodevices are considerably smaller than dust particles, skin flakes and oil residue derived from humans. Although the repeatability, reliability and functionality of the devices may on occasion be questionable under these conditions, ways can currently be found around this.

At the outset of the report an effort was made to do a thorough cleaning of the cleanroom. All surfaces were washed, equipment cleaned and unlabeled containers removed. The fine air filters were replaced and coarse filters were washed and returned.

Currently the equipment available in the laboratory are:

- RF AC Milling unit
- DC Sputtering unit
- Eletron Spin Resonance (ESR) Spectrometer
- Thermal Evaporator
- Quartz Ovens
- AFM/STM Combination
- UV lithography Exposer
- Sonic Wire Bonder
- Optical Microscopes with computer interface
- Photoresist Spinner
- Sonic Bath

- Heated Beaker Spinner
- Hot plate
- Electroplating System

External to the laboratory, but at its disposal are:

- PLD - Physics Department
- E-Beam Lithography - iThemba Labs
- X-Ray Diffraction(XRD) and Electrostatic Discharge (ESD) - Chemistry Department
- SEM - Geology Department, UWC and UCT

Some of the laboratory equipment have undergone considerable modification. The AFM has been upgraded with a software package that allows for tip scratching. A module was also added to enable in-motion stepping of the samples. This controlled motion bed, on top of the stable table, allows the user to search for relevant geometry on the sample, or adjust scans on the fly.

The thermal deposition unit was acquired as just that, a thermal depositor. A sensor was installed to allow for the deposition rate and thickness to be measured, followed by a substrate heater, and eventually a second crucible for dual depositions.

5.2 Basic Procedures in the Microelectronics Laboratory

In the use of the cleanroom there are four pieces of equipment whose use are commonplace and are sure to form part of the project. This section has been set apart for the explanation of their use, with advice as to obtaining effective results from them.

The equipment in question are the photoresist spinner, UV exposer, thermal deposition unit and the AFM. Combinations of the equipment can be used for three consecutive procedures, namely the application of a photoresist mask, deposition of material and subsequent scanning of the sample.

Photomasks

Starting with a silicon substrate cleaned in acetone and heated to 200°C, one then proceeds to the photoresist spinning setup. The substrate is placed in the spinner and turned up to 4000rpm. Photoresist is dripped onto the substrate and left to spin for 30 seconds. After being baked for 2 minutes at 115°C the sample is ready for UV exposure.



Figure 5.3: Photoresist spinner and associated chemicals

In Figure 5.3 the photoresist spinner can be seen, along with all the accompanying chemicals, namely photoresist, developer and photoresist remover. In Table 5.1 the manufacturers and serial numbers of the equipment, and chemicals used are provided.

Table 5.1: Photoresist equipment

Equipment	Manufacturer	Number
Photoresist spinner	Headway Research Inc.	1-EC101D-R485
Photoresist	Micro resist technology	ma-P1225
Developer	Micro resist technology	ma-D331
Photoresist remover	Micro resist technology	mr-Rem 660
UV exposer	Karl Suss KG	401000

The UV exposer, shown in Figure 5.4, is equipped with a mask containing the pattern to be imprinted. After the sample is placed into the UV exposer, the machine is set for the exposure time and turned on. For the resist used here, the exposure time is 30 seconds.

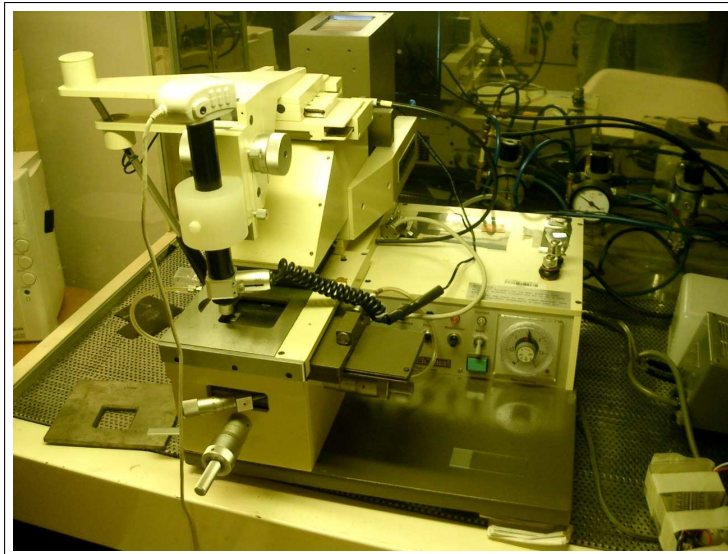


Figure 5.4: UV exposer

The sample is then placed into the photoresist developer for 60 seconds to remove the softened photoresist. It should be noted that the type of resist, as well as the exposure time and the post spin baking, affect the required developing time.

Another effect on the resulting pattern is the mask used for the exposure. Four different types of masks were available and investigated for use. The chrome mask, masks manufactured using Printed Circuit Board (PCB) technology, masks printed onto transparency film and rubber masks. The manufactured masks are shown in Figures 5.5 to 5.8.

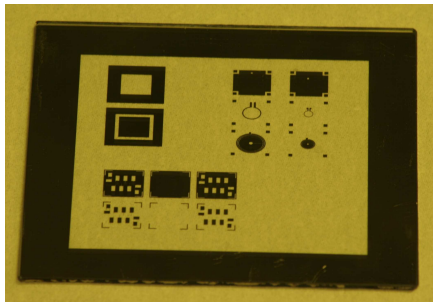


Figure 5.5: Chrome Mask

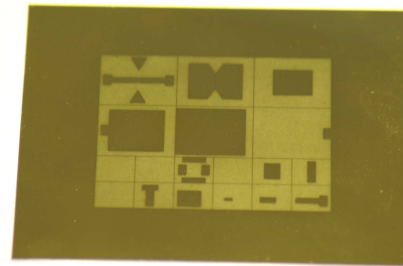


Figure 5.6: PCB mask

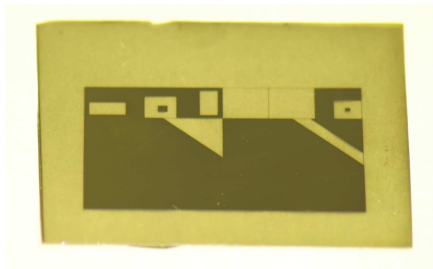


Figure 5.7: Printed mask

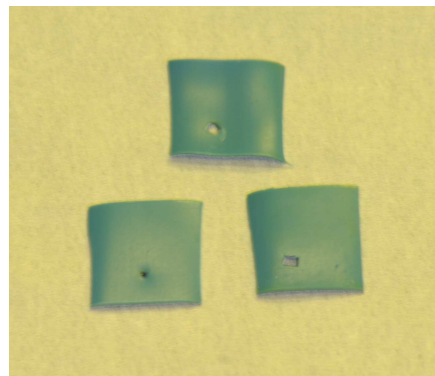


Figure 5.8: Rubber mask

The results obtained from the different masks vary. In Figure 5.9 the step edge of the chrome mask, a clean solid line with solid photoresist, can be seen.

Figure 5.10 shows the PCB step edge, which is straight but unclear. The photoresist side is also broken. This is a result of the blocked out layer of the mask not being dense enough, allowing UV light to filter through and

compromise the photoresist. This type of mask can work, if a denser mask layer can be achieved.

Figure 5.11 shows the result of the mask printed onto transparency film. The step edge is unclear, uneven and the photoresist is compromised. This is a result of the loose packing of the toner onto the film.

Lastly, Figure 5.12 shows the rubber mask step edge. The line is uneven but clear, also the photoresist is unbroken. The step unevenness is due to hoe the rubber was cut. A more solid cut will yield a finer step edge.



Figure 5.9: Photoresist profile of a chrome mask

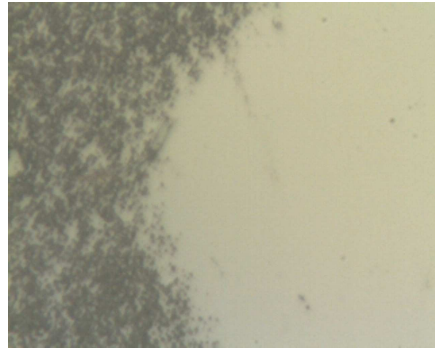


Figure 5.10: Photoresist profile of a PCB mask

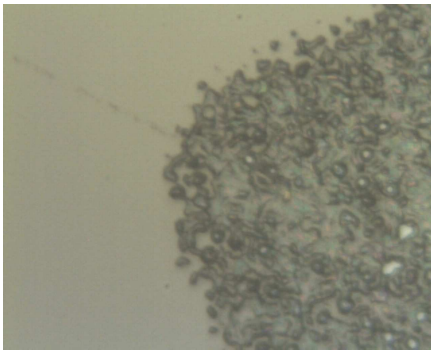


Figure 5.11: Photoresist profile of a printed mask



Figure 5.12: Photoresist profile of a rubber mask

Given the results and the geometries of the masks it is noted that the rubber mask is only usable for larger pattern geometries. While improved forms of the PCB and printed masks can be used for smaller geometries, the chrome mask is the only one that can be used for micron and sub-micron structures.

The microelectronics laboratory usually acquires outdated photoresist, due to the cost of fresh photoresist. For the use that it gets employed in the clean-room, the only real difference is that the outdated resist does not provide such a well defined a under-etch and the time parameters of the sample preparation also change slightly.

Thermal evaporation

Once a sample is ready for material deposition, one method of doing so is by using the thermal deposition unit. In Figure 5.13, the laboratory's RIBER model thermal evaporator can be seen.



Figure 5.13: Thermal evaporation unit

The thermal evaporation unit requires a crucible, coil or basket to be clamped between its electrodes for heating, as shown in Figure 5.14. The cleanroom mostly uses tungsten crucibles for thermal deposition. A material placed in the crucible sublimates and deposits on the waiting sample. Before depositing a new material, a crucible must first be prepared. This entails cleaning it with acetone and then annealing it in the thermal evaporator.

The annealing process requires the crucible to be placed into the thermal evaporation unit without material in it. The unit is then sealed, as for a normal deposition, and then turned up to maximum current. This burns the crucible clean and expunges any latent gas in the crucible. A crucible being annealed in a dark room can be seen in Figure 5.15.

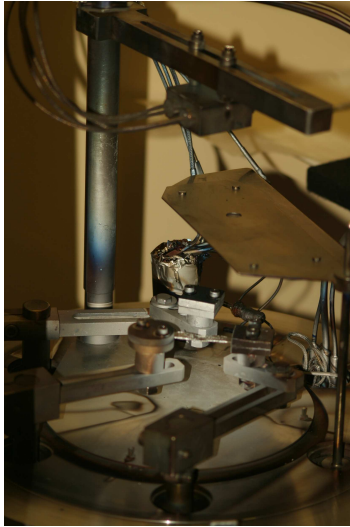


Figure 5.14: Thermal evaporation unit crucible



Figure 5.15: Thermal evaporation unit during annealing process

Once the crucible is annealed, it is loaded with a suitable material and a sensor placed in the QCM. The sample also is placed in the thermal evaporator. The glass dome is put in place and the vacuum is allowed to reach 10^{-6} mbar. the current is slowly increased until the required deposition temperature is reached.

The QCM is used to control the deposition rate and thickness of the deposited material. Having completed this phase, the current is turned down and the vacuum is vented. This completes the deposition process. Having removed the sample, it is placed in the photoresist remover to corrode the extraneous material, leaving the required structure behind.

It should be noted that the sensor needs to be calibrated for the first deposition and again for every 10% loss of sensor life. For even more accurate depositions a calibration sample can be placed in the unit, along with every deposition, for continuous calibration.

Slow heating and cooling of the crucible is important since heating it too quickly can destroy the crucible. This should be avoided due to material loss and the waste of the 2 hours required for a deposition.

The components of the QCM are shown in Figure 5.16. For the accurate operation of the QCM the Z-factor, tooling factor and the density of the

material to be deposited need to be known.

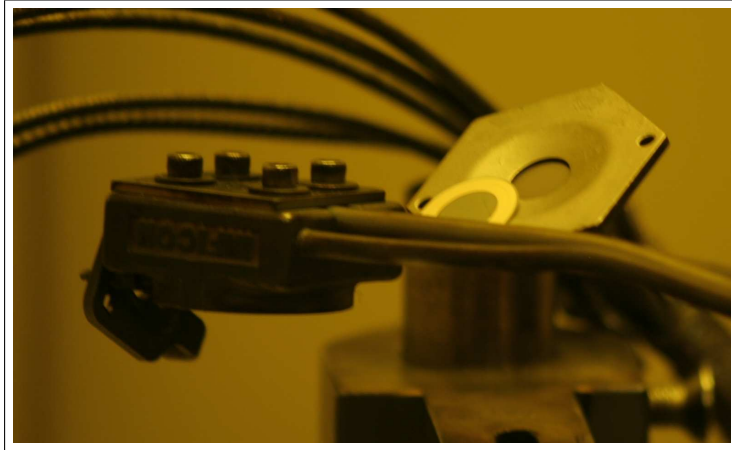


Figure 5.16: QCM sensor and housing

The Z-factor is the ratio between the acoustic impedance of quartz and the deposition material. Acoustic impedance is a measure of how quickly sound travels through a material. The Z-factor is defined as

$$\text{Z-factor} = \frac{\text{Acoustic impedance of quartz}}{\text{Acoustic impedance of material.}} \quad (5.1)$$

The tooling factor is a parameter that correlates the position of the sensor to that of the sample. Different positions in the thermal evaporator result in different degrees of deposition. By compensating for the positional difference, a thickness reading is received relative to the QCM sensor. This means that, when the configuration of the unit is changed, the tooling factor needs to be re-calibrated

The calibration is done by depositing a sample and then measuring a step height on the sample. From these 2 readings the tooling factor is then modified according to Equation (5.2).

$$\text{Tooling factor} = \frac{\text{Thickness}_{AFM}}{\text{Thickness}_{QCM}} \times \text{Old tooling factor} \quad (5.2)$$

AFM

The Nanosurf Easyscan2 and its peripherals can be seen in Figure 5.17. The peripherals include a stable table and a motorised stepper. The stable table is used to cancel out the vibrations from the environment, since the AFM probe is highly sensitive.

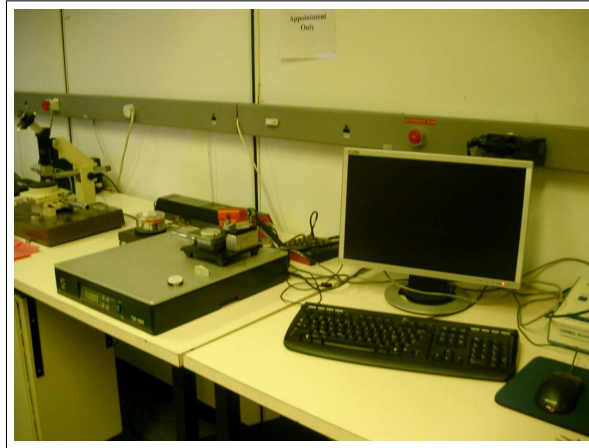


Figure 5.17: AFM station

The stepper is used to move the sample around before or during a scan to get to the right position for scanning. In Figure 5.18 a closer view of the AFM and stepper is provided.

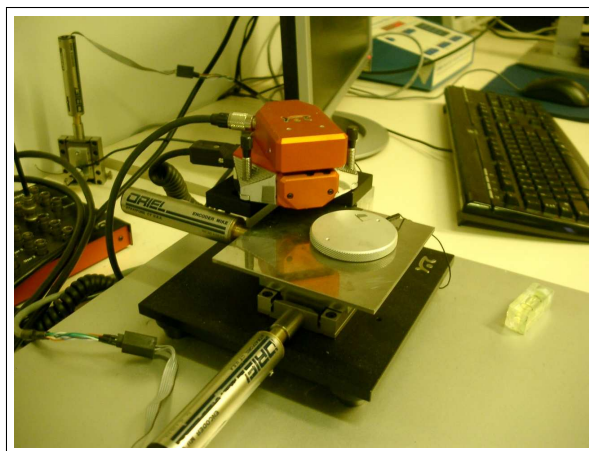


Figure 5.18: The AFM and motorised sample base

Once a sample has been placed under the AFM, the tip is advanced towards the sample and then allowed to make the final approach on its own. This is to prevent the tip from crashing into the surface.

The scan starts automatically. When the scan is completed, the data can be represented as a line graph, colour map or 3D representation. The tip withdraws on its own, to prevent vibrations or swivelling to damage it on the surface.

Structures higher than 1 micron should not be scanned with the AFM, since the height differences during the scan can damage the probe. The correct tip for the scan to be undertaken should be selected, to ensure accurate readings and mode operation.

When attempting AFM scratching, contact tips should be used. These tips are shorter and sturdier than the tap mode tips. This makes them less flexible and better for scraping away material.

5.3 Choosing a Device

In Chapter 3, a brief overview of some of the nanoswitches currently making progress and impact on the field of sub-micron switching was given. Now it is necessary to make a choice between these switches for the next step in the research objective. To this end a means must be found to choose between the available 9 switches:

1. Silver sulfide nanoswitches
2. Phototransistor type nanoswitches using nanoribbons
3. Metal/Organic insulator/Metal type photoswitches
4. Nanofiber switches
5. CNT one side suspended cantilever nanoswitches
6. CNT double suspended cantilever nanoswitches
7. CNT actuated bearing type nanoswitches
8. C₇₀ - CNT nanoswitches
9. Organic motor nanoswitches

To this end a variation on the decision-matrix, or Pugh's method was used. In this method, important criteria for the final device are defined and given relative values. Each of the devices is then rated against these criteria, and the device with the highest score is then considered the most viable [39]. The weighting value was taken out of a total of ten, with no two criteria allowed to have the same weighting, in this case 4, 3, 2 and 1.

Four criteria for the nanoswitches were identified, in descending weighting order:

- **A: Manufacturability** of the device in the microelectronic laboratory
- **B: Applicability** to mechanical switching and logic gates
- **C: Cost** of materials and manufacture
- **D: Switching rate** of the device

The resulting Pugh's matrix can be seen in Tabel 5.2

Table 5.2: Pugh's matrix for nanoswitches

Device	A (Wt.4)	B (Wt.3)	C (Wt.2)	D (Wt.1)	Total
1	6	8	3	6	60
2	3	3	5	5	36
3	7	7	8	6	71
4	1	3	5	5	28
5	3	8	6	8	56
6	3	8	6	8	56
7	2	8	6	8	52
8	1	5	4	7	34
9	2	5	3	3	32

So out of a possible hundred, the highest scoring device was the Metal/Organic insulator/Metal Photoswitch with 71. This will therefore be the main device. In evaluating the alternatives two interesting phenomena were discerned.

The 2nd place silver sulfide switch was disqualified due to its possible high cost and uncertain manufacturability. However, this device embodies the spirit of this project, as it is a switch that works on mechanical detachment, utilises the nanoscale properties of its structure and has promising logic gate applications.

The group off 3rd placed carbon nanotube devices, which where removed from the running by the manufacturing stage as well. Its high applicability rating and switching ratios, not to mention its application to further reaching implementation makes it hard to ignore.

It was decided, therefore, to attempt the manufacture of the photoswitch and the Ag₂S switch. The CNT switches would be modelled for an aid to further study, should the manufacturing be simplified in the future.

5.4 Manufacture

Photoswitch

In the original article appertaining to photoswitches of the type metal/organic insulator/metal by Xinjun Xu *et al.* [28] a series of devices were manufactured. These devices were created using varying thicknesses of polymethylmethacrylate, polystyrene, gold (Au) and aluminium (Al). The materials were layered onto a glass substrate with an ITO coating, which would serve as the bottom contact and the incidental surface for the UV exposure. The structure of the three main devices are represented in Table 5.3, as the organic and metal materials that were deposited onto the ITO glass.

Table 5.3: Photoswitch device configurations for manufacture

Device	Thickness PMMA	Thickness PS	Thickness Au	Thickness Al
1	-	30nm	30nm	-
2	-	65nm	30nm	-
3	100nm	-	-	50nm

To gain a quick feel for the structure involved, two devices were attempted. The first was ITO glass (9-15 sq/ Ω), PMMA photoresist, hard baked, and then layered with gold using the DC sputtering unit. The second was ITO, the organic semiconductor copper phthalocyanine (CuPc) and gold sputtering. The experiments yielded several results for contemplation. These initial devices are shown in Figure 5.19.

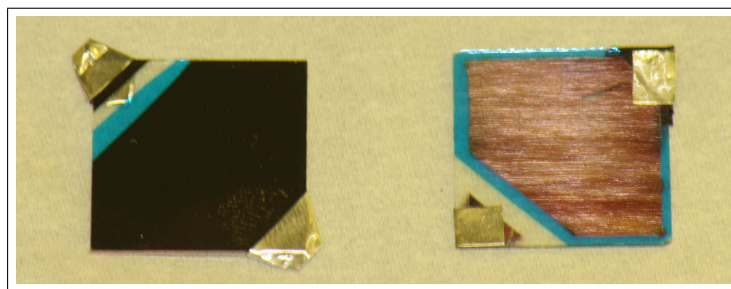


Figure 5.19: Test run photoswitches

The PMMA photoresist did not work well as an organic insulator, due to the soft nature of the layer, even after baking. At the time, there was also no reliable way to verify the layer thicknesses of the spun on PMMA photoresist or the sputtered gold.

The metal electrodes needed to be deposited at a rate of $0.5\text{\AA}/\text{s}$ in a thermal evaporation unit at a vacuum of at least 1.5×10^{-4} . This being known and with the experience of the first attempt, it was noted that the Quartz Crystal Microbalance (QCM) sensor could be used to control the deposition rate and control the layer thickness.

The QCM sensor works by measuring the change in frequency of the quartz crystal resonator, which is dependant on the deposition of material on its acoustic interface. This allows for the accurate determination of deposition rates and film thicknesses, given the density, acoustic impedance and a calibration run to determine the tooling factor of the sensor.

Further research into the deposition of PMMA and PS material eventually led to a reference on isolating individual zinc oxide nanotubes from one another for an electroluminescence application [40]. It states that PS depositions typically involve solutions of PS in toluene.

In an extract from the doctoral work of Alexis Ryan Abramson [41], it was found that polystyrene could be used to add mechanical strength to a loose nanocomposite. The polystyrene was dissolved in a 1:10 mass ratio of PS to toluene. The resulting organic layer had good mechanical strength and a softening temperature of 200°C . It was also stated that its chemical resistance was questionable.

The final result for the manufacture of the organic polymer for device delivery used $2\text{mg}/\text{ml}$ of polystyrene in a mixture of toluene and xylene in a 1:1 ratio at room temperature [42]. The solution is then sonicated for 10 minutes to ensure thorough particle distribution.

Care should be taken to prevent water from being included during the mixing process, since it causes the polystyrene to particulate. This is easily spotted, since the solution will turn a milky white if this occurs.

The nanophotoswitch article used polystyrene (M_W 65000) for its organic layer [28]. A polystyrene development kit was therefore purchased from Sigma Aldrich. The kit contained 250 mg of polystyrene in a series of molecular weights ranging from M_W 5000 - 58000. This would allow testing of a variety

of devices and provide extra material for the testing of spin on thicknesses of the polymer.

From photoresist theory it was found that thicknesses as a result of spinning on the solution can be determined by:

$$h = \frac{KC^{\beta}\mu^{\gamma}}{\omega^{\alpha}} \quad (5.3)$$

where

K = Overall calibration constant

C = Polymer concentration in g/100ml solution

μ = Intrinsic viscosity

ω = Rotations per minute (rpm)

β , γ and α are exponential factors that need to be determined. The absence of a time term, however, makes this equation of lesser use for this application. The thinning of liquid films results from radial convective flow due to centrifugal force, and evaporation [43].

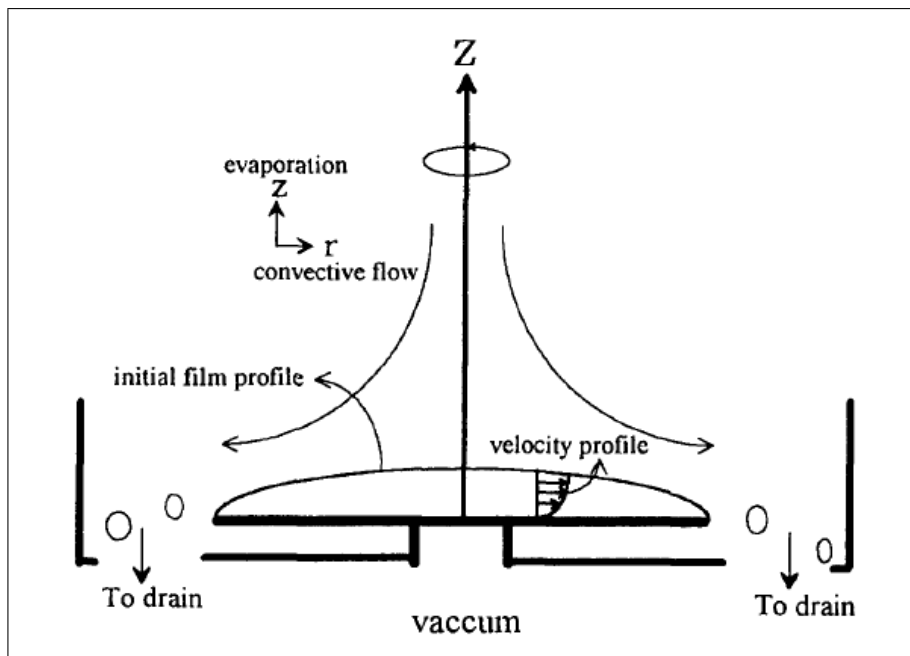


Figure 5.20: Diagram for thin film theory [43]

Considering an isothermic, incompressible and homogeneous Newtonian fluid, the spinning forces represented in Figure 5.20 can be represented by Equation 5.4. For fast spinning, faster than 1000rpm, this equation can be reduced to the form of Equation (5.5).

$$h = \sqrt{\frac{h_0^2}{\frac{4}{3}\rho\omega^2\mu h_0^2 t + 1}} \quad (5.4)$$

$$h = \frac{\sqrt{3}}{2\omega\sqrt{\rho\mu t}} \quad (5.5)$$

in these equations h is the thickness of the film, h_0 is a characteristic scaling factor, ω is the rotational speed of the disc in rpm, ρ is the density of the fluid, μ is the viscosity of the fluid and t is the spinning time.

It should be noted that initial film thickness has no effect on the final film thickness [43], unless the amount of fluid was insufficient to coat the surface.

Molar mass of polystyrene is dependant on the clustering of the molecules and can be controlled by the manufacturing process and quality control. The specific molecular weight of the material used should always be stated with the material.

Health considerations, when using toluene and xylene, depend on exposure and duration, as well as genetic susceptibility and age. Toluene can cause tiredness, confusion, weakness, drunken-type actions, memory loss, nausea, and loss of appetite under low exposure. High levels of exposure can precipitate dizziness, sleepiness, or unconsciousness. Death is also possible, due to how toluene interferes with the way breathing and the way the heart beats. It does not, however, cause cancer [44]. With short term exposure xylene can cause irritation of the skin, eyes, nose, and throat, difficulty in breathing, impaired function of the lungs, delayed response to a visual stimulus, impaired memory, stomach discomfort, and possible changes in the liver and kidneys. The effects of long term exposure to xylene is similar to that of toluene, but the possibility of it causing cancer has not as yet been properly tested [45]. Polystyrene has been classified as a possible carcinogenic material.

Therefore, while working with the compounds for the production of the organic insulation layer, gloves, mask and eye protection will be worn, in ac-

cordance with laboratory protocol, and work will not be conducted in the presence of people not properly attired.

For the organic layer work, the properties of the chemicals used are listed in Table 5.4 for reference and shown together with the mixing equipment in Figure 5.21.

Table 5.4: Material Properties for the Organic Layer

Material	Mol. Formulae	Molar Mass	Density	Viscosity
Toluene	C_7H_8	92.14 g/mol	0.8669 g/ml	0.590 cP
Xylene	C_8H_{10}	106.16 g/mol	0.88g/ml	0.812 cP
Polystyrene	C_8H_8	n/a	1.05 g/ml	n/a

The unit for viscosity, poise (P) is equivalent to $1 \text{ g}\cdot\text{cm}^{-1}\cdot\text{s}^{-1}$ and a centipoise is a hundredth of a poise. Converted to SI units, $1000 \text{ cP} = 1 \text{ Pa}\cdot\text{s}$.



Figure 5.21: Organic layer components and equipment

During a sequence of spin tests with the 25mm×25mm ITO glass samples, the following effects were observed at the different speeds. Also, representative samples are shown in Figures 5.22, 5.23 and 5.24.

Speeds < 3000 rpm : Surface coverage was incomplete

3000 - 5000 rpm : Decent surface coverage and finish

Speeds > 5000 rpm : Surface abnormalities occurs

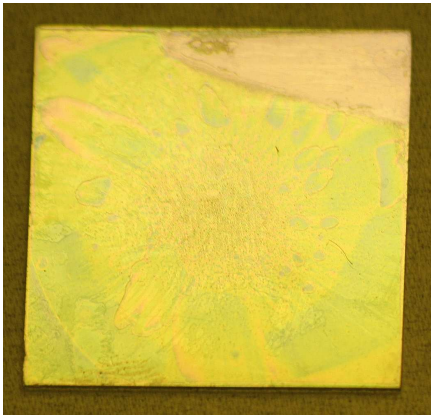


Figure 5.22: Polystyrene spun on at 3000rpm

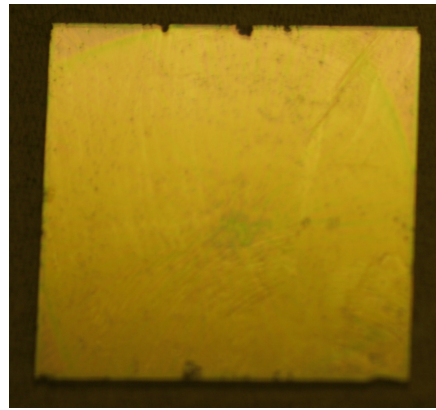


Figure 5.23: Polystyrene spun on at 4000rpm

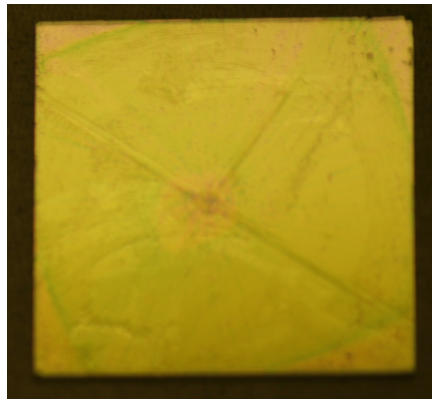


Figure 5.24: Polystyrene spun on at 5000rpm

Since no definitive manner could be found to calculate the viscosity of 2 merged organic liquids, 4000rpm (also the laboratory standard spinning speed) was chosen for full coverage and fine film development on the substrate. Using the viscosity of the xylene as a upper limit and the toluene as lower limit, the correct spinning time could be interpolated experimentally.

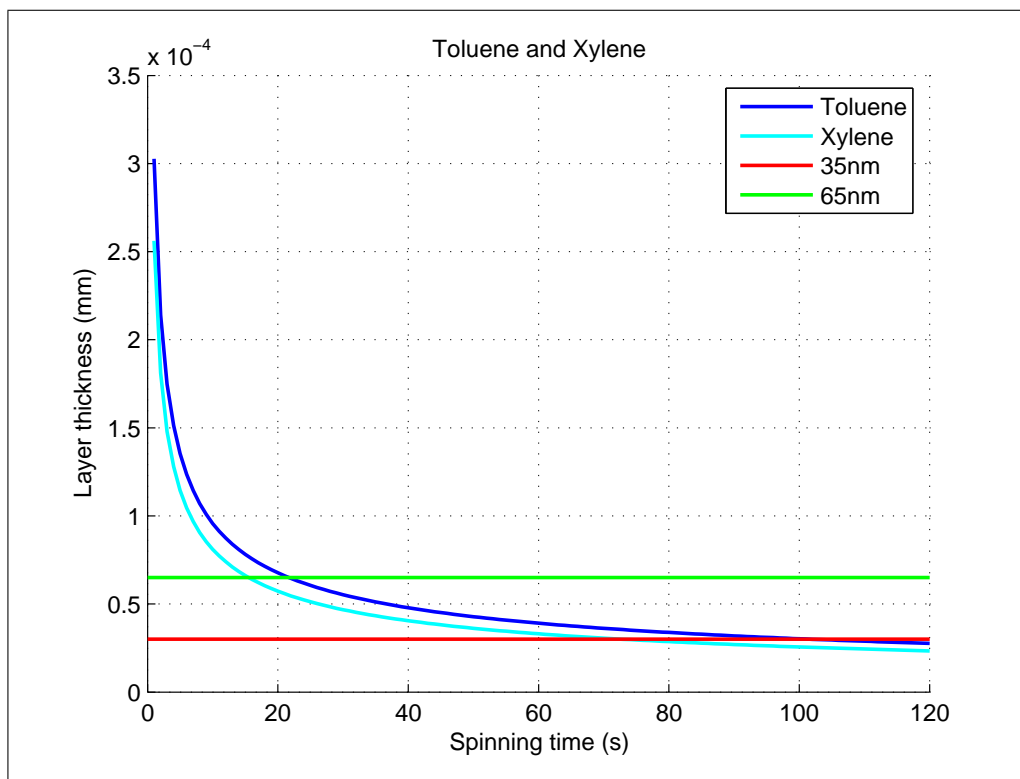


Figure 5.25: Graph for layer thicknesses

In Figure 5.25, the thickness profiles can be seen. The green line represents the 65nm thickness, which intersects from 14s to 21s. The red line, corresponding to the 30nm thickness, intersects from 65s to 90s.

Using the AFM's upgraded software and new tips, the organic layer was scratched down to the substrate and then scanned, enabling a accurate height measurement undisturbed by material build-up or surface effects present in the other available height determination methods.

The surface scans of the spun on organic layer from the chosen speed were smooth and uniform. Surface scans of the polystyrene layer can be seen in

Figure 5.26 as a colour map, where height is represented by brightness, and as a 3D image in Figure 5.27.

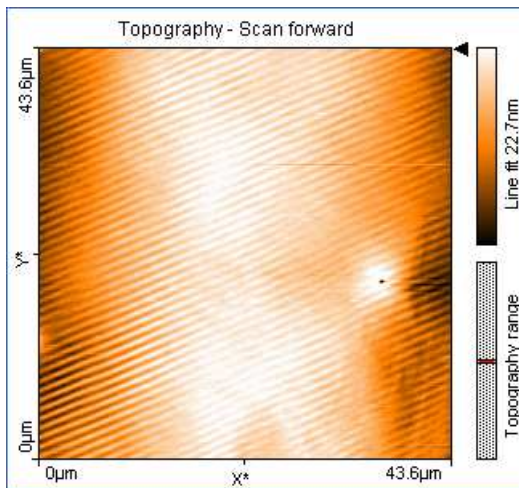


Figure 5.26: Colour map AFM scan an organic layer

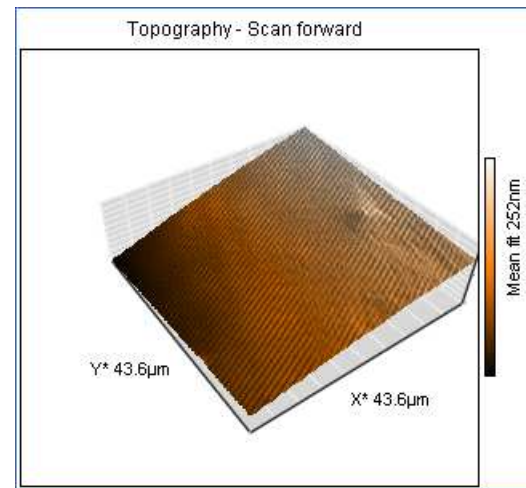


Figure 5.27: 3D graph AFM scan of an organic layer

Using the scratched samples, an example of which can be seen in Figure 5.28, the spinning times were verified. Extra scanning was performed on the 90 second spin samples to obtain a statistically certain height measurement.

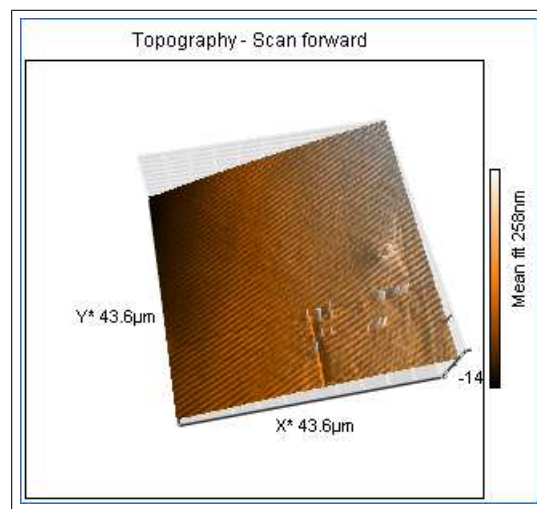


Figure 5.28: 3D graph AFM scan of an organic layer

This was required since the cross cuts of the scratches, as in Figure 5.29 were not consistent. From a sample group of thickness data shown in Table 5.5, finite statistics can be used to obtain the mean value and the standard deviation of the measurements.

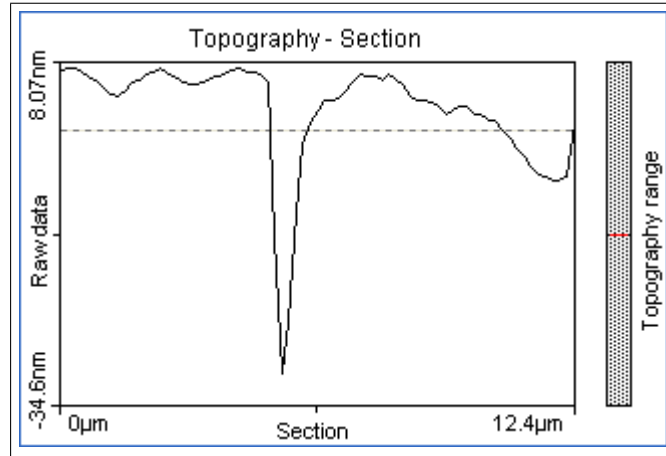


Figure 5.29: Cross section of the AFM scratch

Table 5.5: Organic layer thickness readings

Sample i	Thickness x (nm)
1	25.94
2	24.91
3	22.24
4	31.05
5	51.52
6	10.08
7	25.09
8	22.08
9	31.61
10	37.02

Having first removed terms 5 and 6 due to there being sample anomalies, the working of the data could commence. Using a Gaussian statistical distribution [24], from Equation (5.6), given that there are N samples with

(x_i) being the i -th measurement, the mean (\bar{x}) of the system is 27.49nm. This yielded the sample deviance through the measurements as 5.29nm, from Equation 5.9, meaning that 68% of the thicknesses will lie in the range of 22.20nm to 32.78nm.

$$\bar{x} = \frac{1}{N} \sum x_i \quad (5.6)$$

$$S_x^2 = \frac{1}{N-1} \sum (x_i - \bar{x})^2 \quad (5.7)$$

$$S_x = \sqrt{S_x^2} \quad (5.8)$$

$$= \sqrt{\frac{1}{N-1} \sum (x_i - \bar{x})^2} \quad (5.9)$$

The reason for this can be seen in Figure 5.30. Inside the scratched trench there are height anomalies, probably due to loosened photoresist and ITO peaks. From this scan, the flattening depth of the scratch can be seen to be 26nm, very close to the calculated mean and well within the deviance range. The difference can be explained by finite statistics using only a limited number of data points. Should an infinite number of data points be used, the calculated mean would be theoretically identical to the lengthwise cross section.

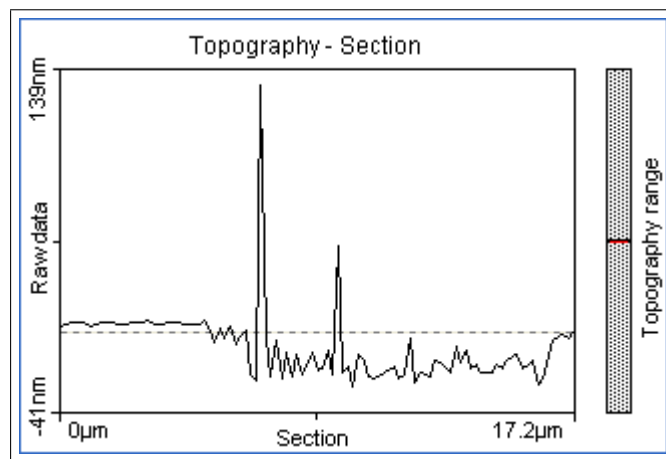


Figure 5.30: Cross section along the AFM scratch

The height values deviated from the values for toluene and xylene, as expected, due to the mixed fluid and suspended polystyrene. This data was plugged back into Equation 5.5 to obtain the characteristic profile for the mixture.

The first round of adapted photoswitches that were attempted with 30nm PS and 30nm aluminium, seen in Figure 5.31, did not function satisfactorily. There was continuity through the device.

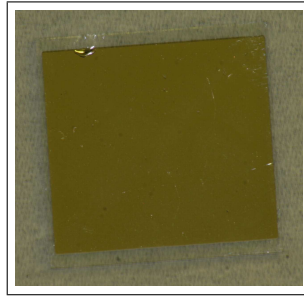


Figure 5.31: First complete photoswitch

Looking at the surface roughness of the ITO glass, seen in Figure 5.32, which in some areas show varying peaks of up to 60nm. In Figure 5.33 the cross cut of the ITO surface can clearly be seen to have a high level of variance.

A device using the parameters of 120nm PS and 50nm aluminium was to be created. This would place the top electrode 100nm, plus the additional mean ITO height difference of 20nm, above the ITO contact.

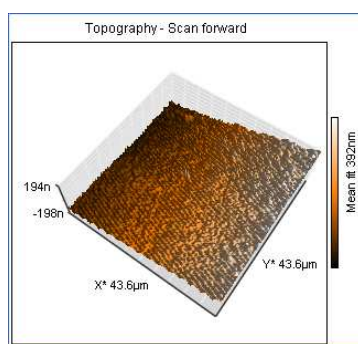


Figure 5.32: 3D graph AFM scan of the ITO glass

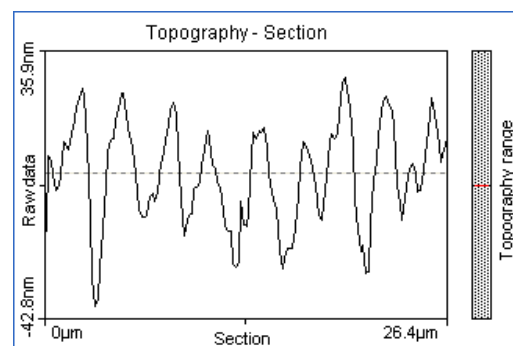


Figure 5.33: Cross section of the ITO glass surface

Ag₂S Switch

According to the work by Terabe *et al.*, the The construction of the silver sulfide switch is accomplished by taking a silver nanowire and sulphurize it. This provides the silver sulfide coating, which is augmented with a 1nm layer of silver where the platinum nanowires are to cross [27]. A SEM image of their developed device is shown in Figure 5.34.

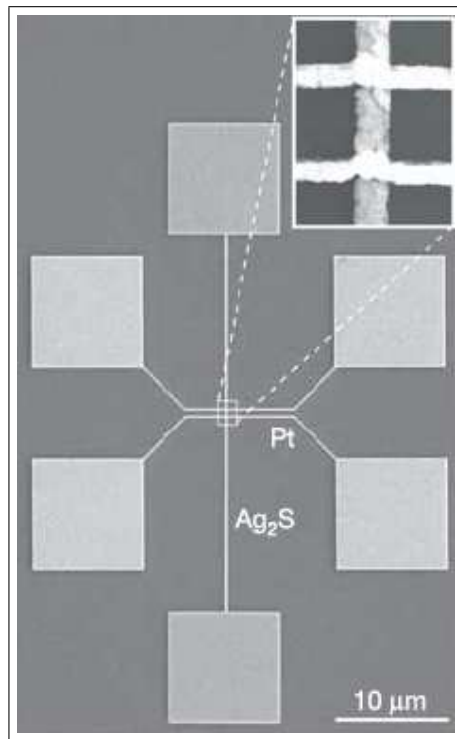


Figure 5.34: SEM image of an actual Ag₂S switch [27]

The diameter of the nanowires are 100nm, but the critical point of the device is the silver sulfide interface and a silver layer of 1nm. While the manufacture and positioning of nanowires are currently beyond the capabilities of the microelectronics laboratory, if the silver sulfide layer can be reproduced, the 1nm of silver could be attained through thermal deposition.

Since deposition in a sulphur atmosphere isn't viable here, 25g of silver sulfide was obtained from Sigma Aldrich. Having obtained the material, the deposition was attempted in the laboratory's thermal evaporation unit. Results were disappointing, the attainable vacuum was insufficient for the transfer

of the silver sulfide, instead the heat split the compound producing sulphur gas and silver deposition.

Since the silver sulfide couldn't be added onto the silver, ways were sought to infuse the sulphur without using a sulphurous atmosphere. It was found that old Russian jewellers used a compound called niello to produce blackened silverware like that seen in Figure 5.35. This compound is a mixture of silver, lead, copper, sulphur and ammonium chloride. The specific formula is jeweller dependant and is handed down within a family of jewellers, although a standardised commercial variant is available.

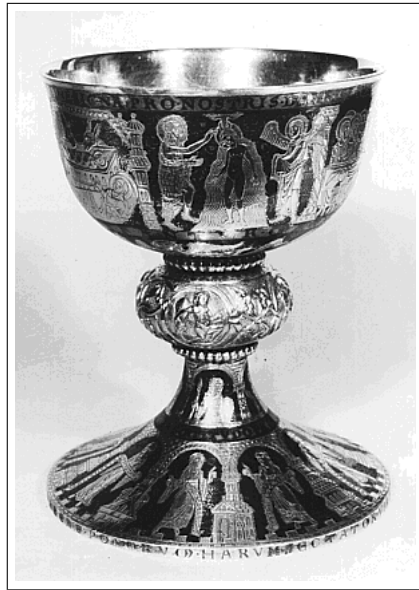


Figure 5.35: Niello Silverware [46]

Jewellers' preferred method for the sulphurization of silver, however, is using liver of sulphur. This mixture is prepared as a brown clump, as in Figure 5.36, by combining sulphur and potassium carbonate. A diluted solution of this compound can be used to sulphurize silver. However, the fumes given off during this process is toxic.



Figure 5.36: Liver of Sulphur

A less toxic method, along the same lines, is to use lime sulphur. It is considerably cheaper than liver of sulphur and available at most agricultural suppliers as a pesticide. The chemical name is calcium polysulfide, and it is created by mixing calcium hydroxide and sulphur [47].

A test was done to determine if this method would yield satisfactory results. To determine the nature of the result, a 69% solution of nitric acid (HNO_3) would be used, since it dissolves silver but only attacks silver sulfide. First the discerning test was attempted with plain silver and the acquired silver sulfide. The silver dissolved and the Silver sulfide remained, as seen in Figure 5.37.

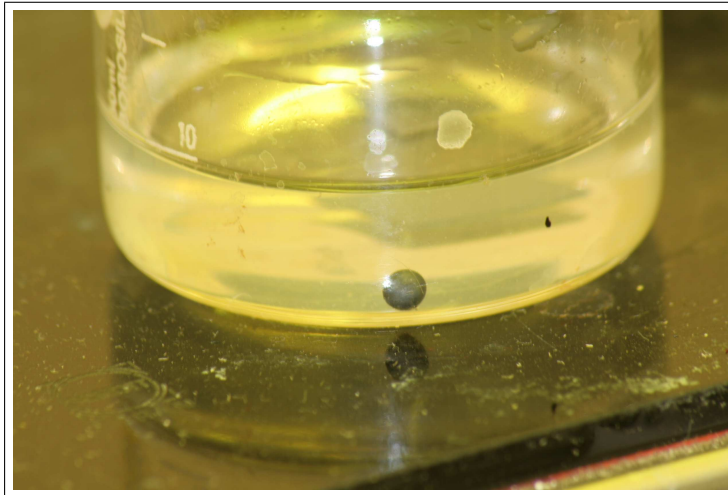


Figure 5.37: The impregnated silver tested in nitric acid

A substrate was prepared with silver and dipped in the lime sulphur, to be corroded and removed from the substrate. A kernel of silver was then left in the lime sulphur. The black covering that it obtained overnight was not removed by the nitric acid. Sulphurization thus occurred, but the strength of the solution was corroding the silver off the substrate.

The reaction accompanying impregnation at a solid-liquid interface is effected by the solution's pH and the temperature of the reaction [48], but a dilute solution did not yield decent impregnation and a heated sample caused a waxy buildup over the impregnated section.

Heating of the 50% dilute solution to 150°C did however present the required result of repeatable and decent sulphur impregnation of the silver. The setup for impregnation is seen in Figure 5.38. The results are shown in Figure 5.39, where a silver substrate is shown along with 2 silver beads, the one on the left having been submerged in the lime sulphur solution.

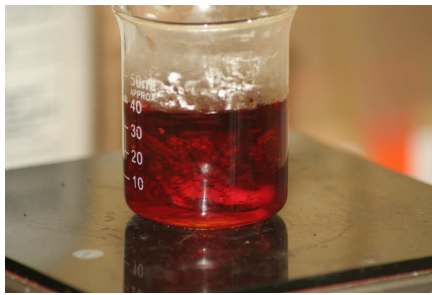


Figure 5.38: The impregnation solution and heating base

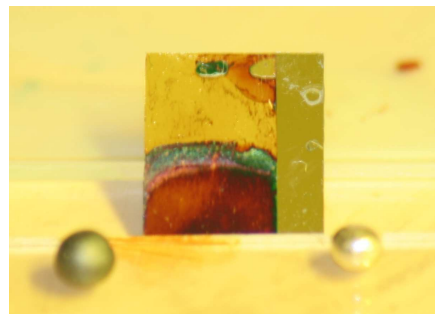


Figure 5.39: Impregnated silver samples

Further enquiry showed that blacksmiths have know for generations that lime sulphur could be used to blacken metal, for ornamental work. While the metal is usually heated and dipped in the solution, silver is an exception, requiring the solution to be heated and the metal inserted cold.

To ensure the validity of the results, a sample was taken to be scanned in the XRD. A new sample holder needed to be machined to allow the ITO samples to fit into the XRD sample holder. Exact dimensions where required to ensure the sample be flush with the external sample holder, so as to allow the X-rays direct impact on the surface and reflection to the pickup. The machined holder can be seen in Figure 5.40

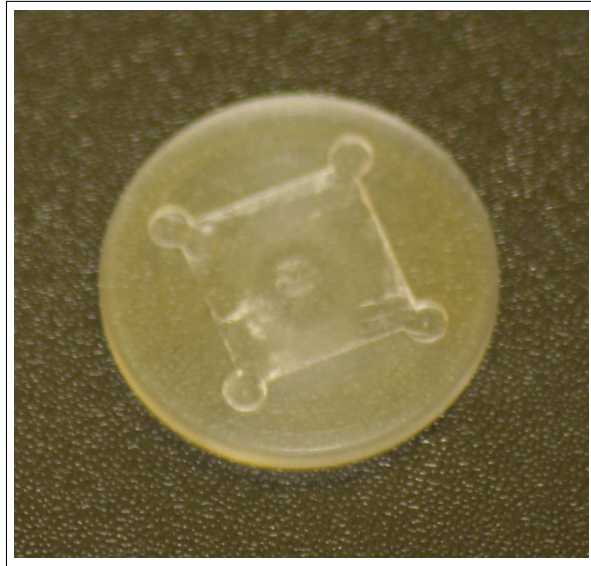


Figure 5.40: XRD sample holder

In Figure 5.41 the scanned spectrum can be seen. The relevant peaks for silver sulfide were identified and verified. An explanation of the verification of the silver sulfide and other relevant materials can be found in Addendum C.

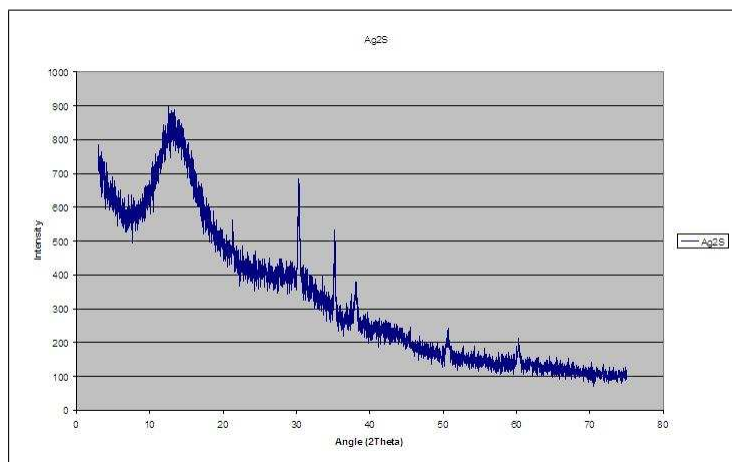


Figure 5.41: XRD results for silver sulfide development

The silver sulfide can thus be reproduced and the small 1nm thick interface can be reproduced using the organic insulator from the photoswitch, making

an AFM scratch and deposition of the controlled silver with the thermal evaporation unit.

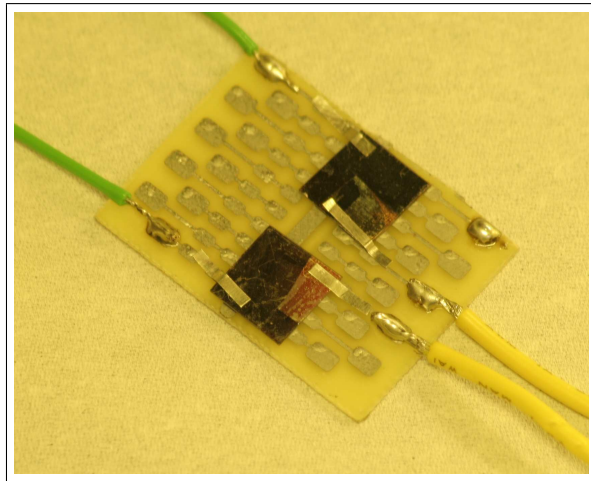


Figure 5.42: Test run device for the silver sulfide switch

Having the critical components in order, a test switch seen in Figure 5.42 was to be built, non functional, just to test the off-state characteristics of the switch. Since the platinum is very expensive, the system was to be checked to make sure it would in fact deposit the material.

Table 5.6: Material Data for Thermal Deposition (in Celsius)

Material	Melting Point	Sublimation at 10^{-5} mbar
Silver	962°C	958°C
Platinum	1772°C	1492°C
Boron	2300°C	1548°C
Palladium	1554°C	992°C
Aluminium	660°C	821°C

Some thermal evaporation data has been provided in Table 5.6 [49], with the full list available in Addendum B.

The rated temperature for platinum deposition seemed somewhat high for the available unit, so a sample was made with some available boron, having a similar deposition temperature. The thermal evaporation unit was barely

able to reach the required temperature and vacuum, at the same time glowing like a light bulb. After the annual service of the unit, could not reach the required temperature again, due to a reduction in resistance of the crucible arm. Platinum could thus not be deposited.

To find a metal with similar chemical properties as platinum, materials in group 7 of the periodic table were looked at. Palladium, being in the same column and only one row removed seemed like a promising candidate. At 992°C it is also well within the capability of the thermal evaporation unit. Purchase of the material became unnecessary when iThemba Labs donated 2g of Palladium to the project.

An XRD scan was made of a palladium deposition to ensure purity, since during thermal evaporation it releases an inordinate amount of oxygen. During the first calibration runs, the material even started to spit and catch alight due to the poor vacuum caused by its de-gasing. By allowing the vacuum to reach a level of 5×10^{-6} mbar the de-gasing problem is overcome, but the reachable temperatures only allow for thermionic deposition.

Once all the materials had been calibrated and synthesis ensured, a device was made. The parameters for the silver sulfide switch, in order, were to be 100nm silver, a 20nm insulation layer, the 1nm silver layer and 100nm palladium layer.

A primary device was made simply layering the materials, without the insulator. This was to develop a feel for the process and have a reference to the device on state. the device showed an on current of 55mA for 600mV activation voltage, hence an internal resistance of 10.91Ω. Having seen that the completed test device had through conduction, this was followed by a plan for the full device.

The silver base electrode is deposited onto the Silicon substrate and the organic insulator spun on. The sample then has a few trenches scratched into the insulator and placed into the lime sulphur for impregnation. Then to the thermal evaporation unit for deposition. The 1nm silver and 100nm palladium is done directly after one another to prevent contamination in the atmosphere. This double deposition without breaking vacuum is possible due to the two crucible modification of the thermal evaporator.

5.5 Results

In the final manufacturing procedures, all attention was given to ensure as clean a working environment as was possible. All surfaces and equipment were washed of with acetone or ethanol, depending on their requirements. Samples were treated in an acetone sonic bath and then annealed. No cross contamination of materials was allowed and all stages of production were treated with nitrogen to prevent oxidation and the occurrence of foreign particles.

Photoswitch

The last iteration of photoswitch production, yielded 3 devices of a testable calibre. A testing area was prepared around the UV exposer and 2 multimeters were acquired along with a 8V/40V power supply. The complete setup can be seen in Figure 5.43, along with a closer view of the exposure zone in Figure 5.44.

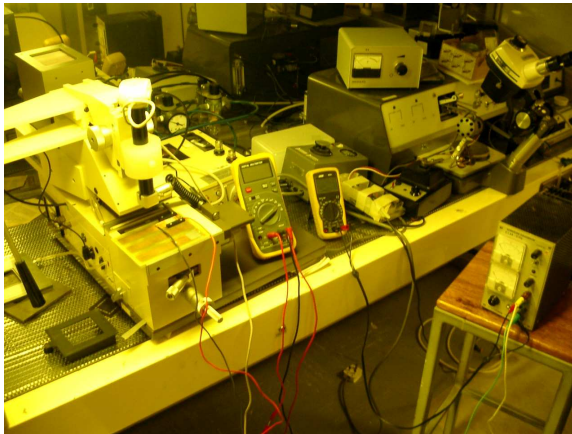


Figure 5.43: Photoswitch testing area

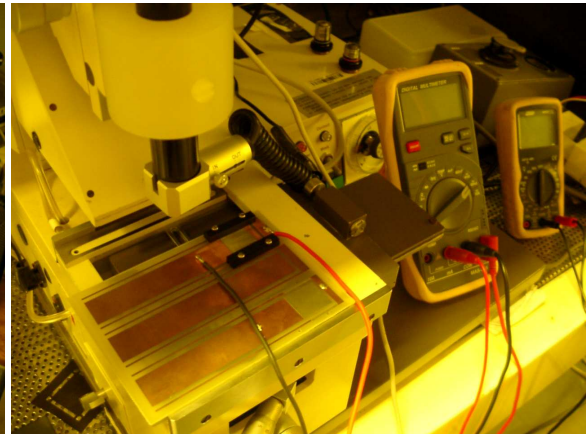


Figure 5.44: UV exposure zone

The first multimeter was used to measure the current through the device while the second was used to verify the supply voltage. All masks and covers were removed from the UV exposer.

The initial sample was placed on the test rig with an ionic water solution to ensure electrical contact. Unfortunately, due to the reactive nature of copper, water surface tension and the very thin layer of aluminium, the device's surface suffered cavitation. An image of the device, post cavitation, is given in Figure

5.45, with a microscope image of the water bubble damage in Figure 5.46. Device failure was verified when a direct ITO response was obtained from the device.



Figure 5.45: Photoswitch with water cavitation

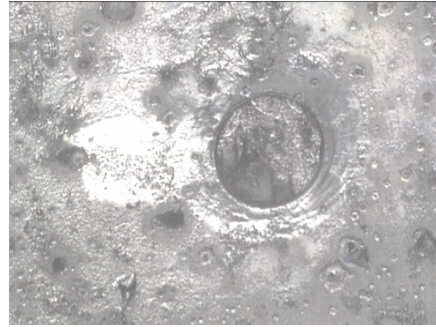


Figure 5.46: Layer damage from water drops

The second device was mounted after silver contacts were made on the test rig and the residual water removed. A reverse bias of 42mV was recorded over the ITO to aluminium electrodes, where a straight through connection would have shown a reverse bias in either direction of 80mV for the ITO.

While increasing the supply voltage, the small current leakage [28] was observed in the sub mA range. In the vicinity of 1.56 volts the current jumped somewhat, to 0.8 mA.

It was not enough to prove a definitive presence of tunnelling, so the voltage was increased to 8V where the current jumped to 0.5A and promptly lit up the device with blue sparks and resulted in device failure. The aluminium surface showed signs of variation towards the ITO contact. A microscope image of the surface transition can be seen in Figure 5.47, followed by a magnified view of the ruffled aluminium surface in Figure 5.48.



Figure 5.47: Aluminium distortion transition



Figure 5.48: Magnified view of aluminium deformation

Following the current breakthrough, a test was run on a standard ITO glass. When the power reached 4 Watts the ITO cracked due to electrical stresses. The height of the cracked sections exceeds 1 micron, making it impossible to scan with the AFM. In Figure 5.49 the device and ITO glass that underwent arcing can be seen, along with a microscope image of the ITO cracking in Figure 5.50.

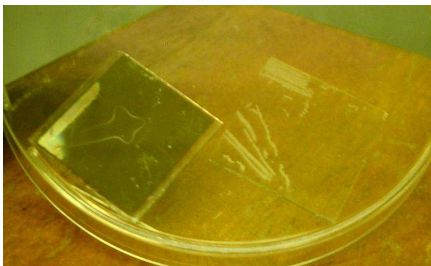


Figure 5.49: Arc damaged samples

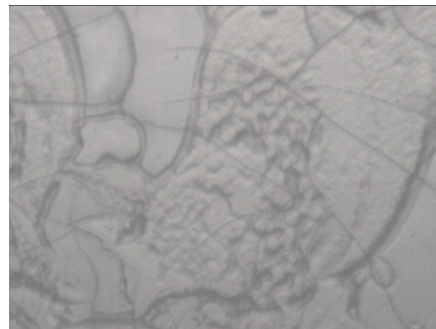


Figure 5.50: Magnified ITO fractures

The final device was then mounted on the test rig with only touch contacts. Diode testing showed a reverse bias of 35mV. The current was then increased to the initial current jump to activate the metal tunnelling. From 2.0V up to 2.5V a gradually speeding increase of current could be seen as, theoretically, tendrils penetrated the organic layer. Reducing the input voltage to 0.5V, the sample was exposed to UV light after which the 200mA current vanished.

A deviation from the relevant literature at this point was that, to rearm the device, the voltage needed to be ramped up to 1V to reinitialise the metal

filaments for current flow, after which the UV again reduced the current to zero.

After 7 runs of switching, however, the device also failed due to condensation from the UV exposer.

The voltage span of 0.5V to 1V for metal filament growth and switching follows the expected behaviour. Also, the current achieved was congruent with similar devices in the literature. Unfortunately the actual off-state current could not be measured since it should be in the pico ampere range, but a definite off-state was evident.

Although tenuous, the fabricated switch configuration thus was operational and showed repeatable switching.

Silver Sulfide Switch

Two devices were produced using the techniques developed during the previous section. Additionally, a calibration sample was included with the production sample at every thermal evaporation step to ensure accurate layer thicknesses, particularly during the 1nm silver deposition.

For the palladium deposition, a powder crucible was used instead of the slug crucible used previously. The powder crucible has a higher resistance, hence a higher temperature can be achieved, even melting the palladium.

To test the silver sulfide switches they will be placed on a test rig with a 600mV activation voltage applied, positive to the palladium. If the switch turns off, without it being due to device failure, the reverse voltage should reactivate the switch.

Neither switch functioned. While both were conductive and showed a 0.06mA current through the device and the bias resistor, no switching was evident. After the application of a increased activation pre-biasing, for approximately an hour, the devices did show a 10% drop in their current.

Possible reasons for the device failure, from the available data, are material or interface problems. The material problems may explain why there is no switching and could be as a result of the palladium or the silver sulfide.

Issues arising from the palladium are that it is a substitute for platinum, and while having the same valence electrons and characteristics, may not share all of its properties. While sulphur penetration was verified on the switch samples, the penetration depth and molecular configuration from the impregnation method used may be non-conductive to this type of switching.

From the slightly reduced current flow after extended biasing, however, it would seem that some electrolytic processes took place. This moves the problem towards the material interfaces. While the active silver layer is 1nm thick, the length and width of the contact trenches may be too large. Where the existing device had contact areas of $100\text{nm} \times 100\text{nm}$, the trenches made on the AFM were $9\mu\text{m} \times 2\mu\text{m}$. This equates to an area variation in the order of 10^3 , which affects the volume of material to be absorbed.

Another possibility is impurities within the trenches, either from dust or residual photoresist from the scratching process. This may be overcome by milling, but the effects on the organic layer must then be tested as well, in order to confirm no adverse effects on the insulation.

5.6 To Summarise

In this chapter the origins of the cleanroom were related, as well as giving a list of the facilities available there and explaining the use of the more prevalent equipment.

The method used to choose the switches for manufacture was discussed and shown along with the reasoning behind the portions of work to be undertaken.

Following this preamble, the iterative design and manufacture processes for the photoswitch and silver sulfide switch was shown. This covered the initial research, the test switches and solving of the resulting manufacturing obstacles.

The final devices were then characterised and manufactured, the testing of these devices was recorded comprehensively to show the problems encountered in the verification process.

Of the two switches, the photoswitch was found to be a complete success, while the silver sulfide switch only showed signs of possible silver absorption. Some suggestions were given as to possible problems in the device, as well as ways that they may be overcome.

Chapter 6

Simulation

The side-clamped nanoelectromechanical device configuration, seen in Figure 6.1, has become prevalent in the field of nanotechnology, being used for disease detectors, cancer treatment, catalyst improvement and beyond.

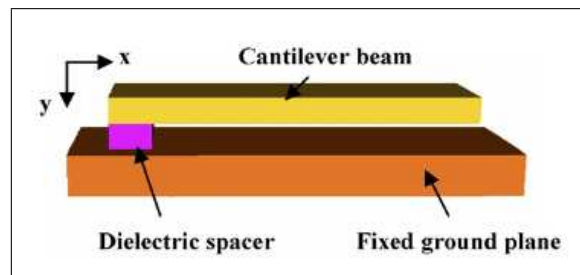


Figure 6.1: Schematic of a cantilever switch [50]

Since it is such a far reaching design, this switch type cannot be ignored. While not being able to produce switches of this type, their simulation is equally important, in order to predict their responses, and most importantly, predicting device failure.

Simulation code will therefore be written to emulate the bending and shifting in CNT cantilever switches in order to predict failure from the device geometry.

6.1 CNT Simulation Theory

The analysis of a NEMS structure involves the mechanical analysis of the structure, as well as the electrostatic analysis. Usually these type of mechanical structures would be analysed using molecular dynamics (MD) models. Due to the relatively large size of the CNT cantilever switch and the large number of atoms involved, however, it will be too time and computation intensive.

Elastostatic models from the continuum mechanics theory have been widely used for the analysis of microstructures, and with a few modifications for quantum effects and material adaptation, are viable for NEMS analysis [51].

In standard elastostatic theory, the relation between a material's stress (σ) and strain (ϵ) is given by Equation (6.1) [52]. The relating constant E is Young's modulus, but due to small scale effects, like reduced material imperfections and close range adhesion, this relationship changes in the nano regime. Two ways to compensate for this is by including the small scale parameter correction e_0a [53] or by modifying the material parameters to reflect these changes.

$$\sigma(x) = E\epsilon(x) \quad (6.1)$$

$$\sigma(x) - (e_0a)^2 \frac{d^2\sigma}{dx^2} = E\epsilon(x) \quad (6.2)$$

$$(6.3)$$

Both the material parameters and e_0a are obtained from experiments and MD simulations. The new form of the stress-strain equation is given by Equation 6.2.

The equilibrium requirements of the static states are given by Equations (6.4) and (6.5), where q is force, Q is the shear force in the beam and M is the bending moment. From this the relationship between force and moment can be derived, as seen in Equation (6.6).

$$-q(x) = \frac{dQ}{dx} \quad (6.4)$$

$$Q = \frac{dM}{dx} \quad (6.5)$$

$$q = \frac{d^2M}{dx^2} \quad (6.6)$$

The deflection (y) of the beam can be related to the strain by means of a relation constant in the form of Equation (6.7).

$$\epsilon = -z \frac{d^2y}{dx^2} \quad (6.7)$$

Now, by substitution of Equation (6.7) into Equation (6.2), the non-local constitutive Equation (6.8) [53] is obtained. This, along with the equilibrium equations, can be used to derive the governing equation of the nanobeam, given in Equation (6.9).

$$M(x) - (e_0a)^2 \frac{d^2M}{dx^2} = -EI \frac{d^2y}{dx^2} \quad (6.8)$$

$$\frac{d^4y}{dx^4} = \frac{q}{EI} - \frac{(e_0a)^2}{EI} \frac{d^2q}{dx^2} \quad (6.9)$$

Here I is the second moment of area, which, together with Young's modulus, form the rigidity of the beam. Now, using the beam property that shear stress is the derivative of the beam moment, which is the second derivative of the beam deflection [52], the bending and shear force equations can be derived.

$$M(x) = -EI \frac{d^2y}{dx^2} - (e_0a)^2 q(x) \quad (6.10)$$

$$Q(x) = -EI \frac{d^3y}{dx^3} - (e_0a)^2 \frac{d^2q}{dx} \quad (6.11)$$

This covers the mechanical aspects of the system, which leaves the electrostatic portion. This part of the analysis actually contributes the force, as

can be seen in Equation (6.12). F_e is the electrostatic force and F_n is a force derived from the small scale parameter, dependant on the size of the device.

$$q = F_e + F_n \quad (6.12)$$

$$F_e = \frac{\epsilon_0 w V^2}{2(g-y)^2} \left(1 + 0.65 \frac{g-y}{w}\right) \quad (6.13)$$

$$F_n^w = \frac{Aw}{6\pi(g-y)^3} \quad (6.14)$$

$$F_n^c = \frac{\pi^2 \hbar c w}{240(g-y)^4} \quad (6.15)$$

Here, ϵ_0 is the permittivity of a vacuum, A is the Hamaker constant, w is the beam width, V is the applied voltage, g is the electrode to beam gap and c is the speed of light.

The F_n variances F_n^w and F_n^c are the Van der Waal's forces and Casimir forces per unit length of the beam respectively. When the gap between the beam and the fixed electrode is smaller than 20nm, F_n^w is used, while for gaps larger than 20nm, F_n^c is used [50].

In MEMS and NEMS cantilever devices, the critical phenomenon of pull-in must be observed. This refers to the voltage at which the nanobeam will separate and end device functionality. Additionally, for NEMS devices, the effect of intermolecular forces may cause failure even when no voltage is applied, depending solely on device geometry [50].

6.2 Implementation of Simulation Theory

Both forms of electrostatic modeling yield non-linear equations for the distributed load, therefore complicating the solution of the 4th order derivatives required to solve for the cantilever systems. The material adaptation method, however, while neglecting fringe effects, yields empirical solutions for the critical device constraints of pull-in voltage, maximum beam length for off- and on-states as well as minimum gap height.

Work done by Asghar Ramezi *et al* [50] and J Yanget *al* [53] shows that, neglecting the fringe effects in the simulation, reduces the voltages by 40%, making them less optimistic, and adding further device protection. Also, a measure of fringe theory was included in the geometry constraints since, without the electrostatic intermolecular interaction, they could not be derived at all. After analysis of the pull-in voltages yielded by this method, it was found that at nanoscale the small scale parameter needs to be included here as well, since the molecular interactions become very important to the force calculations.

The equations obtained to predict nanobeam device failure are shown below. The pull-in voltage is given by.

$$V_{PI} = \frac{e_0 a}{L} \sqrt{\frac{3.654g^3 EI}{\epsilon_0 w L}} \quad (6.16)$$

and the Casimir force geometry restrictions by.

$$L_{max}^{on} = g \sqrt[4]{\frac{20.498gEh^3}{\pi \hbar c}} \quad (6.17)$$

$$L_{max}^{off} = \frac{8}{5} g \sqrt[4]{\frac{2gEh^3}{\pi^2 \hbar c}} \quad (6.18)$$

$$g_{min} = \sqrt[5]{\frac{\pi^2 \hbar c L^4}{20.498Eh^3}} \quad (6.19)$$

Lastly, Van der Waal's force geometry restrictions are given by.

$$L_{max}^{on} = \sqrt[4]{\frac{0.657\pi Eh^3}{A}} \quad (6.20)$$

$$L_{max}^{off} = \frac{1}{2}g\sqrt[4]{\frac{27\pi Eh^3}{4A}} \quad (6.21)$$

$$g_{min} = L\sqrt[4]{\frac{A}{0.657\pi Eh^3}} \quad (6.22)$$

In Figure 6.2, the pull-in voltage V_{PI} can be seen for a CNT nanoswitch of length 180nm, gap height of 20nm and consisting of a SWNT. The simulation was modelled over a series of nanotube widths from 10nm to 90nm. The wall thicknesses were varied to reflect the corresponding nanotube diameters.

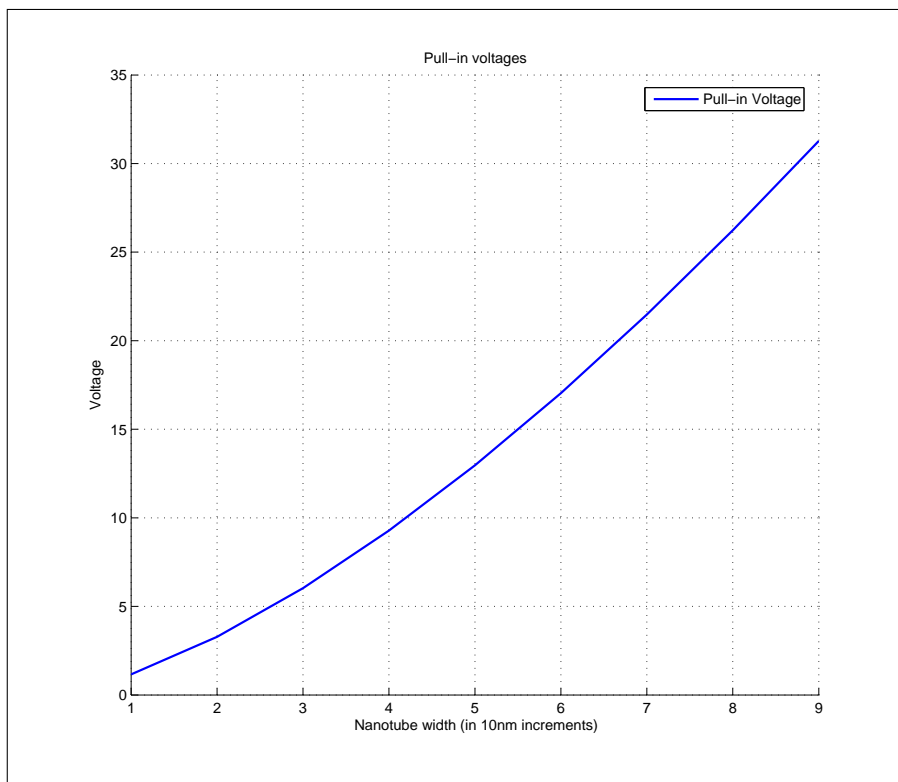


Figure 6.2: Graph of the pull-in voltages as a function of geometry

As can be expected, the voltage required to bend the nanotube increases as the diameter and increasing wall diameter increase its stiffness.

In Figure 6.3, the maximum CNT length, L_{max} , is shown for when there is an applied voltage, and when there is none.

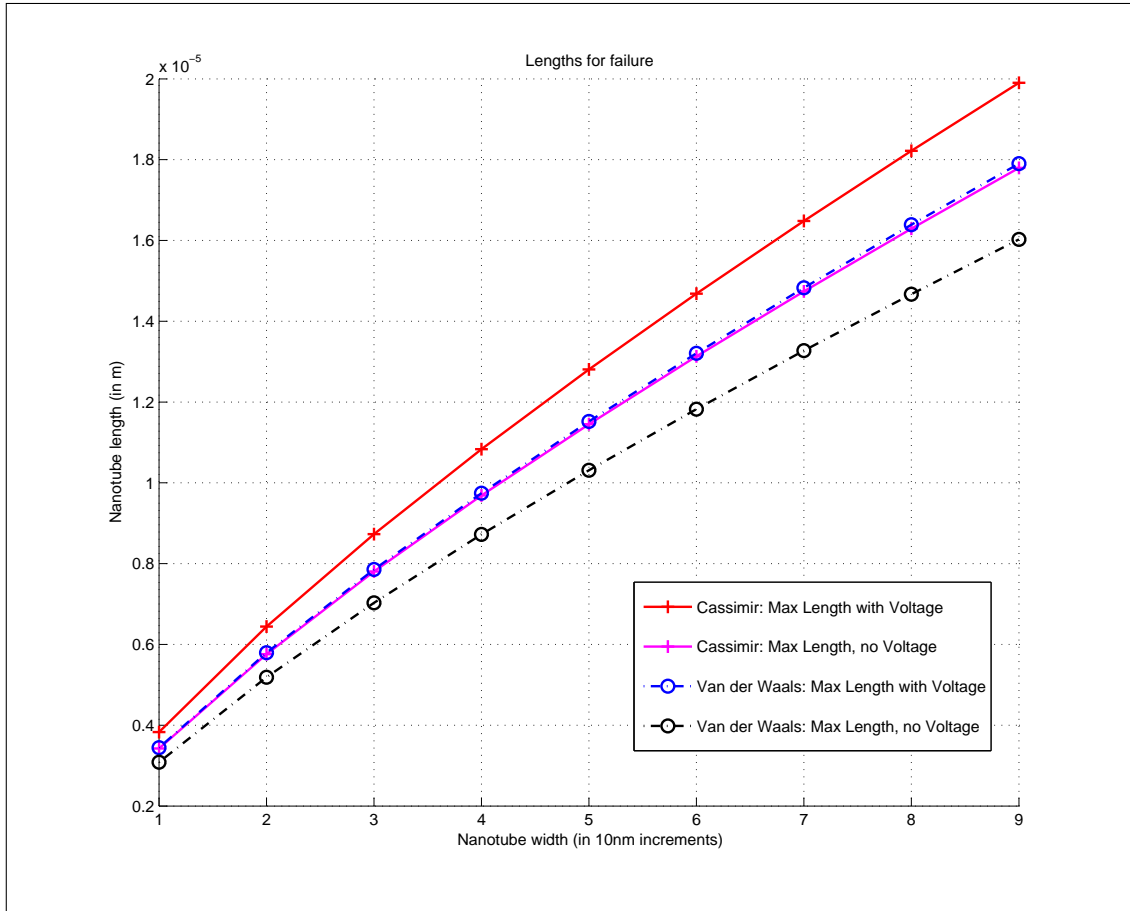


Figure 6.3: Graph of the nanotube lengths as a function of nanotube diameter

The differing values caused by the Casimir and Van der Waal's forces are also shown. Once again, the result reflects the increased strength of the thickening nanotubes. Longer nanotubes can thus be used without fear of collapse.

Lastly, the gap height, g_{min} , is plotted in Figure 6.4, showing an allowable decrease in gap height for larger, thicker nanotubes.

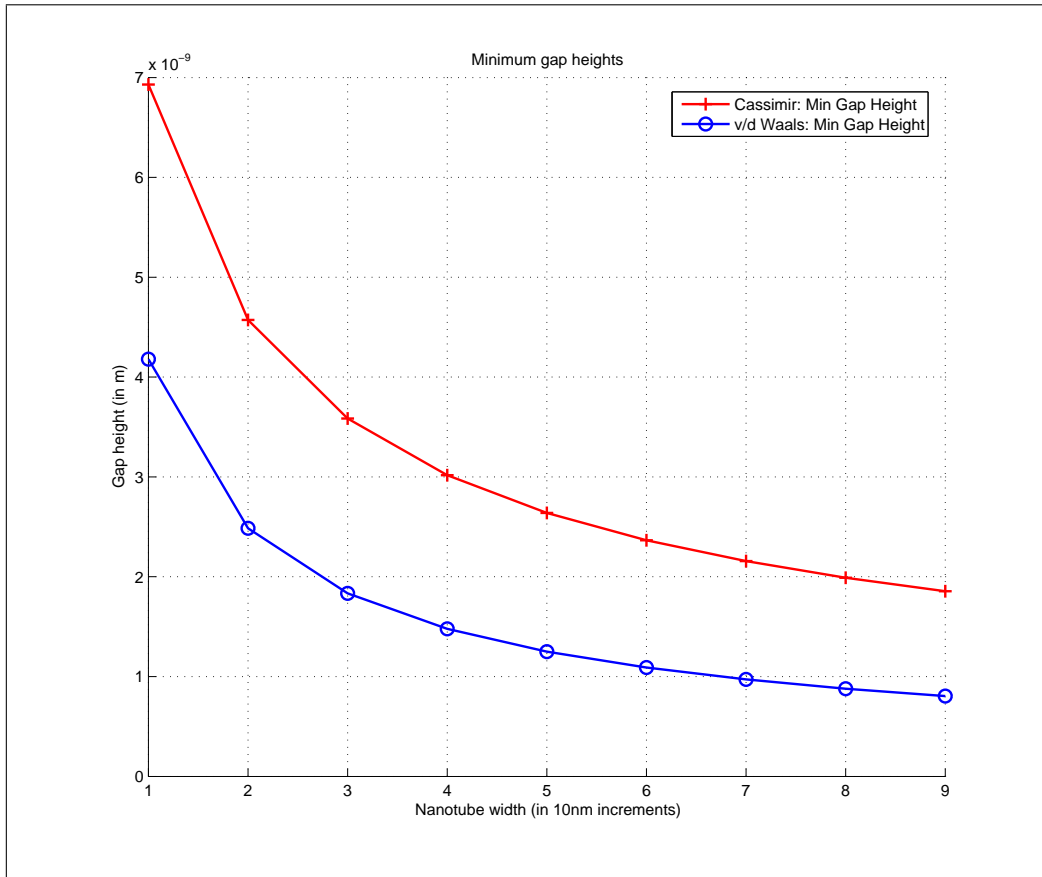


Figure 6.4: Graph of the gap heights as a function of nanotube diameter

The small scale parameter model was also eventually simulated, in order to compare the results of the modified empirical solution with the intermolecular effect model. In Figure 6.5 the raw data of the empirical and simulated models are shown. The pull-in voltages were compared for ranges of lengths and widths.

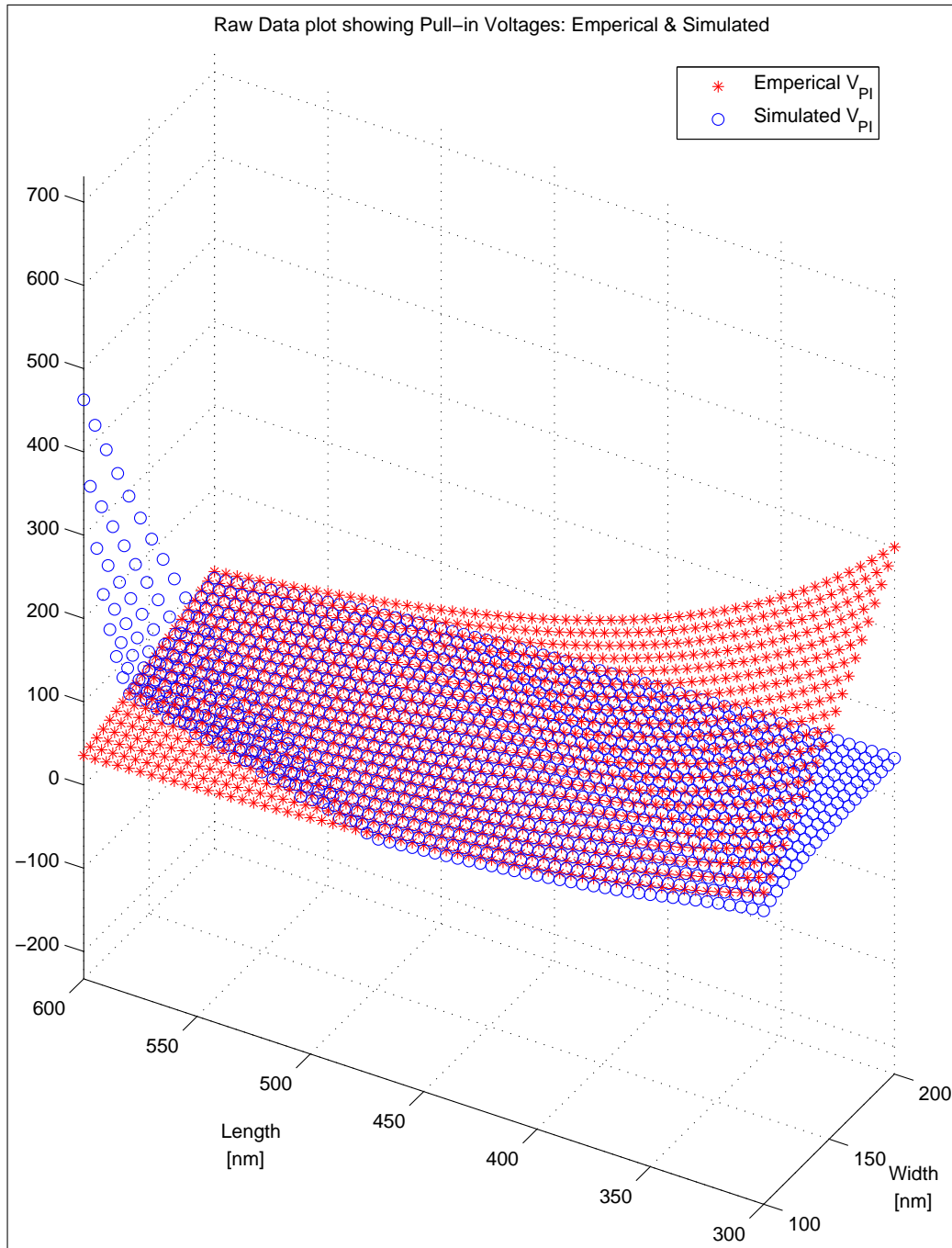


Figure 6.5: Raw data from the empirical and small scale parameter methods

From this data it can be seen that there is a region where the two methods correspond well, but at long lengths and narrow widths, as well as at short lengths and wide widths, the results deviate from one another.

In Figure 6.6 the difference of the results are shown as a percentage of the small scale parameter results. To aid in visual interpretation of the values, the surf plot has been scaled to reflect the dimensions of the cantilever switch.

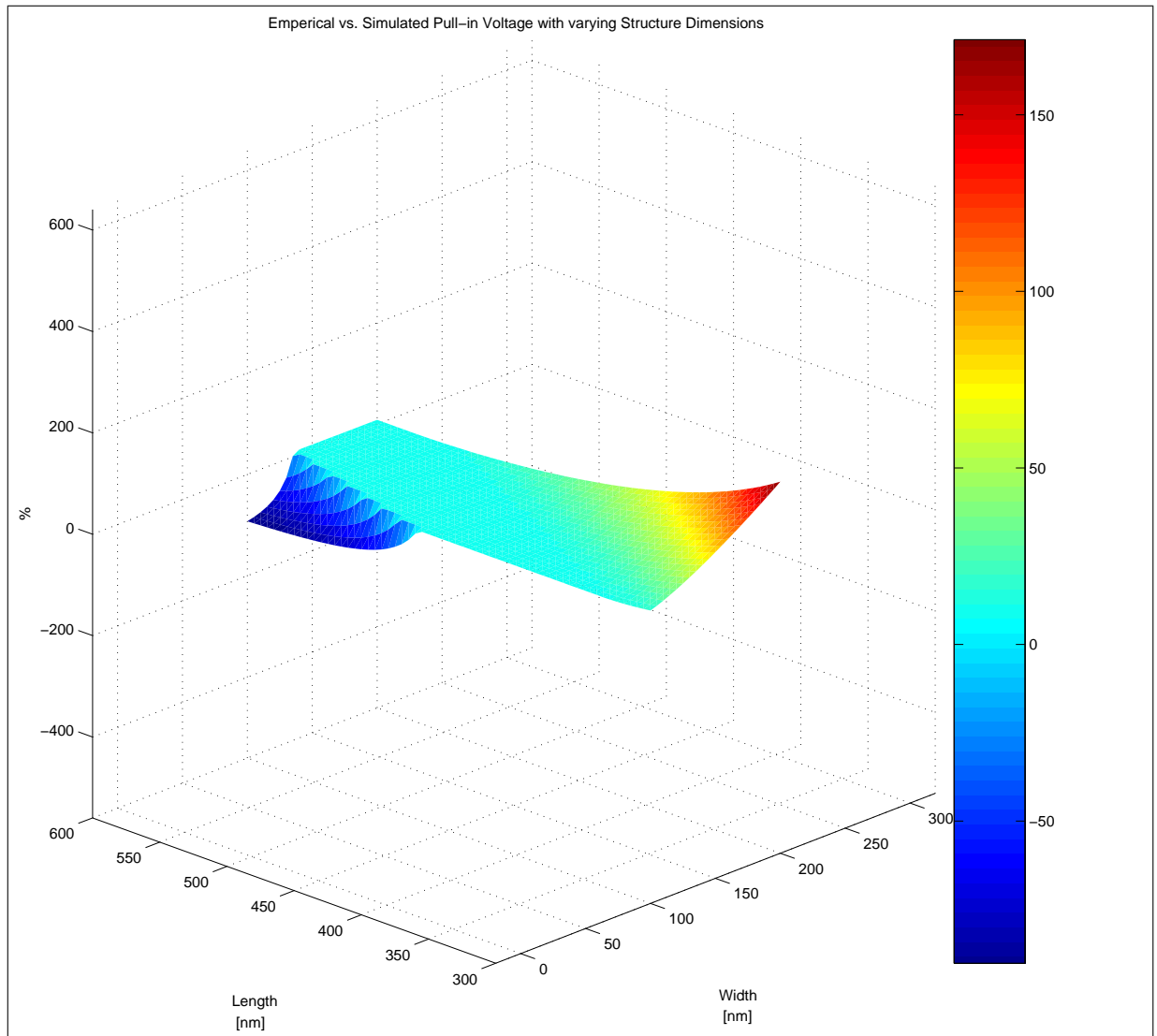


Figure 6.6: Surf plot of the error percentage of the two simulation models

Figure 6.7 shows the results as a contour plot, from which it can be seen that a large portion of the ranges simulated are within a 10% tolerance. The deviations for narrow and stubby cantilevers are understandable, since for long structures the intermolecular forces play a bigger role, while for short structures the beams become rigid.

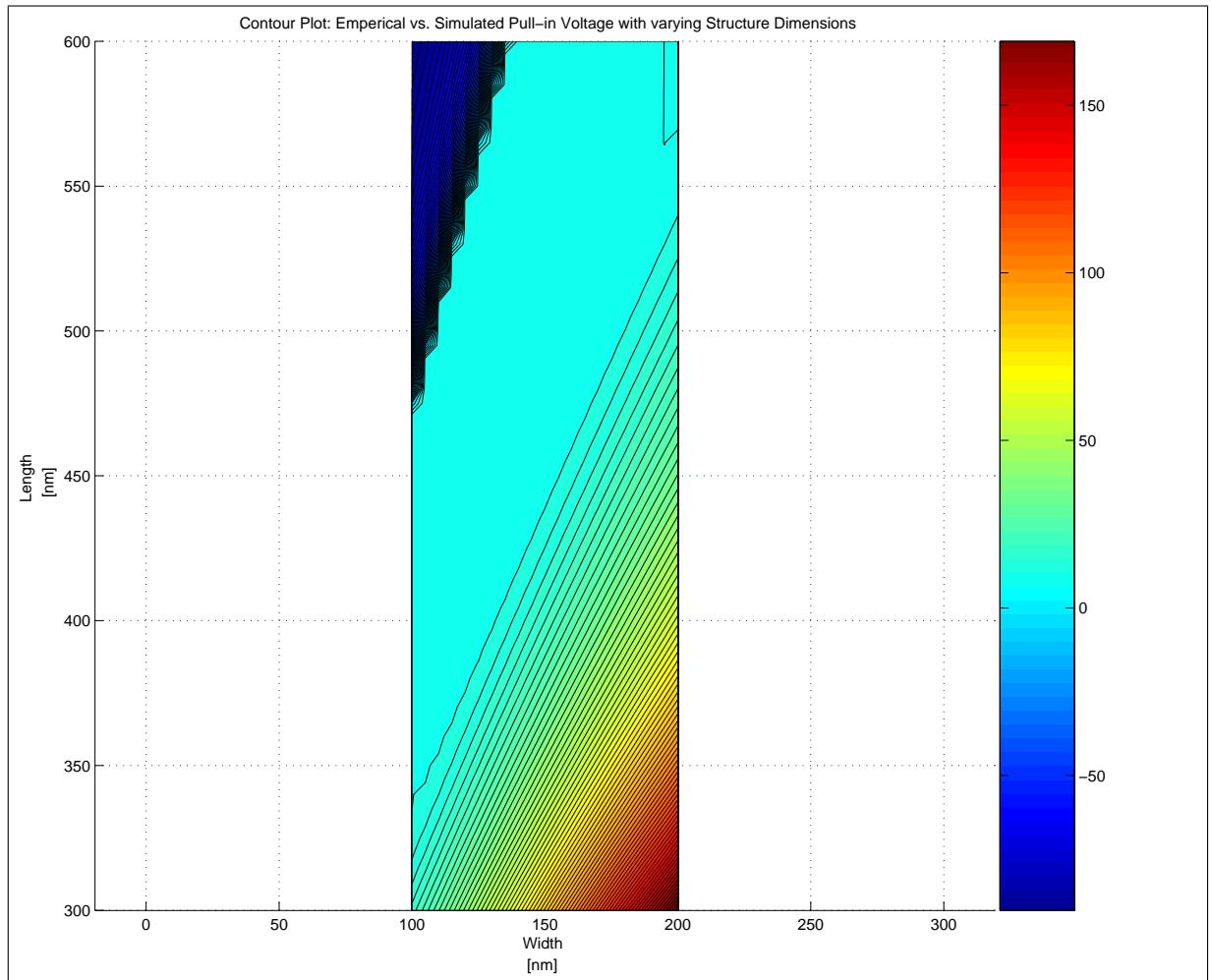


Figure 6.7: Contour plot of the two simulation's error function

The results obtained were for the most part close to results obtained in the literature. The deviations being only slight. Some of the results, however, are not yet testable in a laboratory environment due to manufacturing restrictions. An example is a gap height of less than 10nm. While this is accurate, for a first degree approximation, the current achievable gap height for successful synthesis is 15nm. For a while then, theory yet remains ahead of technology.

From the comparison of the empirical and small scale parameter models it was seen that for devices where the length is in the region of four times the width, the simpler empirical simulation methods yields adequate results. For more complicated, longer or stubbier structures, however, more complex techniques are required.

6.3 To Summarise

The elastostatic model was discussed and ways of implementing it shown. The founding equations having been given, the advantages and disadvantages of implementing either were made apparent.

Having motivated the method used for the simulation, code was written for simulation of failure in cantilever nanoswitches. Once the results had been verified, the code was expanded for use with CNT cantilever switches. The obtained results were shown and correlated with results obtained from external research.

A more complex and accurate method also developed for the simulation of CNT switches. This method was compared to the empirical method and it was found to yield similar results for simple nanostructures, having a ratio of four between its length and width. It must be said, however, that the complex method is more reliable, being more accurate over the entire spectrum of sizes.

Chapter 7

Conclusion

It has been shown that the microelectronics laboratory at the Electrical and Electronic Engineering Department of Stellenbosch University has a wealth of nanomanufacturing resources at its disposal. A section that was recently founded, the Superconducting and Nanodevices (SAND) group, aim to make use of these facilities to spearhead the growing movement into their fields in South Africa.

An extensive literature study led to the choice of appropriate switches and simulation candidates. During the iterative design process, the manufacturing obstacles were addressed and annotated.

A functioning photoswitch was developed, and while it may have proven fragile, it can be reproduced in a simple and cost effective manner. The silver sulfide switch is an ongoing project, since it was not brought to a final working product. Results did however show a strong possibility of success with a few improvements and changes.

The methods developed to address the challenges encountered during the manufacturing of these two devices contributed a new facet to the repertoire of the cleanroom. Like the spinning on of organic insulators, characterised spinning times and the expansion of the aqueous solution fabrication techniques.

Some of the problems in the development phase might have been foreseen earlier, however, double checking every possible source of error is not practical. As a result, a balance between good engineering practice and reasonable faith in accuracy of supplies and functionality of equipment must be found.

The microelectronics laboratory has exceptional equipment, many of which were constructed or modified in house over the years and through the evolution

of the facility. An important part of the investigation was to ensure that equipment and facilities in the cleanroom were at an acceptable level. This helped to become familiar with the equipment and protocols of the laboratory. Yet there is still an above average amount of dust and contaminants. The filters, meant to be changed twice a semester, are only changed every second year due to the inordinate cost of the materials needed. This should not be a cause of concern, however, since the practical experience this grants, as well as the good lab practice this enforces is highly beneficial.

Considering the wealth of instruction, work and innovation already taking place within the lab, the possible improvement to device fabrication would bolster progress immensely.

Simulations undertaken for the prediction of failure in cantilever style nanostructures, showed the myriad of approaches and views on sub-micron physics models. While results were obtained with correlation to literature and experiments, they are restricted to areas where their assumptions hold true, as could be seen in the comparison of the two simulation techniques that were developed.

The quantum mechanical model is certainly the most effective, closely followed by the molecular dynamics methods, to the point where the only choice between them is dependant on the size of the simulated system. The computational cost is their only restriction.

For this initial approach to the design and manufacture of nanoswitches, however, only an approximation that basically agrees with synthesised devices is desired. Therefore the models developed should be used to do a first design iteration and then if more accurate results are required, these first level optimisations can be used to reduce the number of advanced simulations required with the MD or quantum methods.

As the quality of the manufactured devices improve, higher order simulations will become more applicable, as the variances in the devices can be controlled and contribute to its functionality.

The successes achieved during this investigation are not to be seen as with the completion of the theme. Crystalline effects of different infusion methods, material specific properties and studies of the viscous effects of multi-polymer suspensions are only a few of the questions arising peripherally to the work in this report.

While this is an end, it is also just another small step amongst the fields of mountains that atoms are.

Appendices

Appendix A

Clean Room

A.1 Servicing Procedure

Daily:

1. Replace entrance mat
2. Wash rubber mats.
3. Switch on de-ionised water pump if required.
4. Check air pressure. If low go switch pump up.
5. Make sure battery charger is working at 13.8 volts.
6. Check that alarm system is working. Run lamp test procedure and check for broken warning lights.
7. Open gas room. Check canister pressures.
8. Empty rubbish bins.
9. Clean where necessary.
10. Check and clean the tables and work stations.
11. Clear the Roster.
12. Replace dirty overshoes.
13. Decant H₂SO₄, H₂O and any other chemicals required for the clean room.

14. Reverse process for closing procedure.

Biweekly:

1. Vacuum clean the clean room
2. Vacuum clean the changing room
3. Clean and vacuum the wash room en chemical room
4. Clean the thick film laboratory and remove rubbish bins

Weekly:

1. Wash the dirty overcloths. Do not include the blue overshoes.
2. Replace the washable filters.
3. Take pressure measurements on the cleanroom gas systems.

Monthly:

1. Check all filters and replace where necessary.

A.2 Clean room Rules and Regulations

Two things Kill IC's: dust and chemical contamination. The object of the following regulations is not to make life unpleasant for the staff of the laboratory, but to ensure good yields of working devices. If all users of the laboratory adopt a positive attitude towards contamination control we will achieve this goal.

1. THINK!!! A small, careless action such as touching a wafer with a finger can cause disaster. To produce working devices requires all your attention - to produce duds is easy.
2. Wear the specified clean room clothing in the correct manner.
3. Keep hands, fingernails and face clean.
4. Do not scratch your face, comb your hair or rub your hands together.
5. No eating, drinking, chewing of gum or smoking allowed.
6. Do not carry excessive numbers of personal items into the laboratory, e.g. keys, combs, cigarettes, books, etc.
7. WORK NEATLY! If you spill something wipe it up. Pack all items (e.g. chemicals, beakers, instruments, etc) away after use. The laboratory is cleaned daily - tables cannot be cleaned when cluttered up. Always leave your workplace as you would hope to find it.
8. Throw all rubbish (e.g. used paper towels, dud wafers, etc) away regularly.
9. Keep all instruments, equipment and laboratory ware as clean and orderly as possible.
10. Wear protective clothing as follows: (i) Handling of dry wafers, quartzware, sputter targets, wafer carriers, masks: woven nylon gloves. (ii) Handling of wafers and masks during wet processing: rubber gloves or disposable plastic gloves (also protective face masks when working with dangerous mixtures).

11. No erasers or pencils must be used in the clean room - felt pens and ballpoint pens are acceptable.
12. All process recipes and operating instructions are to be kept in plastic folders, to minimize dust and to protect the documents. Notes may be made on the folders with a pen.
13. A "dirty" area has been designated in the laboratory. This is the ONLY place where books and loose papers may be used.
14. Two types of cleaning material are provided - the BLUE paper is a highly absorbent material for mopping up spills. It produces some lint and should NOT be used for wafers and masks. The WHITE material is a low-lint wiper suitable for dry cleaning of wafers and masks.
15. No large amounts of chemicals should be stored in the clean room. Chemicals can be decanted daily if necessary.
16. A clean set of tools is kept inside the clean room. If you need other equipment CLEAN IT THOROUGHLY before bringing it inside. After you have worked on a machine, clean up using appropriate solvent and the vacuum cleaner.
17. Observe all administrative procedures such as marking of wafer batches and masks.
18. All wafers and masks must be transported in closed boxes from one laminar flow area to another.

PERSONS CONTRAVENING THESE REGULATIONS ARE LIABLE
TO BE BARRED INDEFINITELY FROM THE LABORATORY

A.3 Personnel Entrance Procedure

1. Read all notices on the outer door before entering.
2. Type in the correct code while holding in the large button. This will disengage the electric lock and the door can be opened. (The code is changed every month but this may be done more regularly for security reasons.)
3. Wipe your feet and enter the laboratory.
4. Walk on the sticky blue mat.
5. Take of any thick clothing, such as jackets and jerseys.
6. Put on the blue overshoes and enter the changing room. Personnel that are going to work in the chemical or washing room must put on lab coats (and gas masks and gloves if dangerous chemicals are going to be used).
7. Enter the changing chamber and put on the white overshoes, over the blue overshoes, while climbing over the partitioning.
8. Take your own Clean room clothes out of the cupboard.
9. The correct order of dressing in the clean room cloths is cap, suite and then gloves if necessary.
10. Pull the shower lever with your left hand, while the right hand rests on your hip (10 seconds). Turn around and repeat the procedure, this time pulling the lever with your right hand (10 seconds).
11. You may now enter the clean room. Please note the General Clean Room Rules.

A.4 Emergencies

1. It is vital that all users of the laboratory are thoroughly acquainted with the hazardousness of the chemicals in use. Complete information on these substances is available. Study this information and make sure that you know what to do in case of an accident. A local general practitioner, Dr. K.H.C von Delft has made a study of the treatment of poisoning by these substances. In case of an accident he is to be summoned together with the ambulance.

TELEPHONE NUMBERS

Ambulance : 3444

Dr. Von Delft : 72820

After hours : 72870

2. IF YOU ARE IN SERIOUS DIFFICULTY, PRESS ANY OF THE RED BUTTONS ON THE WALL ABOVE THE BENCHES.
This will trigger the emergency alarm. If you are outside the laboratory and you hear this alarm (wah-wah sound), immediately enter to render assistance.
3. If there is a H₂ leak, the alarm at the LEYBOLD HERAEUS RF sputtering unit will sound. Leave the room immediately, switching the main power supply off at the switchboard.
4. In case of fire, the red LEDs in the roof-mounted sensors will come on, as well as the alarm at the epitaxial reactor. The alarm in the passage will also sound. Fire extinguishers are available under the benches. The FIRE BRIGADES's number is 71333.

Appendix B

Deposition Materials

The following tables show the properties of the deposition materials as discussed in this investigation:

Materials Guide for Thermal Evaporation

Adapted from Kurt J. Lesker Co. (rows for nonmetallic materials are hidden)

http://www.lesker.com/newweb/menu_evapsources.cfm?CFID=180535&CFTOKEN=48466901§ion=materialeptable&init=skip

Key of Symbols

* influenced by composition ** Cr-plated rod or strip *** All metals alumina coated Ex = excellent G = good F = fair P = poor S = sublimes D = decomposes C = carbon Gr = graphite
Q = quartz Incl = Inconel VC = vitreous carbon SS = stainless steel

Material	Formula / Symbol	MP (°C)	Sublime / Decompose	ρ (g/cm ³)	Temp. (°C) for Given Vap. Press. (Torr)			Thermal Sources			Comments
					10-8	10-6	10-4	Boat	Coil	Basket	
Aluminum	Al	660		2.70	677	821	1010	TiB ₂ , W	W	W	Alloys and wets. Stranded W is best.
Aluminum Antimonide	AlSb	1080		4.30	-	-	-	-	-	-	-
Aluminum, 2% Copper	Al2%Cu	640		2.82	-	-	-	-	-	-	Wire feed and flash. Difficult from dual sources.
Aluminum, 2% Silicon	Al2%Si	640		2.69	-	-	1010	-	-	-	Wire feed and flash. Difficult from dual sources.
Antimony	Sb	630	S	6.68	279	345	425	Mo,*** Ta***	Mo, Ta	Mo, Ta	Toxic. Evaporates well.
Barium	Ba	725		3.51	545	627	735	W, Ta, Mo	W	W	Wets without alloying reacts with ceramics.
Beryllium	Be	1278		1.85	710	878	1000	W, Ta	W	W	Wets W/Mo/Ta. Powder and oxides toxic. Evaporates easily.
Bismuth	Bi	271		9.80	330	410	520	W, Mo, Ta	W	W	Toxic vapor. Resistivity high. No shorting of baskets.
Boron	B	2300		2.34	1278	1548	1797	C	-	-	Explodes with rapid cooling. Forms carbide with container.
Cadmium	Cd	321		8.64	64	120	180	W, Mo, Ta	-	W, Mo, Ta	Bad for vacuum systems. Low sticking coefficient.
Cadmium Antimonide	Cd ₃ Sb ₂	456		6.92	-	-	-	-	-	-	-
Calcium	Ca	839	S	1.54	272	357	459	W	W	W	Corrodes in air.
Carbon	C	-3652	S	1.8-2.1	1657	1867	2137	-	-	-	E-beam preferred. Arc evaporation. Poor film adhesion.
Cerium	Ce	798		-6.70	970	1150	1380	W, Ta	W	W, Ta	-
Cesium	Cs	28		1.88	-16	22	80	SS	-	-	-
Chiolote	Na ₅ Al ₃ F ₁₄	-		2.90	-	-	-800	Mo, W	-	-	n = 1.33
Chromium	Cr	1857	S	7.20	837	977	1157	**	W	W	Films very adherent. High rates possible.
Cobalt	Co	1495		8.90	850	990	1200	W, Nb	-	W	Alloys with refractory metals.
Copper	Cu	1083		8.92	727	857	1017	Mo	W	W	Adhesion poor. Use interlayer (Cr). Evaporates using any source material.
Dysprosium	Dy	1412		8.55	625	750	900	Ta	-	-	-
Erbium	Er	1529	S	9.07	650	775	930	W, Ta	-	-	-

Europium	Eu	822	S	5.24	280	360	480	W, Ta	-	-	Low tantalum solubility.
Gadolinium	Gd	1313		7.90	760	900	1175	Ta	-	-	High tantalum solubility.
Gallium	Ga	30		5.90	619	742	907	-	-	-	Alloys with refractory metals. Use E-beam gun.
Germanium	Ge	937		5.35	812	957	1167	W, C, Ta	-	-	Excellent films from E-beam guns.
Gold	Au	1064		19.32	807	947	1132	W	W	W*** Mo***	DC, RF, Films soft, not very adherent.
Hafnium	Hf	2227		13.31	2160	2250	3090	-	-	-	-
Holmium	Ho	1474		8.80	650	770	950	W, Ta	W	W	-
Inconel	Ni/Cr/Fe	1425		8.50	-	-	-	W	W	W	Use fine wire wrapped on tungsten. Low rate required for smooth films.
Indium	In	157		7.30	487	597	742	W, Mo	-	W	Wets tungsten and copper. Use molybdenum liner.
Iridium	Ir	2410		22.42	1850	2080	2380	-	-	-	-
Iron	Fe	1535		7.86	858	998	1180	W	W	W	Attacks tungsten. Films hard, smooth. Preheat gently to outgas.
Kanthal	FeCrAl	-		7.10	-	-	-	W	W	W	-
Lanthanum	La	921		6.15	990	1212	1388	W, Ta	-	-	Films will burn in air if scraped.
Lead	Pb	328		11.34	342	427	497	W, Mo	W	W, Ta	Toxic.
Lithium	Li	181		0.53	227	307	407	Ta, SS	-	-	Metal reacts quickly in air.
Lutetium	Lu	1663		9.84	-	-	1300	Ta	-	-	-
Magnesium	Mg	649	S	1.74	185	247	327	W, Mo, Ta, Cb	W	W	Extremely high rates possible.
Manganese	Mn	1244	S	7.20	507	572	647	W, Ta, Mo	W	W	-
Mercury	Hg	-39		13.55	-68	-42	-6	-	-	-	-
Molybdenum	Mo	2610		10.20	1592	1822	2117	-	-	-	Films smooth, hard. Careful degas required.
Neodymium	Nd	1021		7.01	731	871	1062	Ta	-	-	Low tantalum solubility.
Nichrome IV	Ni/Cr	1395		8.50	847	987	1217	***	W	W, Ta	Alloys with refractory metals.
Nickel	Ni	1455		8.90	927	1072	1262	W	W	W	Alloys with refractory metals. Forms smooth adherent films.
Niobium	Nb	2468		8.57	1728	1977	2287	W	-	-	Attacks tungsten source. n = 1.80
Niobium-Tin	Nb ₃ Sn	-		-	-	-	-	-	-	-	Co-evaporate from two sources.
Osmium	Os	2700		22.48	2170	2430	2760	-	-	-	-
Palladium	Pd	1554	S	12.02	842	992	1192	W	W	W	Alloys with refractory metals. Rapid evaporation suggested.
Parylene	C ₈ H ₈	300-400		1.10	-	-	-	-	-	-	Vapor-depositable plastic.
Permalloy	Ni/Fe	1395		8.70	947	1047	1307	W	-	-	F, Film low in nickel.
Phosphorus	P	44.1		1.82	327	361	402	-	-	-	Material reacts violently in air. n = 2.14
Platinum	Pt	1772		21.45	1292	1492	1747	W	W	W	Alloys with metals. Films soft, poor adhesion.
Plutonium	Pu	641		19.84	-	-	-	W	-	-	Toxic, radioactive.
Polonium	Po	254		9.40	117	170	244	-	-	-	Radioactive.
Potassium	K	63		0.86	23	60	125	Mo	-	-	Metal reacts rapidly in air. Preheat gently to outgas.
Praseodymium	Pr	931		6.77	800	950	1150	Ta	-	-	-
Rhenium	Re	3180		20.53	1928	2207	2571	-	-	-	Fine wire will self-evaporate.
Rhodium	Rh	1966		12.40	1277	1472	1707	W	W	W	E-beam gun preferred.

Rubidium	Rb	39		1.48	-3	37	111	-	-	-	-
Ruthenium	Ru	2310		12.30	1780	1990	2260	W	-	-	-
Samarium	Sm	1074		7.52	373	460	573	Ta	-	-	-
Scandium	Sc	1541		2.99	714	837	1002	W	-	-	Alloys with tantalum.
Silicon	Si	1410		2.32	992	1147	1337	W, Ta	-	-	Alloys with tungsten; use heavy tungsten boat. SiO produced above 4×10^{-6} Torr. E-beam best.
Silver	Ag	962		10.50	847	958	1105	W	Mo	Ta, Mo	DC, RF
Sodium	Na	98		0.97	74	124	192	Ta, SS	-	-	Preheat gently to outgas. Metal reacts quickly in air. n = 4.22
Strontium	Sr	769		2.60	239	309	403	W, Ta, Mo	W	W	Wets but does not alloy with refractory metals. May react in air.
Supermalloy	Ni/Fe/Mo	1410		8.90	-	-	-	-	-	-	Sputtering preferred; or co-evaporate from two sources, permalloy and molybdenum.
Tantalum	Ta	2996		16.60	1960	2240	2590	-	-	-	Forms good films.
Technetium	Tc	2200		11.50	1570	1800	2090	-	-	-	-
Teflon	PTFE	330		2.90	-	-	-	W	-	-	Baffled source. Film structure doubtful.
Tellurium	Te	452		6.25	157	207	277	W, Ta	W	W, Ta	Toxic. Wets without alloying. n = 1.002
Terbium	Tb	1356		8.23	800	950	1150	Ta	-	-	-
Thallium	Tl	304		11.85	280	360	470	W, Ta	-	W	Very toxic. Wets freely.
Thorium	Th	1875		11.70	1430	1660	1925	W, Ta, Mo	W	W	Toxic, radioactive.
Thulium	Tm	1545	S	9.32	461	554	680	Ta	-	-	-
Tin	Sn	232		7.28	682	807	997	Mo	W	W	Wets molybdenum. Use tantalum liner in E-beam guns.
Titanium	Ti	1660		4.50	1067	1235	1453	W	-	-	Alloys with refractory metals; evolves gas on first heating.
Tungsten	W	3410		19.35	2117	2407	2757	-	-	-	Forms volatile oxides. Films hard and adherent.
Uranium	U	1132		19.05	1132	1327	1582	Mo, W	W	W	Films oxidize.
Vanadium	V	1890		5.96	1162	1332	1547	W, Mo	-	-	Wets molybdenum. E-beam-evaporated films preferred. n = 3.03
Ytterbium	Yb	819	S	6.96	520	590	690	Ta	-	-	-
Yttrium	Y	1522		4.47	830	973	1157	W, Ta	W	W	High tantalum solubility.
Zinc	Zn	420		7.14	127	177	250	Mo, W, Ta	W	W	Evaporates well under wide range of conditions.
Zinc Antimonide	Zn ₃ Sb ₂	570		6.33	-	-	-	-	-	-	-
Zirconium	Zr	1852		6.49	1477	1702	1987	W	-	-	Alloys with tungsten. < >Films oxidize readily.
Zirconium Silicide	ZrSi ₂	1700		4.88	-	-	-	-	-	-	-

Appendix C

XRD Results

C.1 Calibration Sample

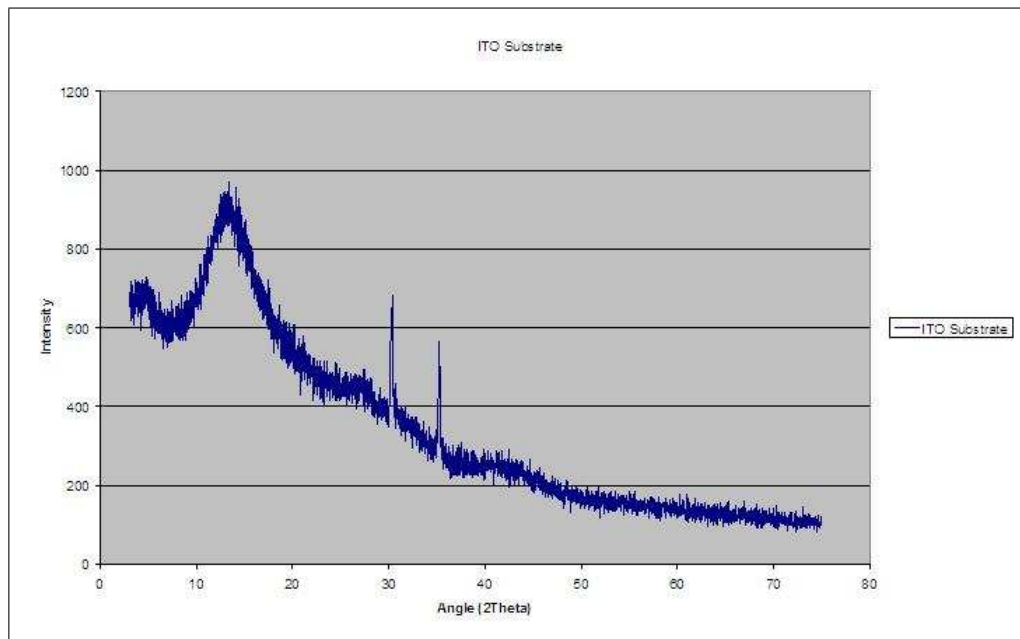


Figure C.1: XRD results for ITO substrate

Here the XRD profile of the glass substrate with ITO is given. The profile, subtracted from the further samples, provides a clean result that can be analysed. The ITO peaks can clearly be seen at 30° and 36° , identifying it

clearly. a smaller peak at around 50° may sometimes appear, depending of the crystalline structure.

C.2 Silver

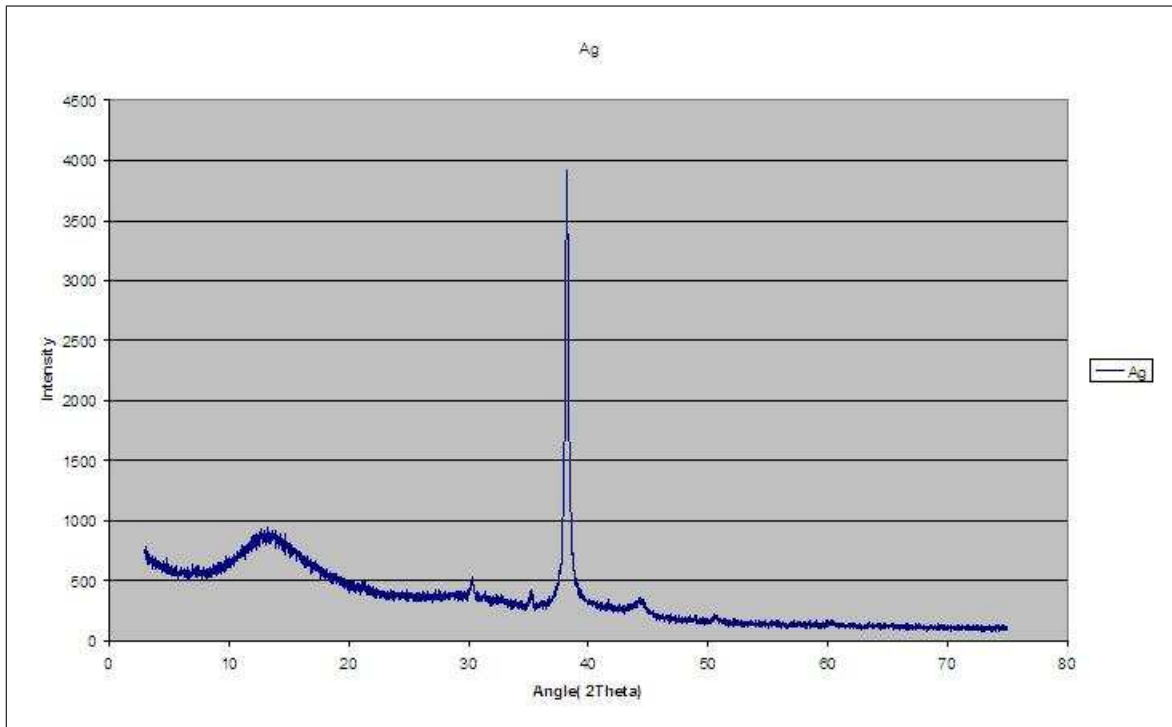


Figure C.2: XRD results for silver deposition

Silver has a strong prevalent peak at 38° , corresponding to its $\{101\}$ plane. The two further characteristic peaks appear at 44° and 60° .

C.3 Silver Sulfide

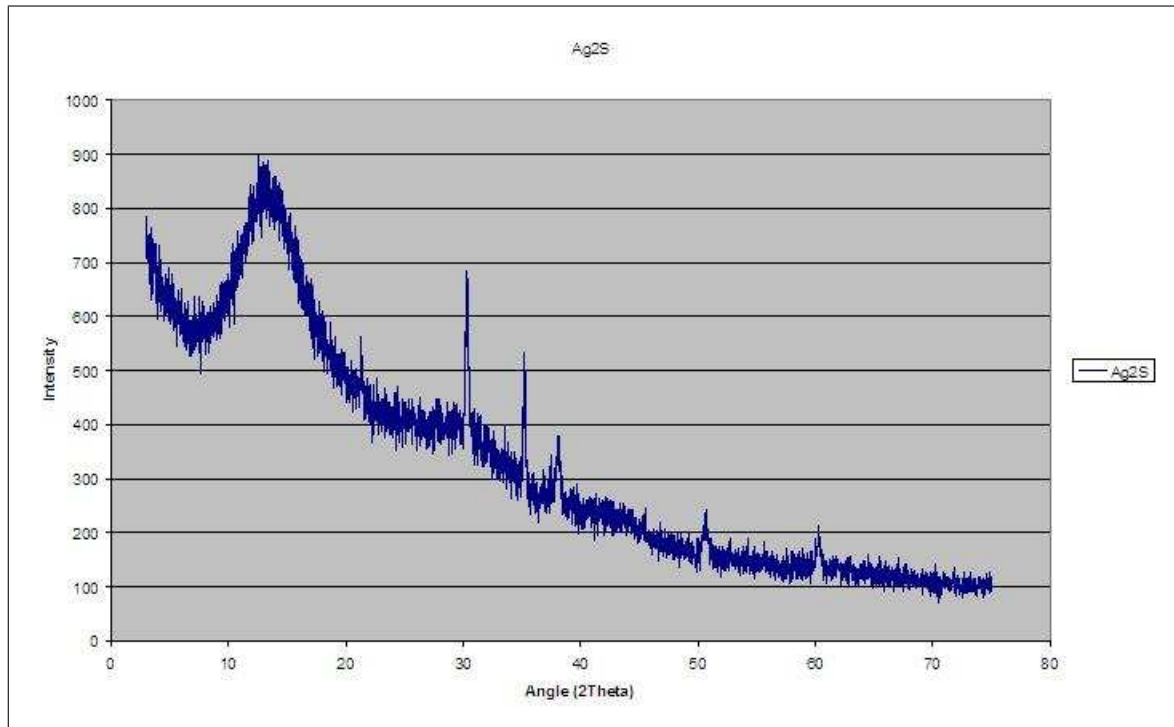


Figure C.3: XRD results for silver sulfide development

Here the silver presence is seen by the peaks at 38° and 60° . The sulphur content is show at 21° , 33° and 37° .

C.4 Palladium

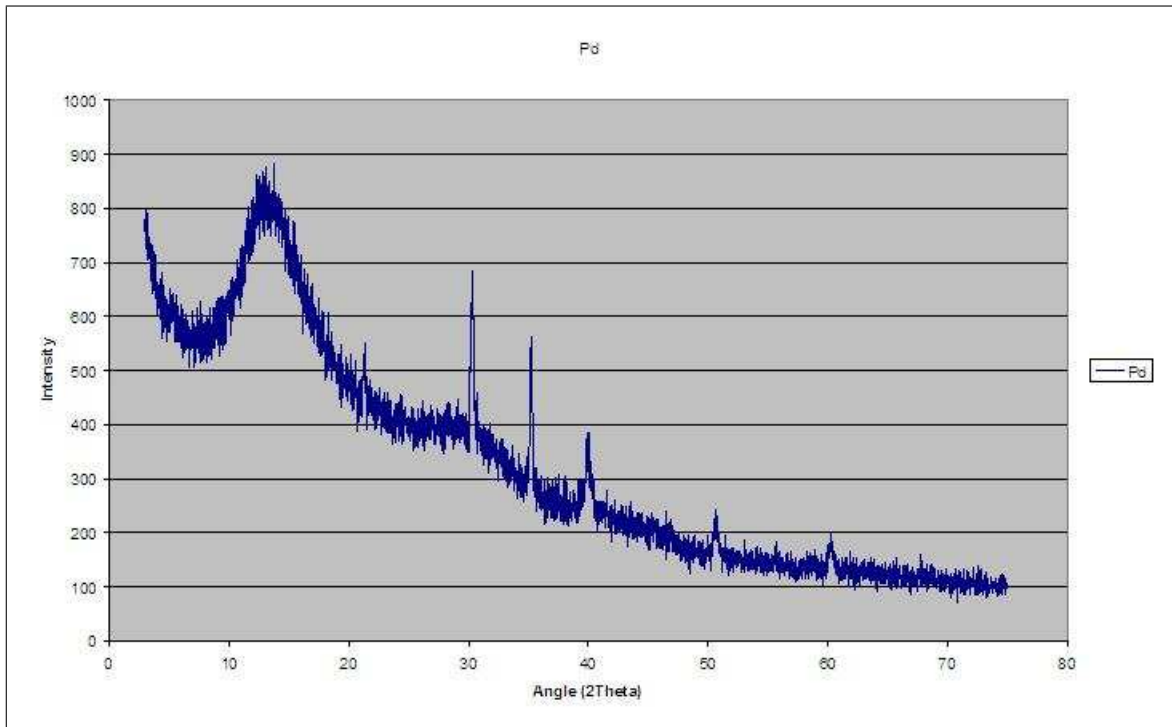


Figure C.4: XRD results for palladium deposition

The peaks at 40° and 60° together identify the material as palladium.

C.5 Aluminium

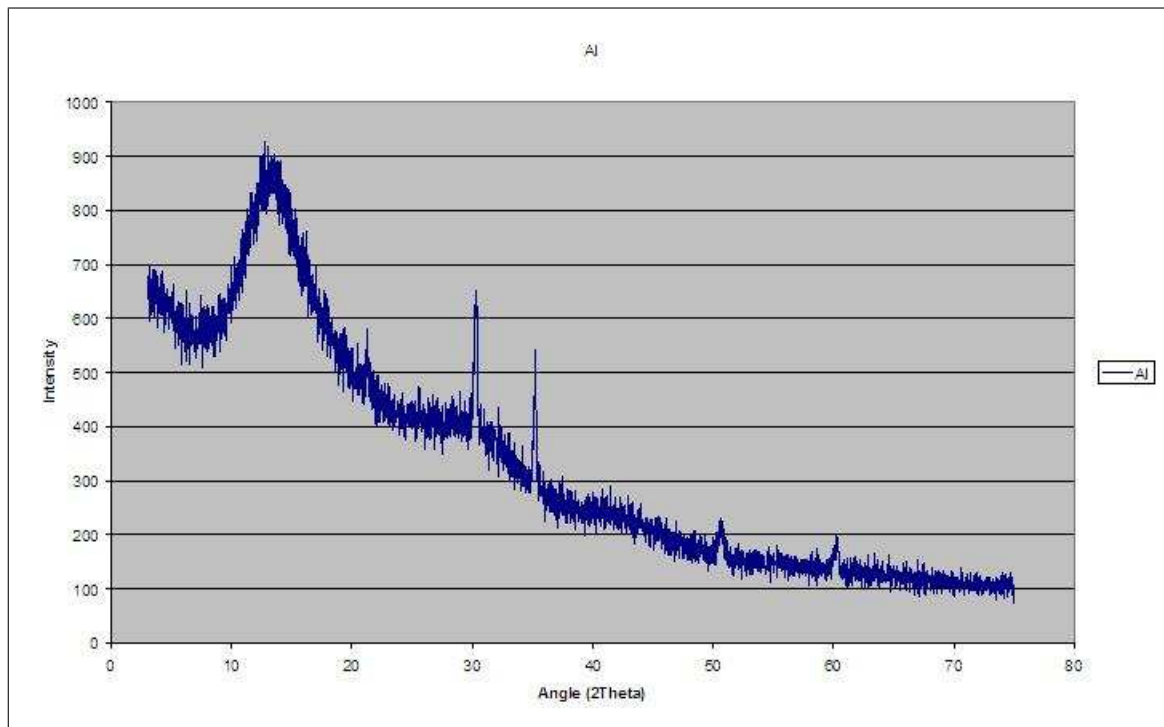


Figure C.5: XRD results for aluminium deposition

The sample aluminium available in the laboratory gave this spectrum. Missing peaks at 44° and 77° , with only the 60° peak present made it impossible to definitively identify as aluminium. Pure aluminium was therefore ordered from Sigma Aldrich.

List of References

- [1] Reith, M.: *Nano-Engineering in Science and Technology: An Introduction to the World of Nano-Design*. World Scientific, 2003.
- [2] O.Brand, G.K.Fedder, C.Hierold, J.G.Korvink and O.Tabata: *Carbon Nanotube Devices: Properties, Modeling, Integration and Applications*. Wiley-VCH, 2008.
- [3] Science museum. Website, July 2009.
Available at: <http://www.sciencemuseum.org.uk/images/I067/10328828.aspx>
- [4] Escutcheons of science. Website, July 2009.
Available at: <http://home.att.net/numericana/arms/schickard.htm>
- [5] Computer history museum. Website, August 2009.
Available at: <http://www.computerhistory.org/collections/accession/102710252>
- [6] Website, August 2009.
Available at: <http://gadgets.boingboing.net/2008/01/>
- [7] Halacy, D.: *Charles Babbage: Father of the Computer*. Crowell-Collier Press, 1970.
- [8] Swade, D.: The babbage engine. Webpage, march 2009.
Available at: <http://www.computerhistory.org/babbage/>
- [9] Carol, A.: Building a calculating machine using lego® pieces. Web Article, March 2009.
Available at: <http://acarol.woz.org/>
- [10] Anthes, G.: Difference engines: The return of the mechanical computer. Web article, March 2008.
Available at: <http://www.computerworld.com/s/article/print/313000/DifferentEngines?taxonomyId=12&taxonomyName=Hardware>

- [11] Us national nanotechnology initiative. August 2009.
Available at: <http://www.nano.gov/>
- [12] Ratner, M. and Ratner, D.: *Nanotechnology: A Gentle Introduction to the Next Big Idea*. Prentice Hall, 2003.
- [13] Busnaina, A.: *Nanomanufacturing Handbook*. CRC Press, 2007.
- [14] MIT: Nanomechanics links. Website, Aug 2009.
Available at: web.mit.edu/cortiz/www/nanomechanics.html
- [15] Answers.com. Website, October 2009.
Available at: <http://www.answers.com/topic/scanning-tunneling-microscope>
- [16] Jijmegen, R.U.: Virtual classroom biology. Website, October 2009.
Available at: <http://www.vcbio.science.ru.nl/en/image-gallery/electron/>
- [17] Greene, B.: *The Elegant Universe: Superstrings, Hidden Dimensions and the Quest for the Ultimate Theory*. Jonathan Cape, 1999.
- [18] Drexler, K.: *Nanosystems: Molecular Machinery, Manufacturing and Computation*. John Wiley, 1992.
- [19] Madou, M.J.: *Fundamentals of Microfabrication: The Science of Miniaturization*. CRC Press, 2001.
- [20] Pelesko, J.A.: *Self Assembly: The Science of Things That Put Themselves Together*. Chapman & Hall/CRC, 2007.
- [21] The art of nano-origami. Online Article, March 2009.
Available at: <http://www.photonics.com/Content/ReadArticle.aspx?ArticleID=36653>
- [22] Mini-origami: Isi folds up tiny packages for drug delivery. Online Article, May 2008.
Available at: http://www3.isi.edu/about-news_story.htm?s=193
- [23] Vayssieres, L.: On the design of advanced metal oxide nanomaterials. *International Journal of Nanotechnology*, vol. 1, pp. 1–41, 2004.
- [24] Figliola, R.S. and Beasley, D.E.: *Theory and Design for Mechanical Measurements*. John Wiley & Son, Inc., 2006.
- [25] Stangroom, J. and Garvey, J.: *The Great Philosophers*. Arcturus Publishing, 2005.

- [26] van Ruitenbeek, J.: Silver nanoswitch. *Nature*, vol. 433, pp. 21–22, 2005.
- [27] Terabe, K., Hasegawa, T., Nakayama, T. and Aono, M.: Quantized conductance atomic switch. *Nature*, vol. 433, pp. 47–50, 2005.
- [28] Li, X.X.L., Yu, G., Di, C.-A., Wei, D., Ye, S. and Liuc, Y.: Nanophotoswitches with a high on/off ratiobased on a structure of indium tin oxide/organic insulator/metal. *Applied Physics Letters to nature*, vol. 92, pp. 043302: 1–3, 2008.
- [29] Tang, Q., Li, L., Song, Y., Liu, Y., Li, H., Xu, W., Liu, Y., Hu, W., and Zhu, D.: Photoswitches and phototransistors from organic single-crystalline sub-micro/nanometer ribbons. *Advanced Materials*, vol. 19, pp. 2624–2628, 2007.
- [30] Benedetto, F.D., Mele, E., Camposeo, A., Athanassiou, A., Cingolani, R. and Pisignano, D.: Photoswitchable organic nanofibers. *Advanced Materials*, vol. 20, pp. 314–318, 2008.
- [31] Lee, S.W.L.D.S., Morjan, R.E., Jhang, S.H., Sveningsson, M., Nerushev, O., Park, Y.W. and Campell, E.E.: A three-terminal carbon nanorelay. *Nano Letters*, vol. 4, no. 10, pp. 2027–2030, 2004.
- [32] O’Connell, M.J. (ed.): *Carbon Nanotubes: Properties and Applications*. CRC Press/Taylor & Fancis Group, 2006.
- [33] Kaul, A.B., Wong, E.W., Epp, L. and Hunt, B.D.: Electromechanical carbon nanotube switches for high-frequency applications. *Nano Letters to nature*, vol. 6, pp. 942–947, 2006.
- [34] Deshpande, V., Chiu, H.-Y., Postma, H., Miko, C., Forro, L. and Bockrath, M.: Carbon nanotube linear bearing nanoswitches. *Nano Letters*, vol. 6, pp. 1092–1095, 2006.
- [35] PuYang, F., Xu, H., Ho, C.-M., Liu, Y., Flood, A.H., Bonvallet, P.A., Tseng, H.-R., Stoddart, J.F., Baller, M. and Magonov, S.: All-carbon nanoswitch based on molecule: a first principles study. *Journal of Applied Physics*, vol. 102, pp. 064501: 1–4, 2007.
- [36] Tsunani, N.: A v6 engine for the nano-age. Website, August 2009.
Available at: <http://www.voyle.net/Nano%20Research-05-100+/research-05-0106.htm>
- [37] Kourens, A.: *Wetenskaplike Skryfvaardighede: Riglyne vir die skryf van tesisse en proefskrifte*. Sun Press, 2004.

- [38] Laboratories, C.: A basic introduction to clean rooms. Website, February 2009. Available at: <http://www.coastwidelabs.com/Technical%20Articles/Cleaning%20the%20Cleanroom.htm>
- [39] Ullman, D.G.: *The Mechanical Design Process*. McGraw Hill, 2003.
- [40] Konenkamp, R., Word, R.C. and Godinez, M.: Ultraviolet electroluminescence from zno/polymer heterojunction light-emitting diodes. *Nano Letters*, vol. 5, pp. 2005–2008, 2005.
- [41] Abramson, A.R.: *Thermal Energy Transport in Micro/Nanostructures*. Ph.D. thesis, University of California, Berkley, 2002.
- [42] Bedair, S.S. and Fedder, G.K.: The 13th international conference on solid-state sensors, actuators and microsystems. In: *Polymer Wicking to Mass Load Cantilever for Chemical Gravimetric Sensors*. 2005.
- [43] Wang, C. and Yen, S.: Theoretical analysis of film uniformity in spinning processes. *Chemical Engineering Science*, vol. 50, pp. 989–999, 1995.
- [44] *TOXICOLOGICAL PROFILE FOR TOLUENE U.S. DEPARTMENT OF HEALTH AND HUMAN SERVICES Public Health Service Agency for Toxic Substances and Disease Registry*, 2000. Available at: <http://www.atsdr.cdc.gov/toxprofiles/tp56.pdf>
- [45] *PUBLIC HEALTH STATEMENT Xylene*, 2007. Available at: <http://www.atsdr.cdc.gov/toxprofiles/tp71-c1-b.pdf>
- [46] Press, B.: Ganoskin. Website, July 2009. Available at: <http://www.ganoksin.com/borisat/nenam/nillo-work-10-1.htm>
- [47] Wood, A.: Alan wood's web site. Website, May 2009. Available at: www.alanwood.net/pesticides/calciumpolysulfid.html
- [48] Chorkendorff, I. and Niemantsverdriet, J.: *Concepts of Modern Catalysis and Kinetics*. Wiley-VCH, 2003.
- [49] Co., K.J.: Materials guide for thermal evaporation. Pdf Guide, August 2008. Available at: http://www.lesker.com/newweb/menu_evapsources.cfm?CFID=180535&CFTOKEN=48466901§ion=materialdeptable&init=skip
- [50] Ramezani, A., Alasty, A. and Akbari, J.: Closed-form solutions of the pull-in instability in nano-cantilevers under electrostatic and intermolecular surface

- forces. *International Journal of Solids and Structures*, vol. 44, pp. 4925–4941, 2007.
- [51] Tang, Z., Xu, Y., Li, G. and Aluru, N.: Physical models for coupled electromechanical analysis of silicon nanoelectromechanical systems. *Journal of Applied Physics*, vol. 97, pp. 114304: 1–13, 2005.
- [52] E.Shigley, J., Mischke, C.R. and Budynas, R.G.: *Mechanical Engineering Design*. McGraw Hill, 2004.
- [53] Yang, J., Jia, X. and Kitipornchai, S.: Pull-in instability of nanoswitches using nonlocal elasticity theory. *Journal of Applied Physics D: Applied Physics*, vol. 41, pp. 1–8, 2008.